

UNIVERSITY OF OKLAHOMA

GRADUATE COLLEGE

CONTINUITY, CONNECTIVITY AND RESERVOIR CHARACTERISTICS  
OF DESMOINESIAN FAN-DELTA CONGLOMERATES AND SANDSTONES,  
ELK CITY FIELD, ANADARKO BASIN, OKLAHOMA

A THESIS

SUBMITTED TO THE GRADUATE FACULTY

in partial fulfillment of the requirements for the

Degree of

MASTER OF SCIENCE

By

BURAK SALANTUR

Norman, Oklahoma

2016

CONTINUITY, CONNECTIVITY AND RESERVOIR CHARACTERISTICS  
OF DESMOINESIAN FAN-DELTA CONGLOMERATES AND SANDSTONES,  
ELK CITY FIELD, ANADARKO BASIN, OKLAHOMA

A THESIS APPROVED FOR THE  
CONOCOPHILLIPS SCHOOL OF GEOLOGY AND GEOPHYSICS

BY

---

Dr. Matthew J. Pranter, Chair

---

Dr. Roger M. Slatt

---

Dr. Shankar Mitra



This thesis is dedicated to my wife, Pelin Salantur, and to my entire family. Thank you for always believing me, giving me the encouragement to achieve this, and reminding me the reality of this life.

## **Acknowledgements**

This research was funded through the Reservoir Characterization and Modeling Laboratory and the sponsors of Granite Wash Consortium: Chesapeake Energy, Devon Energy, QEP Resources, and SM Energy. I would like to acknowledge IHS and SM Energy for providing the data. I thank Schlumberger for the use of Petrel; and IHS for the use of Petra. I would like to thank to Turkish Petroleum for funding me and giving me this great opportunity. I would like to thank Dr. Matthew Pranter for his time, guidance, support, and enthusiasm throughout this research. I would also like to thank Dr. Roger Slatt and Dr. Shankar Mitra for their advice and input as my committee members. I would like to thank the Integrated Core Characterization Center (IC<sup>3</sup>) at OU, Dr. Carl Sondergeld, and his students for the porosity measurements of the core plugs. I thank John Mitchell and my friends at OU: Fnu Suriamin (Ming), Doga Senoglu, Javier Tellez, Antonio Cervantes, Alexander Besov, Andreina Liborius, and Niles Wethington for their time and recommendations. Lastly, I would like to thank my wife and my family for their patience, love, and support during this research.

## Table of Contents

Acknowledgements .....	iv
Table of Contents .....	v
List of Tables .....	vii
List of Figures .....	viii
Abstract.....	ix
Introduction.....	1
Geologic Setting.....	7
Lithologies and Lithofacies.....	16
Conglomerates.....	16
Sandstones.....	20
Muddy Sandstones and Sandy Mudstones .....	21
Mudstones .....	22
Lithology Estimation.....	23
Lateral Variability in Mineralogy and Log Response.....	23
Artificial Neural Network Approach.....	26
Additional Constraints .....	30
Depositional Environment, Stratigraphy and Structure.....	34
Spatial Distribution, Continuity and Connectivity of Fan-Delta Deposits .....	44
Continuity of Conglomerates and Sandstones.....	45
Lithology Distribution .....	46
Porosity Distribution.....	49
Static Connectivity and Pore Volume.....	51
Conclusion .....	56
References.....	59
Appendix A: Paleogeographic Maps.....	62

Appendix B: Core Descriptions .....	64
Appendix C: Thin-Section Photomicrographs .....	88
Appendix D: Spectral Gamma-Ray Data.....	90
Appendix E: Artificial Neural Network Analysis .....	92
Appendix F: Lithofacies and Interpretation of Depositional Setting.....	96
Appendix G: Structural and Stratigraphic Framework.....	98
Appendix H: Upscaled Lithology Logs .....	101
Appendix I: Sea Level Curve for Carboniferous-Permian.....	102
Appendix J: Lithology Models and Maps.....	103
Appendix K: Variograms.....	106
Appendix L: Porosity Modeling.....	122
Appendix M: Connectivity and Pore Volume.....	124

## List of Tables

Table 1: Lithofacies observed in core and interpreted depositional process.....	17
Table 2: Total volume, connected volume, and pore volume of sandstones and conglomerates by zone.....	52



## List of Figures

Figure 1: Geological provinces of Oklahoma and Texas.....	2
Figure 2: Detailed base map .....	5
Figure 3: Anadarko Basin cross section .....	8
Figure 4: Stratigraphic column.....	11
Figure 5: GHK 1-34 Finnell core description and well logs.....	12
Figure 6: GHK 1-27 Niece core description and well logs.....	14
Figure 7: Sandstone and conglomerate lithofacies .....	18
Figure 8: Muddy sand, sandy mud, and mudstone lithofacies .....	19
Figure 9: Longitudinal cross section A-A' .....	24
Figure 10: Artificial Neural Network results for the classification of 5 lithologies .....	28
Figure 11: Artificial Neural Network results for the classification of 3 lithologies .....	31
Figure 12: Cross plot of well logs before and after applying constraints to the ANN .....	33
Figure 13: Illustration of the depositional environment .....	38
Figure 14: Stratigraphic and structural framework (3-D grid).....	41
Figure 15: Vertical proportion curve.....	43
Figure 16: 3-D lithology model cross-sectional views .....	47
Figure 17: 3-D lithology model with slices .....	48
Figure 18: Cross section E-E' with integrated lithology, pore volume and connectivity .....	53
Figure 19: Connectivity and Pore volume by zone and system tract.....	55

## **Abstract**

Marmaton Group (Desmoinesian) Granite Wash deposits of the Elk City Field, in eastern Beckham and western Washita counties, Oklahoma, are composed of sandstones, conglomerates, and mudstones that were deposited as fan deltas with changing proximity to the Amarillo-Wichita uplift. Sandstones, conglomerates and shales can be divided into five zones (Marmaton A-B, C, D, E, F) separated by flooding surfaces. These zones can be further divided into transgressive and highstand system tracts. Structurally, the Elk City Field is composed of a northwest trending anticline bounded by at least two faults on its flanks. Thin section analysis and XRD results suggest that the mineralogy of the sediment source is responsible for the variable well-log responses. An artificial-neural network combined with proper well-log cut-off values and porosity-lithology relations are used to estimate lithologies in non-cored wells by utilizing cores and well logs. The stratigraphic framework, estimated lithology logs, porosity logs, and the spatial statistics from variography are used to construct 3-D lithology and porosity models that illustrate lateral and stratigraphic variability in reservoir quality. Different lithology models show the relation between the sequence stratigraphy and reservoir distribution as well as the effect of using a neural network and porosity-lithology relation in lithology estimation and the resulting reservoir properties. Marmaton C interval has the highest connectivity both for conglomerates (88.1%) and sandstones (67.1%). Marmaton A-B interval has the greatest pore volume. Highstand system tracts have greater amount of reservoir, reservoir connectivity and reservoir pore volume than transgressive system tracts.

## **Introduction**

The Marmaton Group of the Pennsylvanian Granite Wash in western Oklahoma and the Texas Panhandle (Figure 1) is an active producing interval for oil and gas from arkosic sandstones and conglomerates derived from the Amarillo-Wichita uplift and deposited into the southern Anadarko Basin through alluvial fans, fan deltas, debris flows and turbidite flows (McConnell et al., 1990; Mitchell, 2011). Variable factors such as the type of source rock, transportation distance, and accommodation space led to a complex geology for the Marmaton Group in the Anadarko Basin (Mitchell, 2011). Because of the complex geology, lithofacies and petrophysical properties can change both stratigraphically and laterally in such a way that understanding their distribution and correlating the lithofacies become challenging.

The Marmaton Group depositional environment varies from alluvial fans and fan deltas in the proximal areas (near the Amarillo-Wichita Uplift) to deep-marine turbidite deposits in the distal areas (Sneider et al., 1977; Dutton, 1979, 1984; Mitchell, 2011). Sneider et al. (1977) studied the lithological and petrophysical properties of Missourian-age sandstone and conglomerate reservoirs interbedded with shales and carbonates in old Elk City Field. It should be noted that the Elk City field mentioned in this study is larger than the area studied by Sneider et al. (1977). They used spontaneous potential (SP) logs to differentiate reservoir and non-reservoir rocks and found that the amount of shale and carbonate increases basinward. Based on thin sections, they realized that the amount of cement in sandstones and conglomerates is less than 7% and this creates a direct relation between the grain size and sorting. They proposed that, with increasing

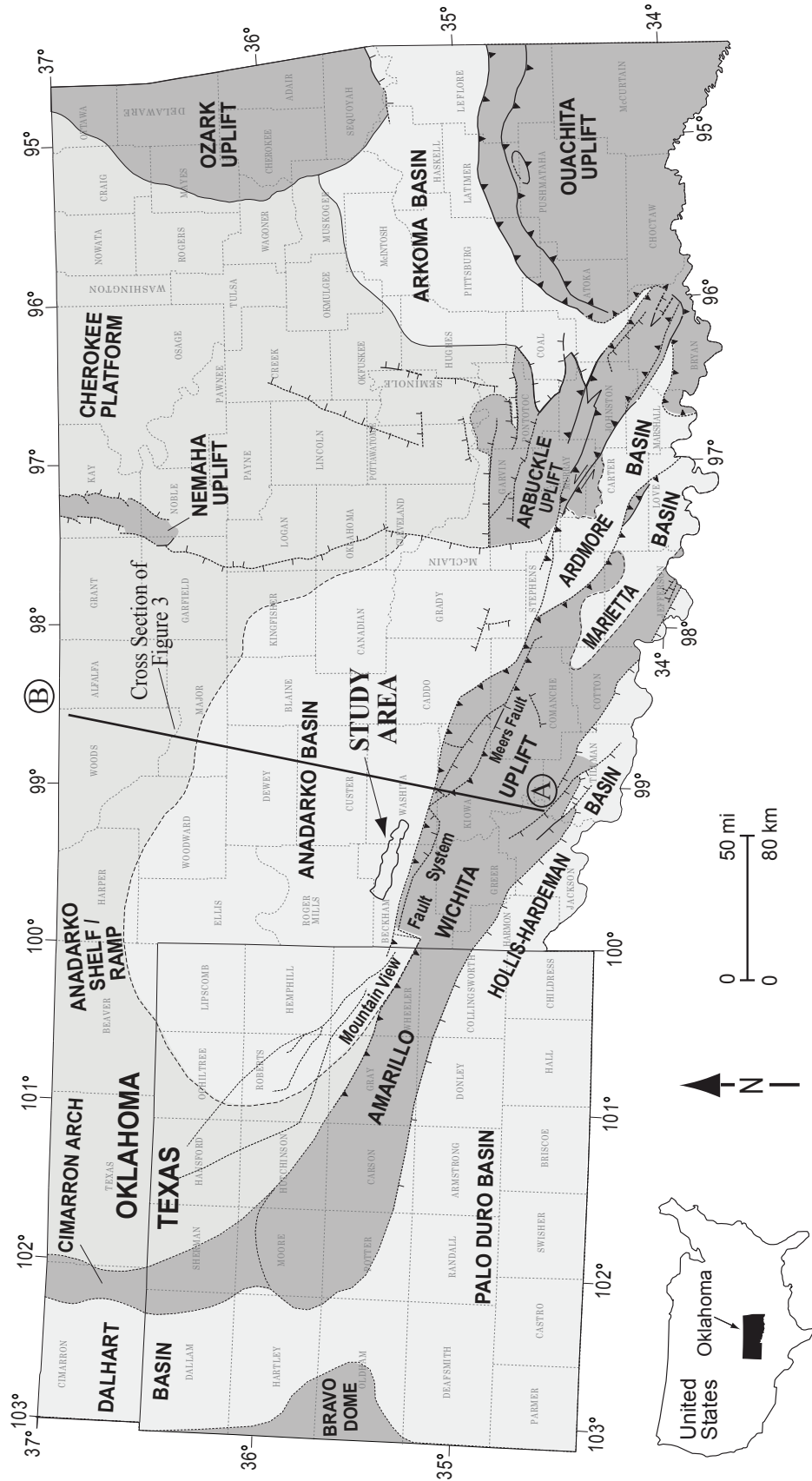


Figure 1. Regional base map showing the geological provinces of Oklahoma and Texas. The study area resides on the deep Anadarko Basin just north of the Amarillo-Wichita Uplift Mountain View Fault System (modified from Johnson and Luza, 2008; Northcutt and Campbell, 1995; Campbell, et al., 1988; Dutton, 1984; LoCricco, 2012, McConnell, 1989).

grain size, porosity decreases and resistivity increases on well logs. They defined four types of sandstone bodies, which are barrier bar, alluvial channel, distributary channel, and deltaic marine fringe indicating a marginal-marine depositional setting.

Proximal areas close to the uplifted source areas are generally defined by alluvial fans or fan deltas. Fan deltas have been described as alluvial fans that prograde into standing bodies of water (marine or lacustrine) from adjacent highlands (Holmes, 1965; McGowen, 1970; Nemeč and Steel, 1988). One criteria used to differentiate between alluvial fan and fan-delta deposits is that fan-delta deposits are often interbedded with marine deposits (Nemeč and Steel, 1988). Based on the fan-delta classification criteria proposed by Ethridge and Wescott (1984), Granite Wash deposits in the deep Anadarko Basin have previously been considered to be a well-developed shelf-type fan delta (McGowen, 1970). By differentiating the sub-aerial and sub-aqueous parts of fan-delta deposits, an accurate classification of depositional settings can be established (Ethridge and Wescott, 1984).

Most of the Granite Wash consists of tight oil and gas reservoirs. In terms of porosity and permeability, Granite Wash deposits show significant variability. Average porosity is approximately 6% and permeability is generally below 0.1 md (Mitchell, 2011). Based on thin sections from Missourian samples in Mobeetie field porosity values are between 0-14% with an average of 5.2% (Dutton, 1984). Based on core plugs, porosity measurements were up to 21% and horizontal permeability values range from 0.1 md to 1.45 md (Dutton, 1984). Missourian conglomerates from western Beckham County (Mayfield 1-2, Mayfield 1-34, and Sage 1-34H wells) have porosity values between 2-8% while sandstones are between 2-10% (Karis, 2015).

The mineralogy of Marmaton Group can have a significant effect on well-log responses and might cause misinterpretations. Gamma-ray logs might have high values because of greater amounts of potassium feldspar. This can cause underestimation of reservoir zones and reserves. Furthermore, high chlorite content might mask the gas-bearing zones by impeding cross-over of the neutron- and density-porosity logs by producing high neutron-porosity readings (Mitchell, 2011). Some metals in the chlorite, such as iron, magnesium, and manganese can cause resistivity logs to have low readings in hydrocarbon-bearing zones, which are normally anticipated to exhibit high resistivity (Sahl, 1970; Dutton, 1984; Mitchell, 2011).

Although previous studies provide examples for the variability of the lithologies and petrophysical properties of the Marmaton Group and the Granite Wash for different regions across the Anadarko Basin, no study has focused on the spatial distribution of lithologies and reservoir characteristics of the Desmoinesian-age Marmaton Group Granite Wash deposits. This study investigates the Desmoinesian-age, Marmaton Group Granite Wash in the Elk City Field located in eastern Beckham, western Washita, and a small portion of southeastern Roger Mills counties, Oklahoma (Figure 2). This area can be considered as a proximal wash field area where more than 1,800 ft (549 m) of Desmoinesian-age Marmaton Group arkosic sandstone and conglomerate were deposited mainly through fan deltas (Lyday, 1985; McConnell et al., 1990; Mitchell, 2011; LoCricchio, 2014). Sandstones and conglomerates are separated by distinct shales that can be correlated regionally (Mitchell, 2011; LoCricchio, 2014).

In this study, the key lithologies and lithofacies of the Marmaton Group in the Elk City Field, their corresponding well-log responses and their relationship with the

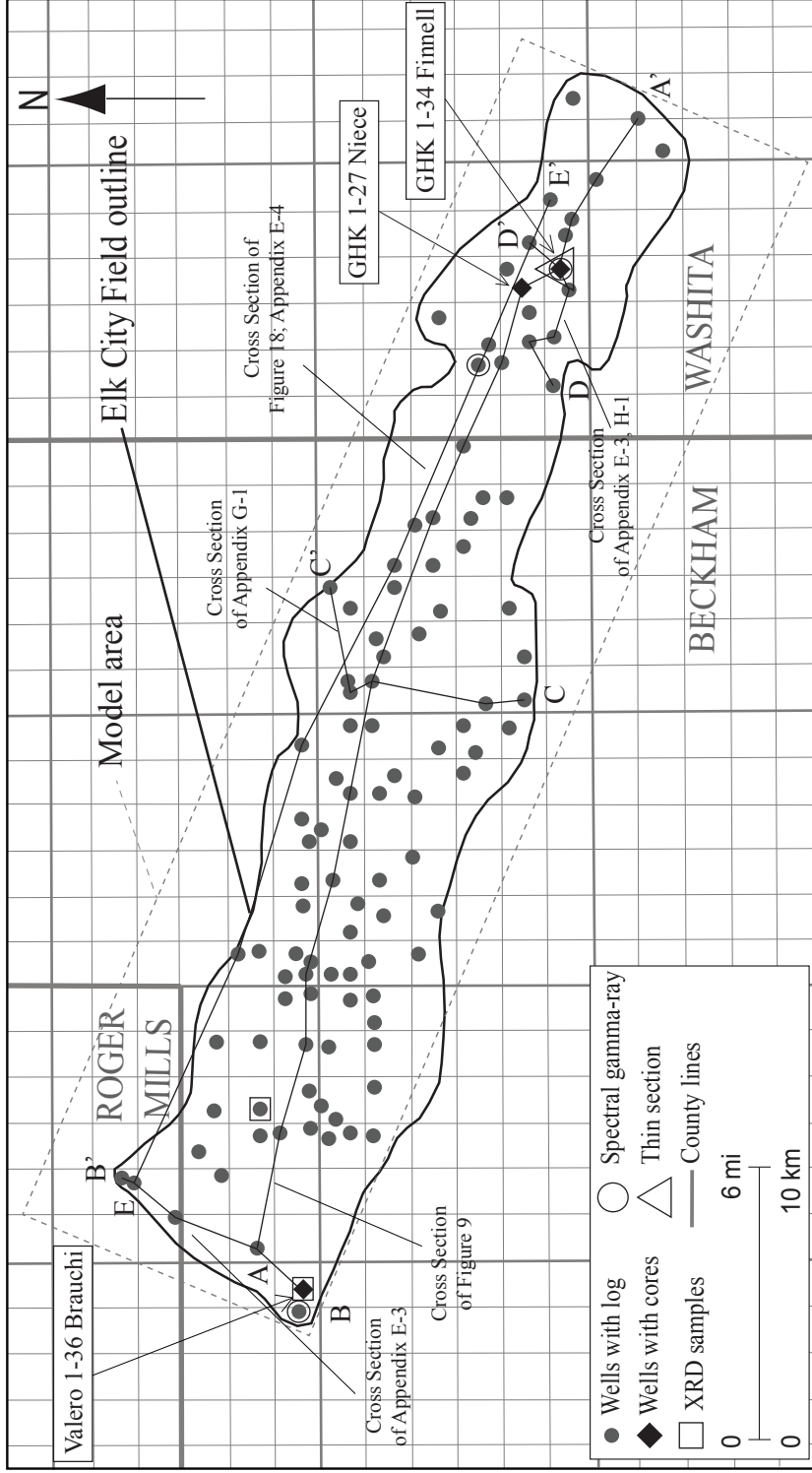


Figure 2. Detailed study area. There are 117 wells with wireline logs. Wells with core, spectral gamma-ray log, XRD data, and thin section data are indicated with different symbols. Elk City Field outline is modified from Boyd, 2002, Maps of Oklahoma Oil and Gas Fields. The model boundary is shown with dashed lines. See Figure 1 for the location of the study area.

porosity are defined; the depositional environment and sequence-stratigraphic framework are interpreted; and the spatial distribution, connectivity, and reservoir characteristics of the sandstones and conglomerates of the Marmaton Group are mapped and their relation to the stratigraphic and structural framework is established.

The study area includes digital logs for 117 wells (Figure 2). Logs for more than 70 of the wells were digitized from raster format to ASCII format by using Petra software. Eighty-nine wells contain gamma-ray (GR), deep-resistivity (ILD), neutron-porosity (NPHI), and density-porosity (DPHI) logs and are used to estimate lithologies. The remaining wells contain a subset of these logs. All wells are used in stratigraphic correlation. Two wells have spectral gamma-ray logs; one of them is located in Beckham County and the other is in Washita County. Two cores housed at the Oklahoma Geological Survey (OGS) - Oklahoma Petroleum Information Center (OPIC) in Norman, Oklahoma were described in detail in regard to lithology, color, grain size, sorting, rounding, sedimentary structures, and additional remarks. The two cored wells, located in Washita County, are 4,115 ft (1,254 m) apart, and are from different stratigraphic zones. GHK 1-34 Finnell core is a butt core 4 in (10 cm) in width and 120 ft (37 m) in length. It is almost completely continuous through the cored interval of the Marmaton C Wash (discussed later). GHK 1-27 Niece core is a slabbed section from a 3.5 in (8.9 cm) core. Of the 119 ft (36 m) of core, only 60% (71 ft, 22 m) of it is preserved. The remaining 40% of the core is missing. This core corresponds to Marmaton E and Marmaton F Wash intervals (discussed later). Porosity and permeability were measured on five core plug samples of different lithologies from the GHK 1-34 Finnell core. Thin sections of these samples were examined for mineralogy



and porosity. Spectral gamma-ray data for the GHK 1-34 Finnell core was provided by OPIC. Also, XRD measurements of ten samples from the cores located in Beckham County and photographs of one of these cores (Valero 1-36 Brauchi), 20 ft (6 m) in length, were provided by SM Energy.

After calibrating the core to the well logs, Artificial Neural Network (ANN) analysis combined with the well-log cut-off values and a porosity-lithology relation were used to estimate lithologies in non-cored wells by utilizing the core descriptions and gamma-ray (GR), deep-resistivity (ILD), neutron-porosity (NPHI), and density-porosity (DPHI) logs. By correlating four laterally extensive shales, a stratigraphic and structural framework (3-D grid) of the study area is established. Lithology logs, porosity logs, a vertical proportion curve, the stratigraphic and structural framework, and spatial statistics from variography are used to construct 3-D lithology and porosity models to evaluate reservoir connectivity and pore volume.

## **Geologic Setting**

The Anadarko Basin, located in western Oklahoma and the Texas Panhandle, is the deepest interior basin in North America (Figures 1 and 3). Locally, the basin has more than 40,000 ft (12,000 m) of Cambrian through Permian sediments, most of which were deposited in deep- to shallow-marine environments (Perry, 1989; Mitchell, 2011). Perry (1989) divided the structural history of the Anadarko Basin into four main stages: 1. Precambrian crustal consolidation, 2. Late Precambrian to Middle Cambrian southern Oklahoma Aulacogen development in which high amounts of igneous intrusion and extrusion occurred along the axis of the aulacogen (Perry, 1989; Gilbert 1992), 3.

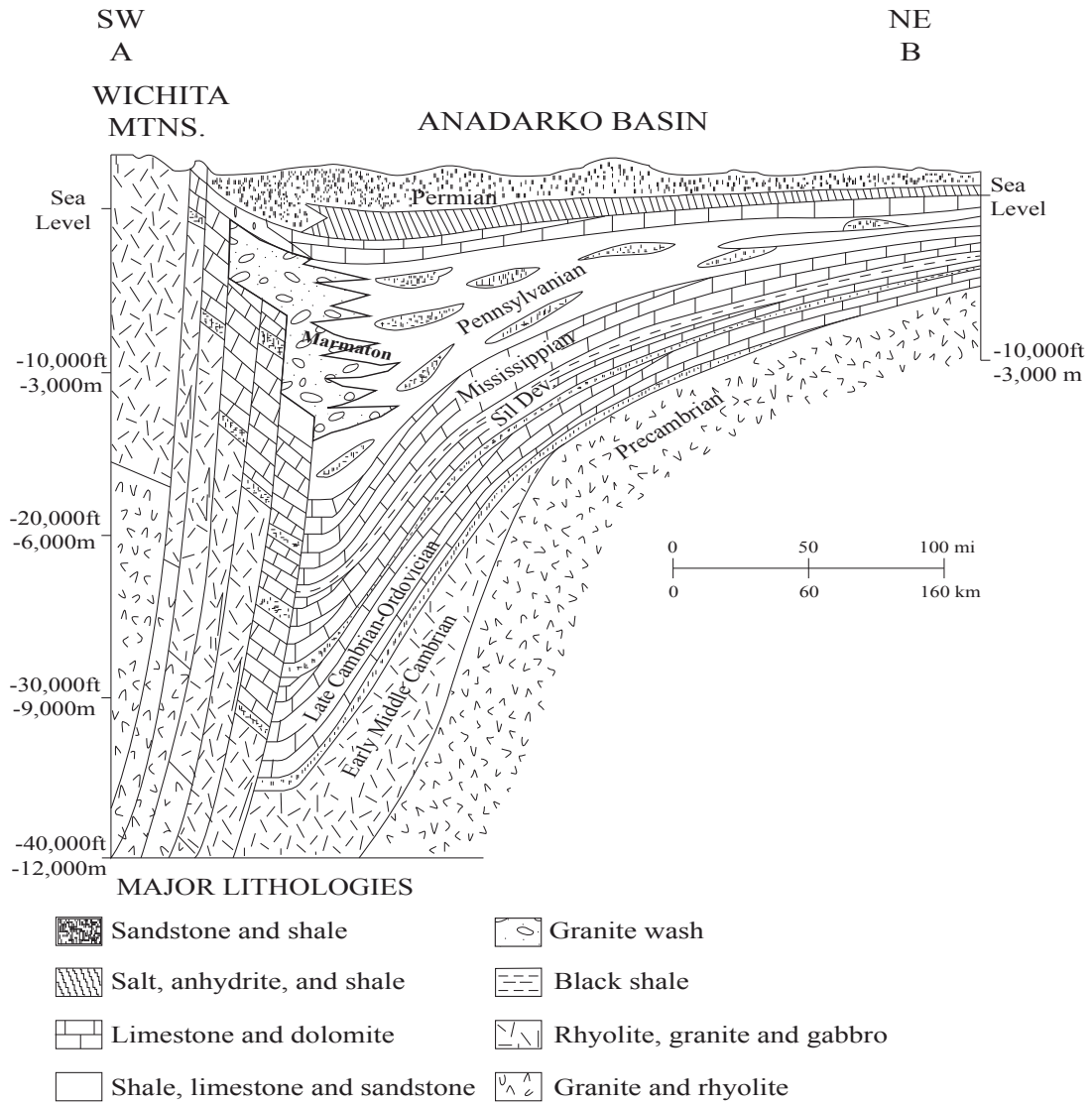


Figure 3. SW to NE structural cross section of the Anadarko Basin. With the change in the stress regime in Early Pennsylvanian, the materials of the Amarillo - Wichita uplift started to erode and were deposited in the basin on top of the igneous rocks and carbonates. Granite Wash deposits pinch out to the north and are transitional with the sediments that are sourced from the north (modified from unpublished H.G. Davis; K.S. Johnson, 1989). The location of the cross section is shown in Figure 1.

Cambrian through Early Mississippian southern Oklahoma trough development during which the region kept subsiding and became a depocenter for carbonates, shales, and sandstones (Johnson, 1989; Gilbert, 1992), 4. Late Paleozoic tectonism associated with the development of Amarillo-Wichita uplift. The Granite Wash deposition started to take place in the fourth stage with the change in the stress regime from extensional to compressional because of the collision of North America with Gondwana. The deepest part of the basin, lying on a basement of faulted Cambrian igneous units, became an upthrust block in this new compressive environment leading to an increase in the subsidence rate of the Anadarko Basin (Gilbert, 1992). With the continued episodic uplift during Early Pennsylvanian through Lower Permian, the Amarillo-Wichita Mountains formed (Sahl, 1980; Lyday, 1985; Johnson, 1989; Perry, 1989; Mitchell, 2011). Appendix A-1 shows the Middle Pennsylvanian paleogeographic map including the locations of the Amarillo-Wichita Uplift, Anadarko Basin, and the study area (Blakey, 2013).

Sediments eroded from the Amarillo-Wichita uplift were deposited into the Anadarko Basin mainly as alluvial fans, fan deltas, debris flows, and turbidite flows between Pennsylvanian Morrowan and Permian Wolfcampian times forming the Granite Wash (Gelphman, 1960; Dutton, 1979; Dutton, 1984; Lyday, 1985; Perry, 1989; Henry and Hester, 1995; Mitchell 2011). Deposition of the Granite Wash in the Anadarko Basin took place in the reverse order of the age of rocks of the Amarillo-Wichita Mountains. During the Pennsylvanian, Precambrian basement rocks were eroded and deposited as arkosic sandstones and conglomerates above the Cambrian to Mississippian rocks that had been previously eroded and deposited (Lyday, 1985; Henry

and Hester, 1995; Mitchell, 2011). High variability of lithofacies and petrophysical properties within short distances in the Granite Wash sediments are attributed to variability of the geological properties of the source rocks, transportation distance, and the amount of local accommodation space in the basin area (Mitchell, 2011). The units become finer-grained and interbedded with shale basinward (Gelphman, 1961; Sneider et al., 1977; Mitchell, 2011; Holmes, 2015). Also, depositional environment and effective transportation mechanism change according to proximity to the Amarillo-Wichita uplift. Because the Granite Wash pinches out to the north and grades into other units that are sourced from the north, it has a complex stratigraphy. Moreover, because the Granite Wash deposition occurred in an extensive area including both Texas and Oklahoma, the nomenclature of the units differs from place to place.

This study focuses on the Desmoinesian Marmaton Group Granite Wash deposits and uses the stratigraphic terminology of Mitchell (2011) for the southern Anadarko Basin (Figure 4). Five zones were defined within the Marmaton Group Granite Wash in the Elk City Field based on the extensive shales (Figures 5 and 6). Top Marmaton Wash, Marmaton A Wash, and Marmaton B Wash are not separated for this study and these zones are combined as Marmaton A-B Wash.

## **Lithologies and Lithofacies**

Marmaton Group lithologies and lithofacies were examined and interpreted based on detailed core descriptions of two cores from the GHK 1-34 Finnell and GHK 1-27 Niece wells (Figure 2). Descriptions include lithology, color, grain size, sorting, rounding, sedimentary structures, and additional remarks. Detailed core descriptions are

ERA	SYSTEM	SERIES	GROUP	UNIT
PALEOZOIC	PENNSYLVANIAN	VIRGILIAN	Shawnee/Cisco	* Shawnee Wash Heebner Shale
			Douglas/Cisco	Haskell Shale * Tonkawa Shale
		MISSOURIAN	Lansing/Hoxbar	* Cottage Grove Wash
			KansasCity/Hoxbar	* Hoxbar Wash/Shale * Hogshooter Wash * Checkerboard Wash * Cleveland Wash
		DESMOINESIAN	Marmaton	<b>Top Marmaton Wash</b>
				<b>Marmaton "A" Wash</b>
				* <b>Marmaton "B" Wash</b>
				* <b>Marmaton "C" Wash</b>
				* <b>Marmaton "D" Wash</b>
				* <b>Marmaton "E" Wash</b>
			* <b>Marmaton "F" Wash</b>	
		Cherokee	* Upper Skinner Shale * Upper Skinner Wash * Lower Skinner Shale * Lower Skinner Wash * Red Fork Ss. and Sh.	
ATOKAN	Atoka	* Atoka Wash 13 Finger Ls.		
MORROWAN	Morrow	* Upper Morrow * Lower Morrow		

Figure 4. Stratigraphic column for the Granite Wash Area of the Anadarko Basin. Nomenclature of the units differs from place to place. Marmaton Wash units can be divided 7 different sub-units in some areas. In this study Top Marmaton Wash, Marmaton A Wash, and Marmaton B Wash units are considered together. Producing intervals are shown by well symbol (modified from Mitchell, 2011).

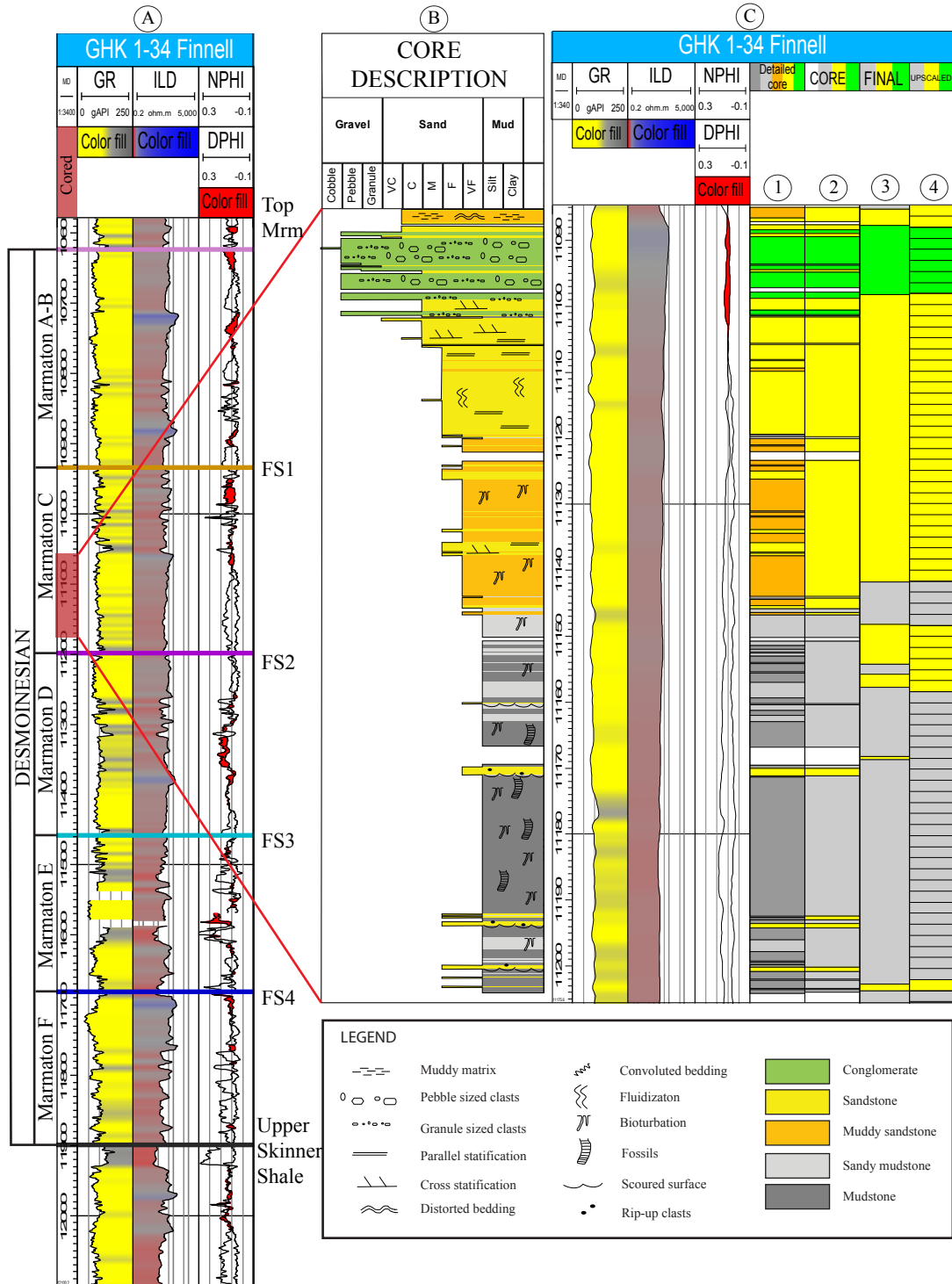


Figure 5. A) Gamma-ray (GR), deep-resistivity (ILD), neutron porosity (NPHI), and density porosity (DPHI) well-log responses for the cored well GHK 1-34 Finnell. Five zones are separated by flooding surfaces (FS). Red bar indicates the cored interval. Color fill in neutron and density porosity logs shows the gas-effect (DPHI>NPHI). Mrm:Marmaton. B) Schematic core description from well GHK 1-34 Finnell. The cored interval has a coarsening-upward cycle from mudstones at the bottom to the sandstones and conglomerates at the top. C) Gamma-ray (GR), deep-resistivity (ILD), neutron porosity (NPHI), and density porosity (DPHI) well-log responses for the cored interval. Conglomerates have cross-over of porosity logs with slightly higher gamma-ray and resistivity values than sandstones. Sandstones have cross-over or slight separation of porosity logs. Mudstones have higher gamma-ray values with high separation between neutron porosity and density porosity. 1) Lithologies observed in the core. 2) Lithology log used in upscaling and modeling. Muddy sandstones and sandy mudstones are merged with sandstone and mudstone, respectively (See Figures 10, 11). 3) Estimated lithology log by combining Artificial Neural Network (ANN) analysis, gamma-ray cut-off values, and relationship between density porosity, neutron porosity, and lithology. 4) Upscaled lithology logs used to constrain 3-D lithology models. 1.5 ft (0.5 m) of average proportional layering was used in upscaling. Measured depth (MD) is in ft.

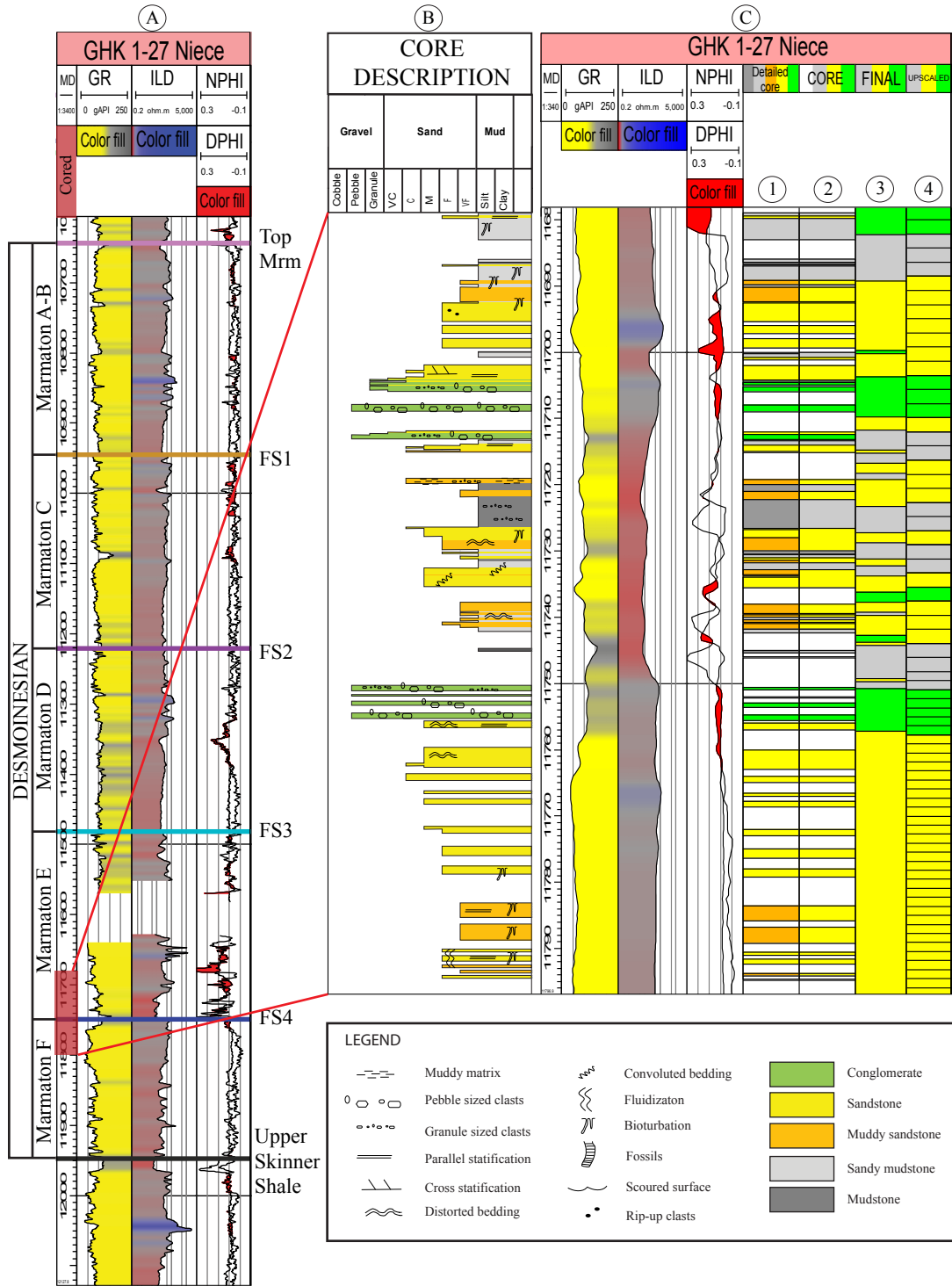




Figure 6. A) Gamma-ray (GR), deep-resistivity (ILD), neutron porosity (NPHI), and density porosity (DPHI) well-log responses for the cored well GHK 1-27 Niece. Five zones are separated by flooding surfaces (FS). Red bar indicates the cored interval. Color fill in neutron and density porosity logs shows the gas-effect (DPHI>NPHI). Mrm:Marmaton. B) Schematic core description from well GHK 1-27 Niece. The cored interval has two coarsening-upward cycles, followed by a fining-upward cycle at the top. C) Gamma-ray (GR), deep-resistivity (ILD), neutron porosity (NPHI), and density porosity (DPHI) well-log responses for the cored interval. Conglomerates have higher gamma-ray values than sandstones and they show cross-over of porosity logs most of the time. Sandstones have low gamma-ray values with cross-over or slight separation of porosity logs. Mudstones have high gamma-ray values and large separation of porosity logs. 1) Lithologies observed in the core. 2) Lithology log used in upscaling and modeling. Muddy sandstones and sandy mudstones are merged with sandstone and mudstone, respectively (See Figures 10, 11). 3) Estimated lithology log by combining Artificial Neural Network (ANN) analysis, gamma-ray cut-off values, and relationship between density porosity, neutron porosity, and lithology. 4) Upscaled lithology logs used to constrain 3-D lithology models. 1.5 ft (0.5 m) of average proportional layering was used in upscaling. Measured depth (MD) is in ft.

provided in Appendix B. Both cored wells are located in Washita County and are 4,115 ft (1,254 m) apart. GHK 1-34 Finnell is an almost completely continuous core through 120 ft (37 m) and corresponds to Marmaton C Wash interval (Figure 5). GHK 1-27 Niece core has a 119-ft (36-m) cored interval of which only 60% is preserved. The cored section corresponds to Marmaton E and Marmaton F Wash intervals (Figure 6). Based on the detailed core descriptions, 5 lithologies and 15 lithofacies were recognized (Table 1; Figures 7 and 8). The lithologies are conglomerate, sandstone, muddy sandstone, sandy mudstone, and mudstone.

### **Conglomerates**

Conglomerates consist of pebble-to-granule-sized, poorly sorted, rounded to sub-angular clasts and granitic rock fragments. They are present in both cores and are classified into two types based on texture; orthoconglomerates (clast supported) and paraconglomerates (matrix supported). The orthoconglomerates are interpreted to have been transported as the bedload material of current flow during high flow rate while the paraconglomerates is likely associated with the debris-flow transport considering the poorer sorting and abundant matrix. Photomicrographs of the conglomerate show they are composed of quartz, feldspars, biotite, glauconite, chert, and granitic rock fragments and are poorly sorted (Appendix C-1 A-D). The grains are mostly rounded to sub-angular. Porosity is relatively higher compared to the sandstone samples. In addition to the very low intergranular porosity, secondary porosity associated with dissolution of feldspars and chert clasts is commonly observed. Quartz overgrowths and carbonate cements are common.

Table 1. Marmaton group lithofacies with description, interpreted depositional processes, and percent distribution in cores.

Lithology	Lithofacies	Description	Depositional Process	%
Conglomerate	Orthoconglomerate (C1)	Pebble-to granule-sized, poorly sorted, rounded to sub-angular clasts mostly granitic with different colors. Clast supported	Bedload; high flow rate (channeled)	3.6
	Paraconglomerate (C2)	Pebble-sized, poorly sorted, rounded to sub-angular granitic clasts floating in fine to medium grained sandstone matrix	Debris flow (unchanneled)	4.8
Sandstone	Parallel-stratified (S1)	Grey to beige, fine-to medium-grained, well sorted, well-rounded	Upper flat-bed regime, unidirectional traction flow	4.6
	Cross-stratified (S2)	Grey to beige, fine-to coarse-grained, well to moderately sorted, low angle cross-bedded	Lower flow regime, unidirectional traction flow	4.5
	Structureless (S3)	Grey, medium-to very coarse-grained, well sorted, well-rounded	Rapid deposition from suspension; soft sediment deformation	10.4
	Granule-pebble-bearing (S4)	Grey, medium to coarse grained, well sorted, rounded to sub-rounded sand with well-oriented granule sized clasts	Sandy part: upper flat-bed regime; granular part: higher energy conditions	0.4
	Bioturbated (S5)	Light to dark grey, fine-to medium-grained, well sorted.	Lower energy conditions	11.0
Muddy Sandstone	Bioturbated (MS1)	Intercalated fine-to very fine-grained sandstone/siltstone and mudstone layers distorted with bioturbation	Mud: settling from suspension during low energy conditions; sand: higher energy conditions.	18.4
	Slumped (MS2)	Medium-to coarse-grained, moderately to poorly sorted, sub-rounded to sub-angular sandstone and black mudstone with deformed structure	Slump; soft sediment deformation	3.5
Sandy Mudstone	Bioturbated (SM1)	Intercalated very fine-grained sandstone and mudstone layers distorted with bioturbation	Mud: settling from suspension during low energy conditions; sand: higher energy conditions.	12.8
	Slumped (SM2)	Dark grey to black mudstones intercalated with grey to beige sandstones. Poorly sorted, chaotic structure	Slump; soft sediment deformation	0.8
Mudstone	Bioturbated (M1)	Dark grey, carbonate rich mudstone with various degree of bioturbation	Very low energy conditions; suspension sedimentation	12.3
	Fossiliferous (M2)	Dark grey, carbonate rich mudstone with abundant fossils, mostly crinoid and bivalves	Very low energy conditions; suspension sedimentation	7.5
	Pebbly (M3)	Light grey, pebble sized, sub-angular to sub-rounded clasts floating in black mudstone matrix	Debris flow	2.7
	Massive (MS4)	Black, massive mudstone with abundant fractures	Very low energy conditions; suspension sedimentation	2.7

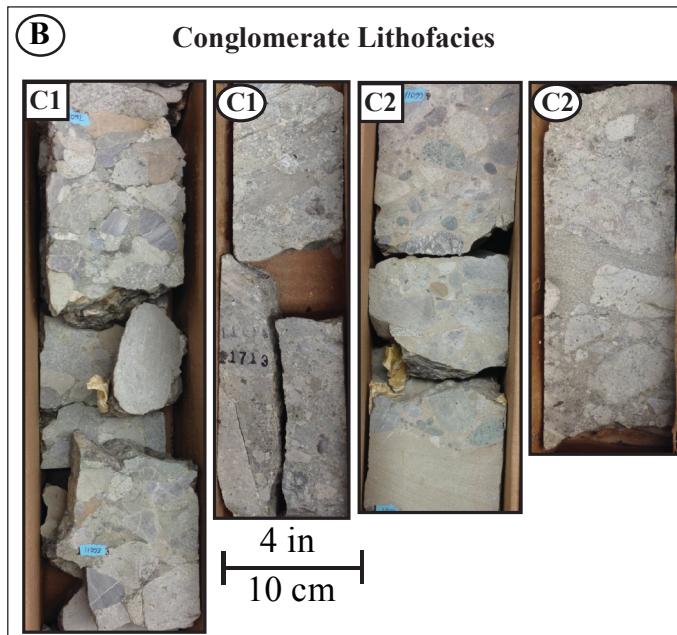
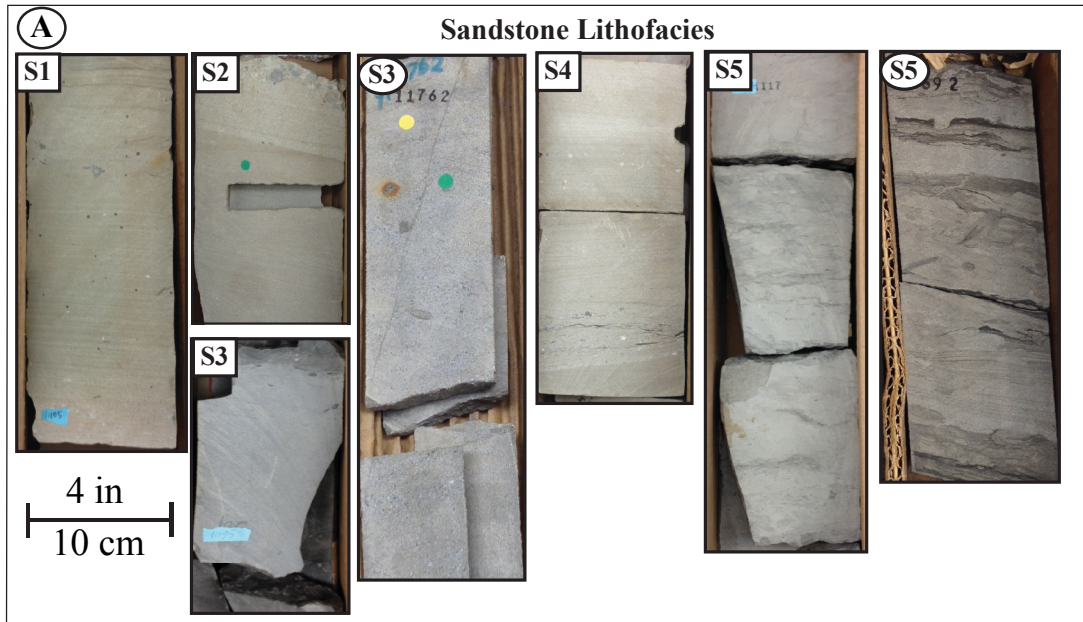


Figure 7. A) Sandstone, B) conglomerate, and C) muddy sandstone lithofacies. Circle: Core from GHK 1-27 Niece; Rectangle: Core from GHK 1-34 Finnell. S1) Parallel-stratified sandstone, measured depth (md) = 11104 ft; S2) Cross-stratified sandstone, md = 11100.5 ft; S3) Structureless sandstone, md = 11195 ft, md = 11762 ft; S4) Granule-pebble-bearing sandstone, md = 11105.5 ft; S5) Bioturbated sandstone, md = 11117 ft, md = 11692 ft; C1) Orthoconglomerate, md = 11092 ft, md = 11712.5 ft; C2) Paraconglomerate, md = 11099 ft, md = 11708 ft; MS1) Bioturbated muddy sandstone, md = 11136 ft, md = 11787 ft; MS2) Slumped muddy sandstone, md = 11086 ft, md = 11719 ft.

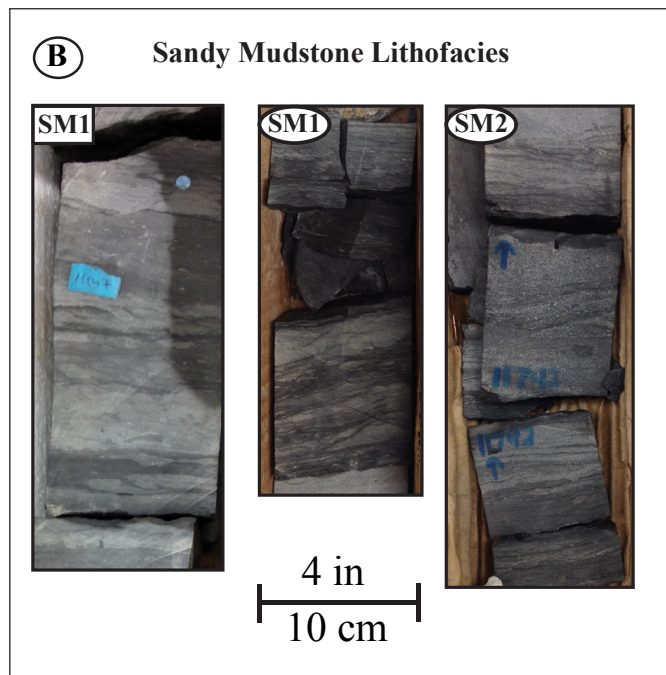
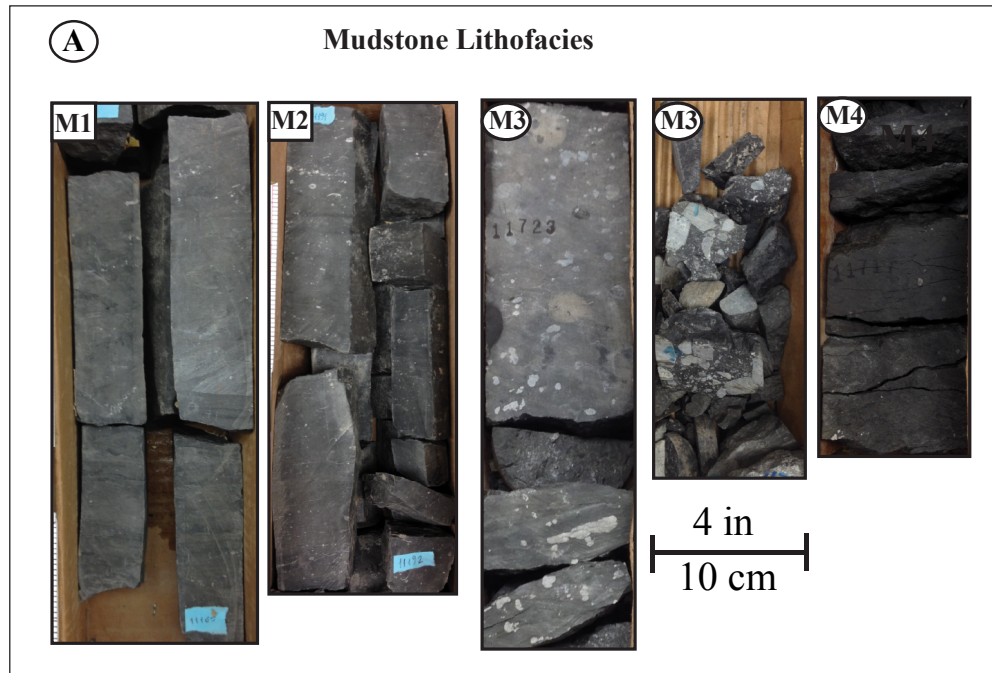


Figure 8. A) Mudstone and B) sandy mudstone lithofacies. Circle: Core from Niece 1-27; Rectangle: Core from Finnell 1-34. M1) Bioturbated mudstone, measured depth (md) = 11164 ft; M2) Fossiliferous mudstone, md = 11191 ft; M3) Pebbly mudstone, md = 11723 ft, md = 11745 ft; M4) Massive mudstone, md = 11717 ft; SM1) Bioturbated sandy mudstone, md = 11147 ft, md = 11713.5 ft; SM2) Slumped sandy mudstone, md = 11742 ft.

## **Sandstones**

Sandstone lithofacies exhibit parallel stratification, cross stratification and bioturbation, and occasionally have granule-to-pebble-sized clasts or are structureless. Parallel- and cross-stratified sandstones are variable in grain size from fine to coarse, transitional with conglomerates, and are interpreted to have been deposited under upper and lower flow regimes, respectively. Medium to fine-grained bioturbated sandstones appear to have previously been structureless sandstones. Burrows in these sandstones are interpreted as *Glossifungites* considering their shape and orientation. This lithofacies is interpreted to have been deposited under lower energy conditions than stratified sandstones. Granule-pebble-bearing sandstone consists of medium to very-coarse sandstones, and sub-rounded to rounded granule-to-pebble-sized grains floating in them and horizontally oriented. It is interpreted that the sandy part of the lithofacies has been deposited under upper flat-bed regime and, with the increase in the energy, the flow is thought to have carried coarser-grained material. Structureless sandstone is present in both cores, and is very fine- to very coarse-grained, but mostly medium-grained. In the GHK 1-34 Finnell well, this lithofacies is present above scour surfaces overlying fossiliferous to bioturbated mudstones and embody small mudstone clasts indicating its erosional effects. In the GHK 1-27 Niece well, it constitutes a higher proportion of the cored section. Photomicrographs illustrate that medium-grained parallel-stratified sandstone and fine-grained slightly bioturbated sandstone have similar characteristics in terms of mineralogy. They are composed of well-sorted, angular to sub-angular grains, mostly quartz, feldspar, glauconite, hematite, and granitic rock fragments (Appendix C-1 E, F). Some of the quartz minerals have fluid inclusions. Primary intergranular

porosity is very low in sandstones. Silica and carbonate cements are common. Most of the porosity is secondary by the dissolution of feldspars. Some part of the porosity is occluded by clay minerals and hematite. Medium-grained sandstone has higher porosity than finer grained sandstone.

### **Muddy Sandstones and Sandy Mudstones**

Muddy sandstone and sandy mudstone differentiation is based on the dominant lithology in the whole rock mass. They are observed to be bioturbated or slump deposits. Moderately to poorly sorted muddy sandstones and sandy mudstones that lack structures or with parallel but distorted bedding are grouped under slumped muddy sandstone and slumped sandy mudstone, respectively. These lithofacies are composed of medium-to-coarse-grained, moderately to poorly sorted, sub-rounded to sub-angular sandstone interbedded with mudstone. They occasionally have soft sediment deformation. Slumping can be the transportation mechanism leading to the deformation and distorted wavy-like bedform. Occasionally, they contain white to grey, sub-angular to sub-rounded, granule-to-pebble-sized clasts which reduce sorting. Poorer sorting and lack of bedding can be indicative of debris flow (Reineck and Singh, 1975).

Bioturbated muddy sandstone and sandy mudstone lithofacies consist of very fine-to-fine-grained, well sorted, well rounded sandstone and mudstone alternation. Parallel or low-angle cross-stratification is disturbed due to wide range of bioturbation intensity. Occasionally, the primary bedding structure can be seen as the degree of bioturbation decreases. Rarely, bioturbated mudstone lithofacies include some brachiopod shells. In the GHK 1-34 Finnell core, bioturbated muddy sandstones overly bioturbated sandy mudstones which overly bioturbated to fossiliferous mudstones. Thin

section sample from bioturbated sandy mudstone lithofacies is composed of angular to sub-angular quartz, feldspar, and glauconite minerals with abundant clay minerals (Appendix C-2 A, B).

### **Mudstones**

Mudstone lithofacies are commonly bioturbated, fossiliferous, pebbly, or massive. Bioturbated mudstones and fossiliferous mudstones are observed only in the GHK 1-34 Finnell core. They react to hydrochloric (HCl) acid, suggesting that they have carbonate content. Thin section analysis shows that some of the mud-sized grains are carbonate and there are some bioclasts including *Brachiopod* and *Bryozoa* (Appendix C-2 C, D). Burrows in the bioturbated mudstone are likely *Cruziana* ichnofacies given their elongation and preservation along the bedding planes. These two lithofacies are interpreted to have been deposited under very low energy conditions where the sediment influx is low. Bioclast can be observed in core scale, and their content increases with the increasing measured depth. Pebbly mudstone lithofacies were observed only in the GHK 1-27 Niece core. Some of them overly paraconglomerates while others are transitional with slumped sandy mudstones. Black, massive mudstone lithofacies rich in fractures is one of the least abundant lithofacies and is only observed in the GHK 1-27 Niece core.

Based on core-plug porosity from the GHK 1-34 Finnell, well medium-to coarse-grained sandstones (7%) have higher porosity than fine-grained bioturbated sandstones (6%). Although the conglomerate sample has lower porosity (4%) than sandstone samples, because the conglomerates vary in grain size, texture, mineralogy,



and porosity properties from place to place within the rock it is difficult to generalize this result for the whole Marmaton Group.

## **Lithology Estimation**

In order to assess the characteristics of the Marmaton Group in the Elk City Field and to map the lithology variations and petrophysical properties, it is useful to estimate lithologies even in non-cored wells. This study uses a combination of an Artificial Neural Network (ANN), well-log cut-off values, and porosity-to-lithology relations to classify lithology in non-cored wells.

### **Lateral Variability in Mineralogy and Log Response**

Lithology estimation based on only a gamma-ray cut-off in formations with radioactive elements can be misleading and cause the underestimation of pay and reserves. Potassium and thorium values from spectral gamma-ray data for the cored interval in the GHK 1-34 Finnell core show that most of the data are associated with feldspar and glauconite in the cross plot chart for mineral identification (Appendix D-1). Data points within the illite, mixed layer clay, and montmorillonite regions correspond to mudstones.

Well-log responses change considerably from northwest to southeast across the study area (Figure 9). To the northwest, well logs exhibit higher gamma-ray (GR) and higher deep-resistivity (ILD) values with common cross-over (DPHI>NPHI) of density-porosity (DPHI) and neutron-porosity (NPHI) logs. To the southeast, the gamma-ray and deep-resistivity values are relatively lower with less cross-over (DPHI>NPHI) and more separation (NPHI>DPHI) of porosity logs (Figure 9).

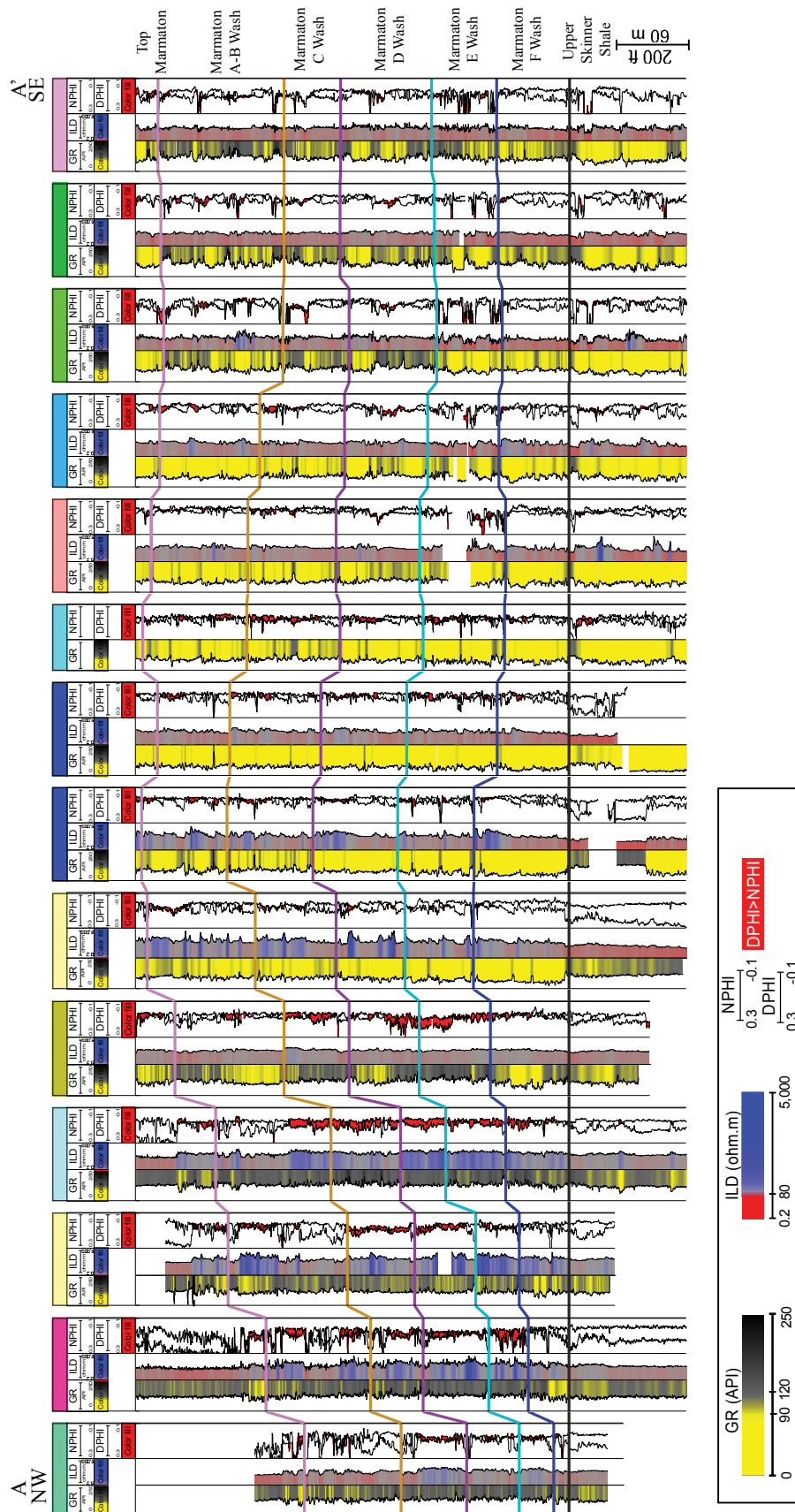


Figure 9. Stratigraphic well-log cross section extending from northwest to southeast and showing stratigraphic zones for the Marmaton Group. GR: Gamma-ray; ILD: Deep-resistivity; NPHI: Neutron-porosity; DPHI: Density-porosity. Upper Skinner Shale (base Marmaton). Refer to Figure 2 for the location of the cross section. The wells are flattened on the Upper Skinner Shale and are equally spaced. Wells on the west have much higher gamma-ray values, higher resistivity, and more cross-over of density and neutron porosities. The regional difference in well-logs responses is probably a result of source-rock mineralogy. More than four flooding surfaces can be defined toward the east side.

Gamma-ray values of sandstones and conglomerates for the cored interval of the Valero 1-36 Brauchi well on the northwest side of the study area are greater than 125 API. According to the Middle Pennsylvanian paleogeographic maps prepared by Ham et al. (1964), the rocks in the source area located on the southwest side of the study area are granitic while they are more gabbroic toward the southeast side of the source area (Appendix A-2). The erosion of mostly the granitic rocks with higher amounts of potassium feldspar is likely responsible for the higher gamma-ray values on the northwest side of the study area while on the southeast side erosion of both granitic and gabbroic rocks likely resulted in relatively lower gamma-ray values. Also, the higher iron and magnesium content in gabbroic rocks can be responsible for the relatively lower resistivity values on the southeast side (Figure 9). X-ray diffraction (XRD) analyses of 10 samples from two different wells (Valero 1-36 Brauchi and Valero 1-27 Hartman) that are located on the northwest of the field show that these samples contain potassium feldspar ranging between 3-13% with an average of 7.5% (Figure 2). Also, potassium (K) – thorium (Th) cross plots for two wells; Chesapeake 1-35 Clenice, from the northwest, and Burlington 1-20 Thomas, from the southeast side of the study area show a greater amount of potassium on the northwest side (Appendix D-2). These data support the idea that the change in the general gamma-ray response in the wells from northwest to southeast is related with the source-area mineralogy, especially related to potassium feldspar content. Because the difference in well-log responses are thought to be the result of the mineralogy but not related with the tool calibration well logs were not normalized. Because of the obvious difference in gamma-ray log responses on the northwest and southeast sides of the study area, lithology estimation was conducted

separately for these regions to correspond with the change in log response. Lithology estimation in this study was done by combining supervised Artificial Neural Network (ANN) analysis, gamma-ray cut-off values, and general rules relating porosity logs and lithology.

### **Artificial Neural Network Approach**

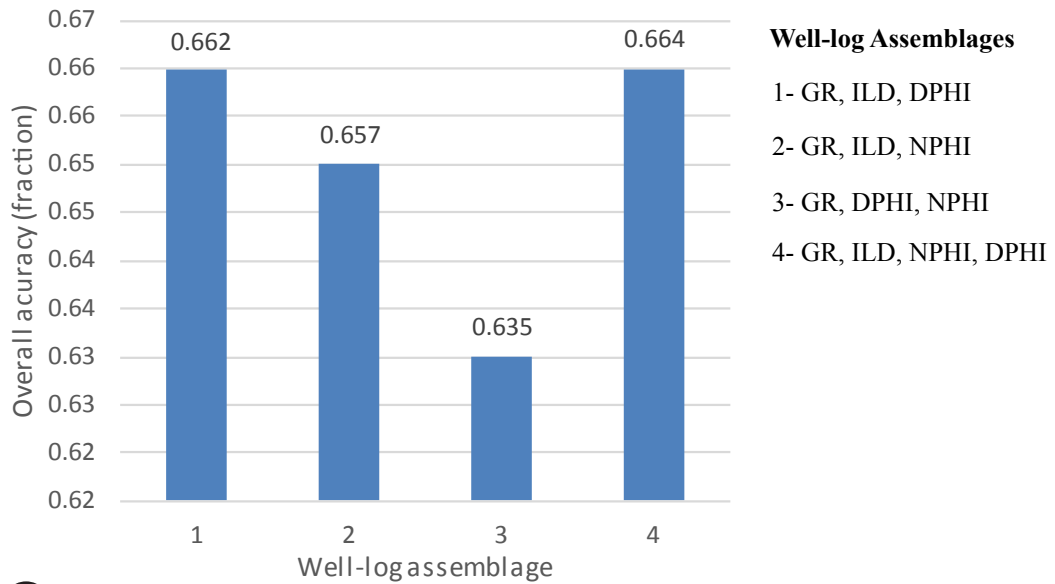
An Artificial Neural Network (ANN) is a mathematical algorithm that was inspired by the human brain in terms of its ability to learn by example (Iloghalu and Aziwike, 2003; Anggraini and Puspa, 2008; Kumar and Kishore, 2006). In geology, this technique can be used to predict the lithofacies, lithologies, or architectural elements by using the well logs. Unsupervised neural network analysis enables only the classification of the well-log patterns. With supervised neural network analysis, well-log responses are trained with the corresponding lithology, lithofacies, or architectural elements described in core so that the network learns the relation between the well-log signatures and the corresponding rock groups. Being trained by the interpreted core observations, the network is forced to yield a particular output (Kumar and Kishore, 2006). A desired portion of the core and log data are used to train the network, and the remaining core and log data are used in testing the result of the neural network (cross validation).

The structure of ANN consists of one input layer, one output layer and one or more hidden layers (Appendix E-1). Each layer contains a number of nodes which are connected to the other nodes in the next layer by simple weighted links. Except for nodes in the input layer, each node multiplies its specific input value by corresponding weight and then sums all the weighted inputs. The weighted numbers are selected

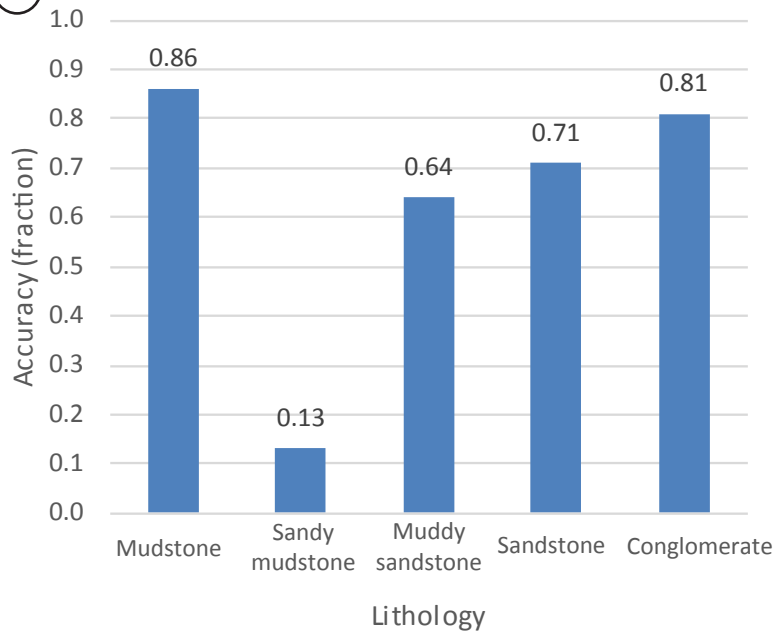
randomly at the beginning and changed iteratively so that the next iteration will produce a closer result to the real output, minimizing the difference between the estimated and known values (backpropagation) (Kumar and Kishore, 2006; Anggraini and Puspa, 2008). This iterative process continues until the desired number of iterations or the tolerated amount of error is reached. Ideally, for realistic results, the well-log signatures for the cored interval should be representative of the entire area for which the lithologies are predicted.

Throughout the cored intervals, well-log signatures do not change in a recognizable way according to the lithofacies of the same lithologies, because the classification of lithofacies is based on properties such as sedimentary structures, texture, and fossil content that may not have different effects on well logs. Also, the lithofacies are transitional with each other and sometimes they are so thin to be captured by the well logs. Therefore, the focus is on lithology estimation. The first aim to estimate lithologies was to apply two different neural-network analyses by separately using the cores located on the northwest and southeast sides of the study area. However, the Valero 1-36 Brauchi core located on the west side is only 20 ft (6 m) in thickness and does not have a representative mudstone interval to train the neural network (Figure 2). Therefore, the GHK 1-34 Finnell and the GHK 1-27 Niece cores were used as desired (target) output to train the neural network. Fifty percent of the cored intervals (95 ft; 29 m) was used in training the neural network while the other 50% was used in cross validation. As input to the neural network, different combinations of gamma-ray, deep-resistivity, neutron-porosity, and density-porosity logs were tested (Figure 10A). Using all of them together gave the best results with an overall accuracy of 66%. A

(A)



(B)



(C)

Actual Lithologies	Predicted lithologies					Total
	Mudstone	Sandy mudstone	Muddy sandstone	Sandstone	Conglomerate	
Mudstone	192	24	1	6	0	223
Sandy mudstone	44	16	53	8	0	121
Muddy sandstone	20	0	125	50	0	195
Sandstone	30	7	28	196	15	276
Conglomerate	3	1	0	10	60	74

Figure 10. A) Histogram showing the overall accuracy of Artificial Neural Network result in the estimation of 5 lithologies within the cored interval for different combinations of well logs (GR: Gamma-ray; ILD: Deep-resistivity; DPHI: Density-porosity; NPHI: Neutron-porosity). Result by using all the available logs has the highest overall accuracy (0.664). B) Histogram showing the accuracy for five lithologies estimated by the Artificial Neural Network using GR, ILD, DPHI, and NPHI. Accuracies are calculated by dividing the number of correctly estimated lithology by the total number of lithology in confusion matrix (See Figure 11 for the merged lithology estimations). C) Confusion matrix associated with the Artificial Neural Network for which all the available well logs (GR, ILD, NPHI and DPHI) are used as inputs. Blue highlighted cells represent the number of correctly predicted lithologies in the cored interval. All the other cells represent mis-predicted lithologies. The number of correctly estimated sandy mudstone is quite low. The numbers of sandy mudstones mis-predicted as mudstones, and mudstones mis-predicted as sandy mudstones (grey highlighted cells) are greater than the correctly predicted sandy mudstones, indicating that if mudstones and sandy mudstones are merged better estimation can be obtained. Similarly, the number of muddy sandstones mis-predicted as sandstones (and vice versa) is high (orange highlighted cells). By merging the muddy sandstones and sandstones high degree of confusion can be avoided.

confusion matrix that shows the numbers of the estimated lithologies for each trained lithology was established and the accuracy for the prediction of each lithology was calculated (Figure 10B-C). Because of the low number of correctly estimated sandy mudstones (13%), high number of sandy mudstones mis-predicted as mudstones (36%), and considerable amount of mudstones mis-predicted as sandy mudstones (11%), these two lithofacies were combined to obtain higher overall accuracy. Sandy mudstones were grouped with sandstones due to significant amount of muddy sandstones mis-predicted as sandstones (26%). In the estimation of 3 lithologies, different combinations of wells logs were tested as done for 5 lithologies to determine the well-log assemblage that provides the highest accuracy (Figure 11A). Again, using all the available well logs provides the highest overall accuracy in the estimation (83%). Accuracy of the estimation for each lithology was also calculated (Figure 11B). As a result of the application of the neural network to the non-cored intervals the lithologies cluster separately in the well-log cross plots that suggests the neural network and the available logs can be used in the classification of these lithologies (Appendix E-2). Generally, mudstones cluster where neutron-porosity and gamma-ray values are high and resistivity values are low. Conglomerates in general, have higher gamma ray, resistivity, and density porosity than sandstones. However, mudstones assigned for very low gamma-ray values, and reservoirs assigned for very high gamma-ray values cause confusion.

### **Additional Constraints**

In addition to the ANN, proper gamma-ray cut-off values and the relation between the neutron porosity, density porosity, and rock type were used to improve the



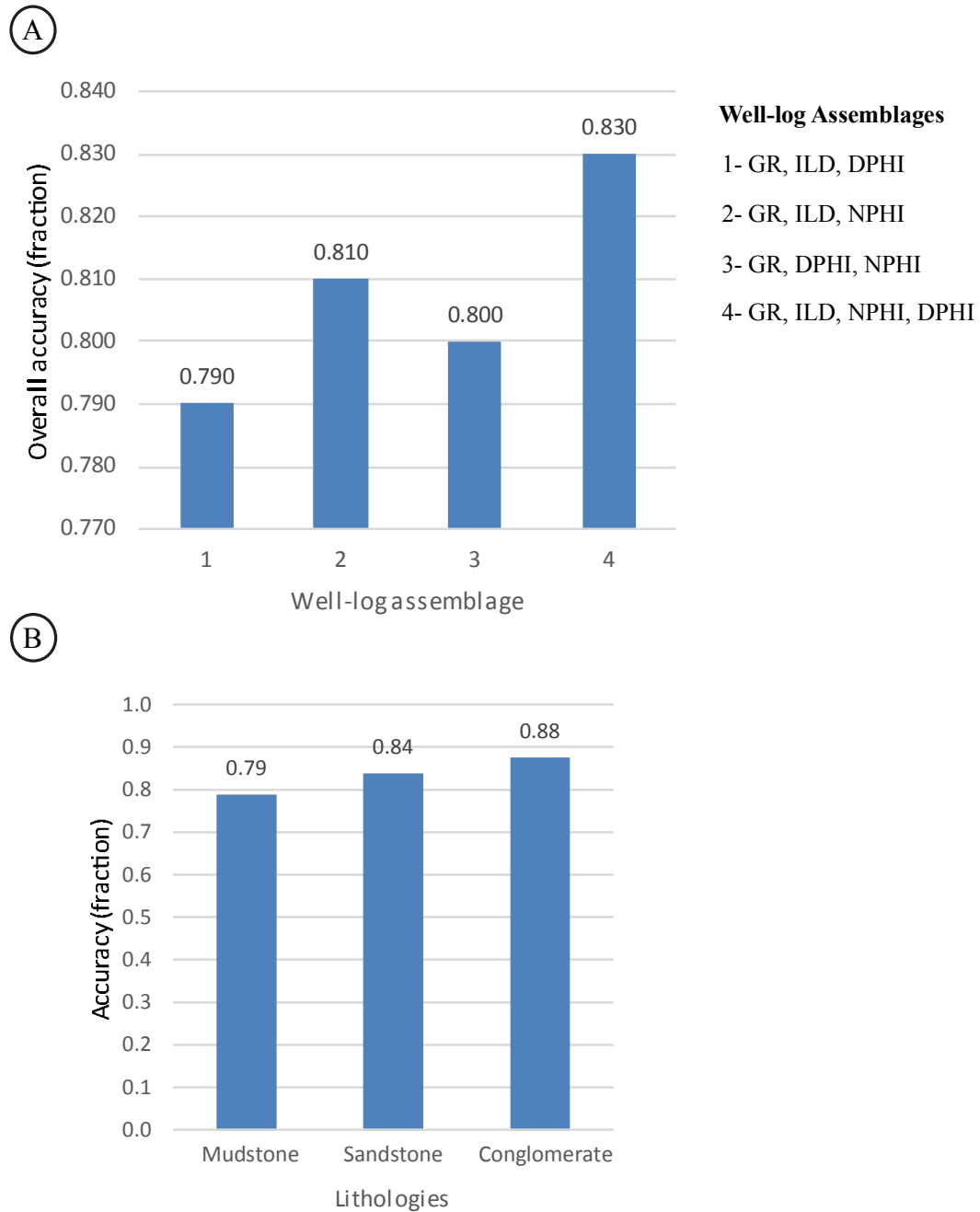


Figure 11. A) Histogram showing the overall accuracy of Artificial Neural Network result in the estimation of 3 lithologies within the cored interval for different combinations of well-logs (GR: Gamma-ray; ILD: Deep-resistivity; DPHI: Density-porosity; NPHI: Neutron-porosity). Result by using all the available logs has the highest overall accuracy (0.830). B) Histogram showing the accuracy for 3 lithologies estimated by the Artificial Neural Network using GR, ILD, DPHI, and NPHI. Accuracies are calculated by dividing the number of correctly estimated lithology by the total number of lithology. The accuracies for all lithologies are satisfactory.

results. Density-porosity logs in this study were calculated from the bulk density assuming a limestone matrix. Density- and neutron-porosity logs together can help in lithology estimations such that cross-over ( $DPHI > NPHI$ ) indicates either a gas-bearing zone or a sandstone whereas log separation ( $NPHI > DPHI$ ) accompanied with high gamma-ray values indicate shale zones. If the separation is accompanied by low gamma-ray values, it is a direct indicator of dolomitic zones (Asquith et al., 2004).

Although ANN analysis for the estimation of the lithologies gave promising results (83% of overall accuracy), application of it to the non-cored wells resulted in some unsatisfying results. For instance, occasionally the network assigned sandstone or conglomerate lithology for very high gamma-ray values with large separations between density and neutron porosities. Also, some intervals with cross-over were estimated as mudstone (Figure 12). Reservoirs in the western part of the Elk City Field usually have cross-over of the porosity logs (J. Mitchell, 2015, personal communication). In order to minimize the misinterpretations, intervals having gamma-ray greater than 105 API and 120 API for southeast and northwest sides, respectively, and having separation of porosity logs were classified as mudstone to modify the result of the ANN. Zones classified by the ANN as mudstone and having a cross-over of porosity logs were re-classified as conglomerate (Figure 12). Because the gamma-ray values of conglomerates are commonly greater than sandstones, the misinterpreted zones with high gamma-ray and cross-over were re-classified as conglomerate (Figures 5, 6). As a result, by constraining the result of the ANN, the lithology log estimates were improved (Figures 5, 6, 12, Appendix E-3).

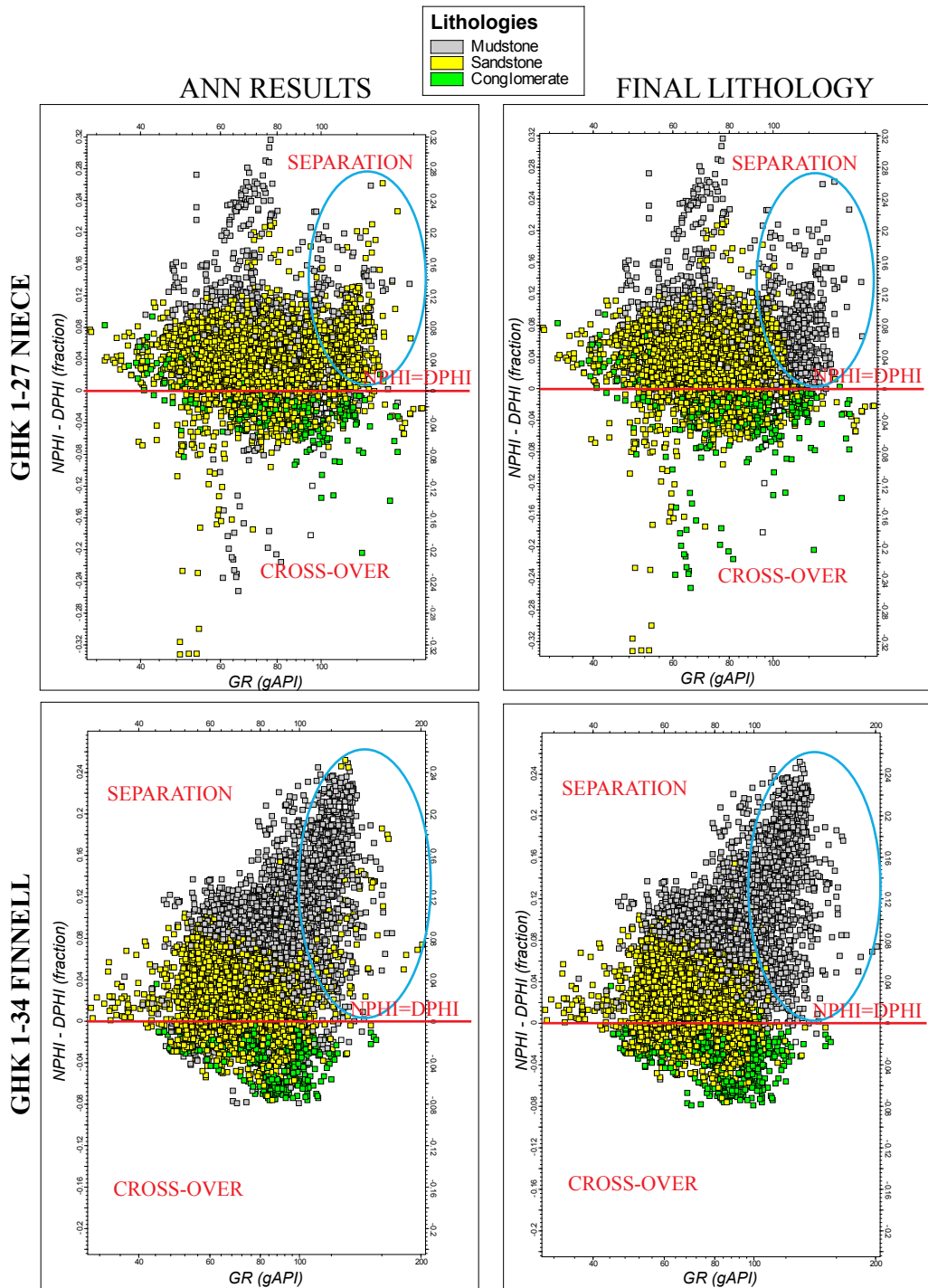


Figure 12. Cross plots of gamma-ray vs. the difference between neutron and density porosities before and after applying constraints to the Artificial Neural Network (ANN) results. Note that lithologies with high gamma-ray and separation in neutron and density porosity were assigned as mudstone in the final lithology (blue). Also, lithologies estimated as mudstone by ANN were changed to conglomerate whenever they have cross-over ( $DPHI > NPHI$ ) of porosity logs.

In order to understand the effect of using the neural network and the relation between the type of lithology and porosity in the estimation of the lithologies, the resulting lithology logs were compared with the lithology logs calculated by using only the gamma-ray cut-off values that are 105 API for the southeast side and 120 API for the northwest side of the study area (Appendix E-4). Pay intervals are seen to be underestimated in the lithology logs calculated by using only a gamma-ray cut-off. By using the Artificial Neural Network and the lithology-porosity relationship, the reservoirs that can be underestimated because of the presence of radioactive elements responsible for higher gamma-ray are correctly estimated.

### **Depositional Environment, Stratigraphy, and Structure**

The stratigraphic and structural framework of the Marmaton Group at Elk City Field was established by correlating 117 wells; each having at least one of the following well logs: gamma ray (GR), deep resistivity (ILD), density porosity (DPHI), and neutron porosity (NPHI). Cross sections were established to correlate top and base of the Marmaton Wash, and four extensive shales that are distinctive in well logs with higher gamma-ray, lower deep-resistivity, and large separation of porosity values. These shales are interpreted to cap flooding surfaces based on the regional well-log correlations across the Anadarko Basin and into Kansas (Mitchell, 2011; LoCroccio, 2014; J. Mitchell, 2015, personal communication). The base of the Marmaton Group corresponds to the top of the Upper Skinner Shale, which is top of the Cherokee Group (Figure 4). The Upper Skinner Shale overlies the Upper Skinner Wash, and it is quite distinctive throughout the study area with its relatively high and blocky gamma-ray, low

and blocky deep resistivity, and large separation between density- and neutron-porosity logs (Figures 9). The thickness of the Upper Skinner Shale on the west was observed to reach up to 800 ft (244 m) in thickness. Eastward this unit gradually thins below 25 ft (8 m) in thickness. The top of the Marmaton Group is overlain by the Cleveland Wash with very large separation in neutron- and density-porosity values. The Cleveland Wash becomes thinner to the east. The correlative shales on the west side of the study area are more prominent because of the difference in well-log responses between them and the zones they separate which have blocky gamma ray and deep resistivity (Figure 9). Toward the east, the shales used in correlation are less prominent because of additional shales in the interval. The additional shales on the east side of the field could be the result of its relatively more distal location.

Based on the lithologies in the cores, their vertical relation with each other, their sedimentary structures, the corresponding well-log responses, and the well-log correlation across the study area, the environment of deposition and the significance of the correlative shales in terms of the sequence-stratigraphic framework were interpreted. In the GHK 1-34 Finnell well, the 2<sup>nd</sup> flooding surface is interpreted to exist approximately 20 ft (6 m) below the bottom of the cored interval (Figure 5A). GHK 1-34 Finnell core (120 ft; 37 m) consists of a coarsening-upward succession of lithofacies extending from bioturbated to fossiliferous mudstones at the bottom to sandstones and conglomerates at the top (Figure 6). The basal mudstones transition into bioturbated sandy mudstones and muddy sandstones that are overlain by bioturbated, cross-stratified and parallel-stratified sandstones, from bottom to top. The conglomerates at the top of the cored interval is interpreted to be capped by another mudstone that can

possibly be interpreted as the base of another flooding surface, considering its well-log responses with higher gamma-ray, lower resistivity and large separation of porosity logs (Figure 5A). Being bounded by the flooding surfaces at the top and bottom, and having a shallowing-upward trend, this cored interval is interpreted to be part of a parasequence. GHK 1-27 Niece core (119 ft; 36 m) has two similar but shorter coarsening-upward intervals that can be defined as parasequences as well (Figure 6). In both parasequences bioturbated sandy mudstones and muddy sandstones are followed by structureless sandstones, poorly sorted conglomerates, and moderately to poorly sorted, deformed, chaotic sandstones and mudstones. There is 7 ft (2 m) of missing section between the two coarsening-upward parasequences. This section includes only remaining of small mudstone fragments, and is interpreted as the mudstones capped by the 4<sup>th</sup> flooding surface regarding the corresponding very high gamma-ray, large separation of neutron and density porosities in the logs, and its separating two coarsening-upward parasequences. In the upper section, structureless sandstones are overlain by bioturbated muddy sandstones and sandy mudstones. This package has the same type of lithofacies as those observed in the coarsening-upward cycles, but have the reverse order reflecting an upward-deepening succession (fining-upward). This suggests a small-scale sequence boundary somewhere above the conglomerates of the second upward-coarsening cycle (Figure 8).

In both cored wells, coarsening-upward cycles in the cores exhibit upward-increasing resistivity (Figures 5, 6). Because of the radioactive minerals, the gamma-ray does not show an upward-increasing trend. Conglomerates are observed to exhibit relatively higher gamma-ray values than sandstones and with cross-over of porosity

logs. Similar well-log responses to the packages in cored intervals can be observed in non-cored wells suggesting the same type of coarsening-upward sequences (Appendix E-3).

Based on the presence of well-developed coarsening-upward sequences in the cores, high bioturbation intensity, presence of *Cruziana* and *Glossifungites* type of burrows, and presence of glauconite, the environment of deposition is interpreted to be a shelf-type fan-delta setting (Brown; 1979; Ethridge and Wescott, 1984). The classification of the fan-delta depositional setting can be established by the differentiation of the proximal, medial, and distal components, and the differentiation of the sub-aerial, transitional, and sub-aqueous components of fan delta (Ethridge and Wescott, 1984) (Figure13). The proximal and medial fan-delta setting form the sub-aerial component, and the distal fan forms the transitional and sub-aqueous components of the fan delta. In general, the grain size decreases and the sorting increases from the proximal to distal fan delta. The recognition of more flooding surfaces on the southeast side of the field is likely the result of the more distal location of this region while the northwest side of the study area can be interpreted to be more proximal because of the presence of thinner and fewer number of mudstones separating the intervals with blocky gamma-ray and deep-resistivity log responses.

The conglomerate lithofacies are interpreted to be deposited in a proximal fan-delta area (Appendix F). The orthoconglomerates can be associated with the braided rivers in the proximal sub-aerial part of the fan delta while the paraconglomerates may be associated with the debris-flow deposits of the fan deltas that might develop in relatively arid conditions in the proximal sub-aerial fan areas (Ethridge and Wescott,

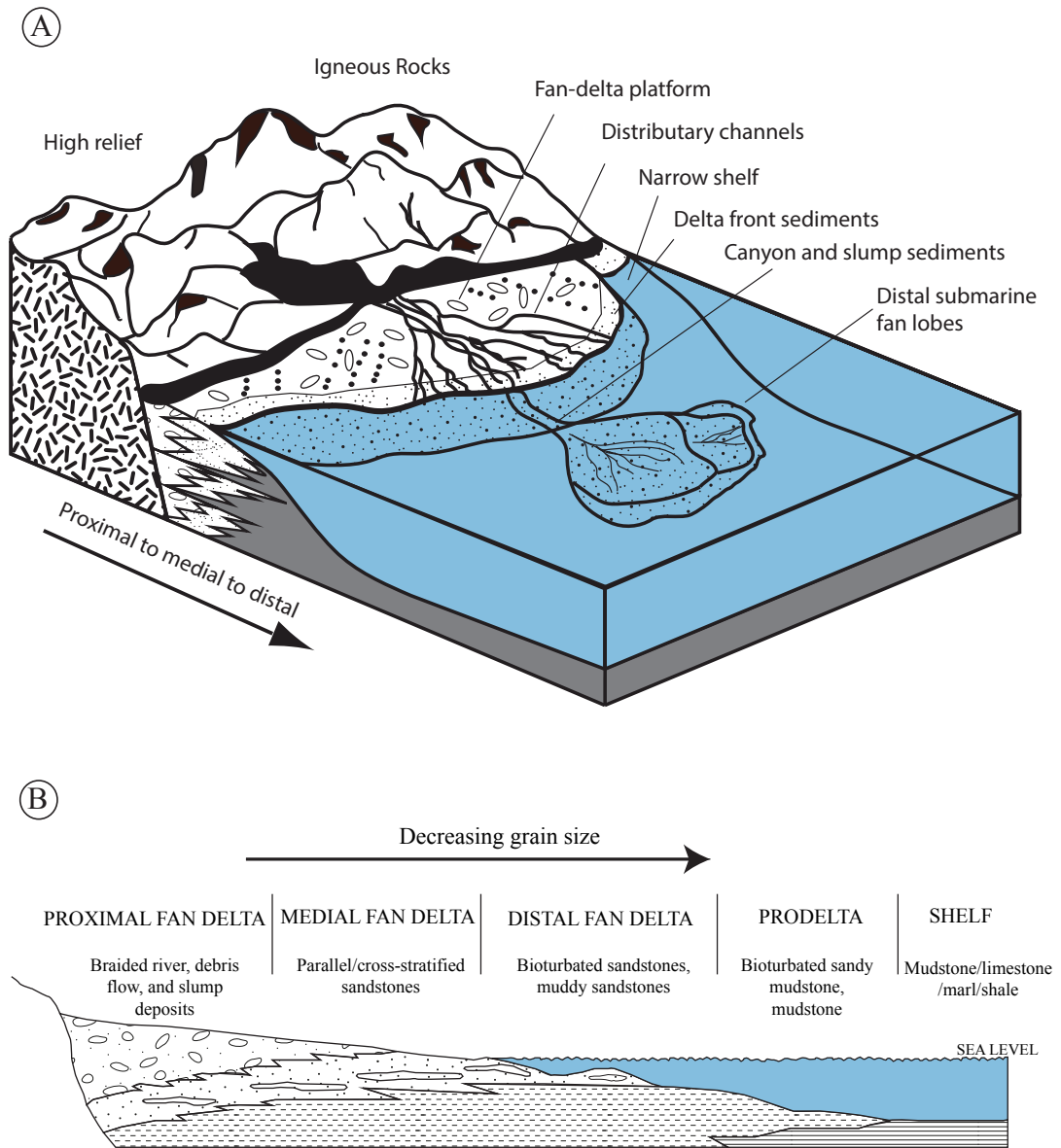


Figure 13. A) Schematic illustration of environment of deposition in deep Anadarko Basin Granite Wash area. Complex geology in the area can be attributed to variation in the source rock, distance of transportation, and accommodation space. Materials eroded from Amarillo-Wichita Mountains are deposited to the mountain front, mainly by fan-deltas. Fine - to coarse-grained submarine deposits transported by sediment gravity flows and slumps can be found in more distal areas (adapted from Bouma, 2000 and Bruner and Smosna, 2000). B) Cross sectional view for the shelf type fan-delta, its components, and typical lithologies. Fan-delta deposits becomes finer-grained from proximal to distal areas (modified from McGowen, 1970).



1984). Pebbly mudstones are interpreted also as proximal to medial fan deposits associated with debris flows considering the abundant mudstone matrix, poorly sorted texture, and their position in the core relative to paraconglomerates. Slumped muddy sandstone and sandy mudstone lithofacies are interpreted to be deposited at the proximal fan delta as a result of slumping and as debris flows. The immature nature of these lithofacies is attributed to a tectonically active environment and short transportation distance. Subaerial mid-fan areas are interpreted to be composed mostly of sandstone lithofacies. Parallel and cross-stratified sandstones, transitional with conglomerates, are interpreted to have been deposited in proximal to medial sub-aerial fan areas, relatively more distal than the conglomerates. Bioturbated sandstone is considered to have been deposited in medial to distal fan areas where there is lower energy. Structureless sandstone is presents together with both conglomerates and mudstones as interbedded and is thought to be associated with channels and deposited in a wide range of setting from medial fan area to prodelta. Bioturbated sandy mudstones and muddy sandstones can be explained as a transitional unit between sub-aerial and sub-aqueous units (Ethridge and Wescott, 1984). The amount of mudstone in these lithofacies may be a measure of relative distance from the shore and the water depth (Figure 5B). Bioturbated mudstones, fossiliferous mudstones, and massive mudstones are interpreted to have been deposited under very low energy conditions on the continental shelf (distal fan to prodelta) where sediment influx is low.

Structure-contour maps of each flooding surface and the top and base Marmaton surfaces show that a northwest to southeast elongated anticline is the dominant structure. Two major faults cut the structure (Appendix G-1). On the north flank of the

anticline there is more than 1,600 ft (488 m) of offset while the offset is around 800 ft (244 m) on the south flank of the anticline. The fault traces (locations) were interpreted by using the structure-contour and dip-magnitude maps of Top Marmaton and Upper Skinner Shale (Base Marmaton) surfaces (Appendix G-2). The faults are interpreted parallel to the structural contours along the highest dips and interpreted to be reverse faults considering the compressional regime (Lyday, 1985; Perry, 1989). There is significant uncertainty for the angle of the faults and the faults could be vertical or normal in character. The interpreted faults are nearly vertical and approximately parallel to the Mountain Front Fault located outside of the study area to the south (Figure 1). The thicknesses of the same stratigraphic zones on both sides of the faults are similar which suggests that the faults are post-depositional.

An isopach map of the Marmaton Group reveals that the thickness is greatest in the south-central part of the area and thins from this region in all directions (Appendix G-3 A). Changes in the thickness of each Marmaton Group wash across the study area can be directly related to the accommodation space at the time of deposition (Appendix G-3 B-F). Marmaton E Wash is the thinnest zone and Marmaton A-B Wash is the thickest zone (up to 650 ft, 198 m). Most zones thin toward the north to northeast.

Using the structure maps and fault surfaces, a 3-D stratigraphic and structural framework (3-D reservoir model grid) was constructed for the Marmaton Group (Figure 14). The model area is rectangular in shape and covers approximately 191 mi<sup>2</sup> (494 km<sup>2</sup>). The grid cells are oriented parallel to the two main faults. The cell sizes are 500 ft x 500 ft (152 m x 152 m) aurally and 1.5 ft (0.5 m) on average vertically with proportional layering. The number of cells in the model is 296x73x809 in I, J, and K

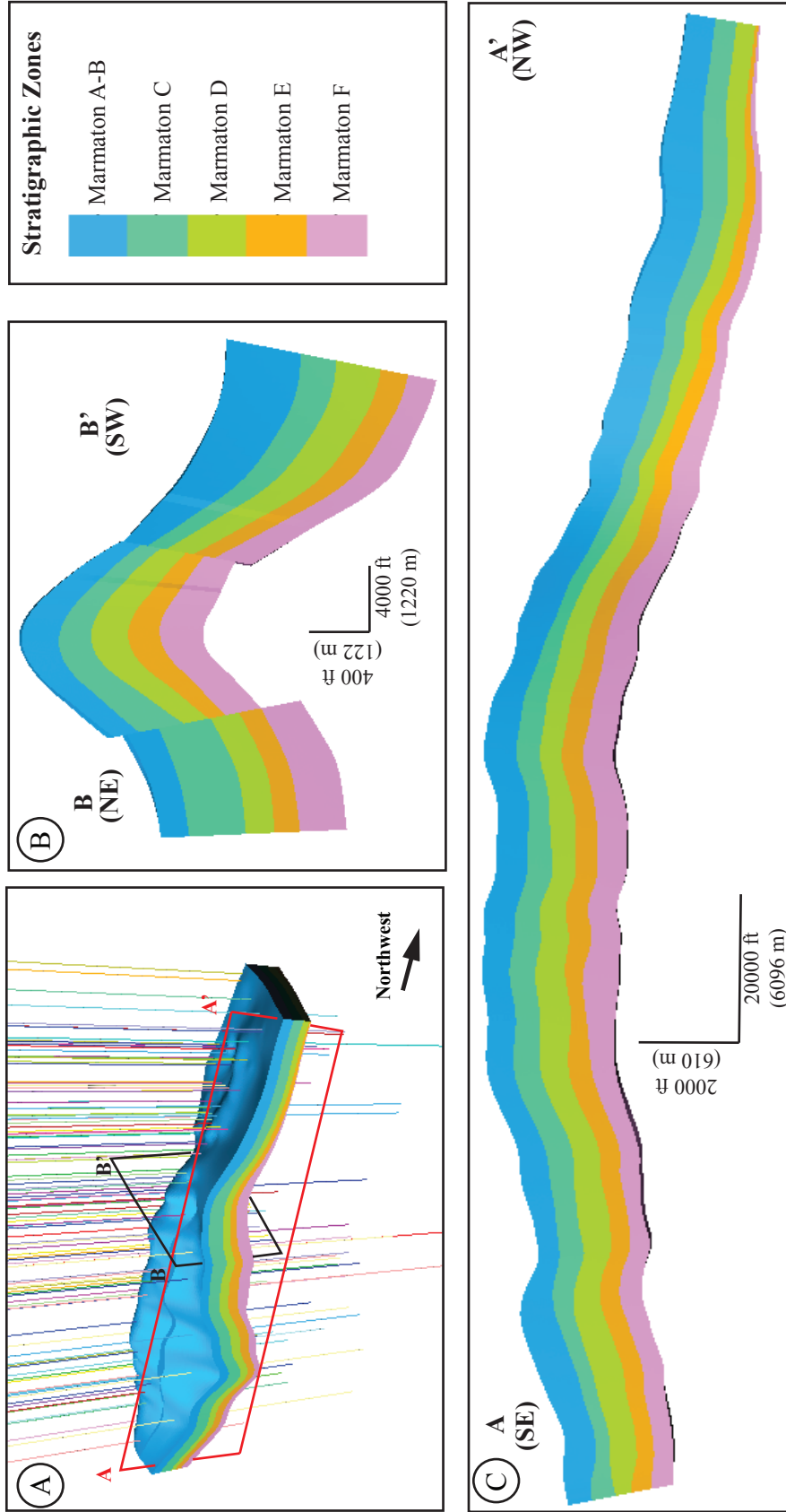


Figure 14. A) Stratigraphic and structural framework of the 3-D model (3-D grid) with view of five stratigraphic zones. B) Transverse slice showing the anticline structure bounded by two faults on its flanks. C) Longitudinal slice across which the zones have similar thickness. Marmaton F zone thins toward northwest. All figures are ten times vertically exaggerated.

directions. The total number of 3-D cells is 17,802,180. Lithology logs were upscaled to populate the grids cells (Figures 5, 6; Appendix H). The type of the lithology that exists in higher proportion within each cell was assigned as the upscaled cell lithology (Appendix H).

A vertical proportion curve is a vertical, 1-D trend (values between 0 and 1.0) that represents the variability in the percentage of lithology stratigraphically or by model layer based on the upscaled lithology logs (Figure 15). The correlated flooding surfaces correspond to the layers with highest mudstone proportion in the vertical proportion curve. According to Ross and Ross (1988) and Haq and Schutter (2008) Pennsylvanian time is composed of around 16 depositional cycles that are 1 million years in duration in average (Appendix I). The Desmoinesian interval approximately corresponds to the upper Moscovian and lower Kasimovian stages in the international time scale (Richards, 2013). Marmaton Group wash zones can be considered to correspond to the 5 cycles in this interval and interpreted as 3rd order regressive-transgressive depositional cycles (approximately 1 million years) bounded by the maximum flooding surfaces that represent the greatest transgression of shallow-marine facies after relative rise in the sea level (Ross and Ross, 1988; Haq and Schutter, 2008) (Appendix I). Flooding surfaces separating the wash zones can be considered as maximum flooding surfaces. The relative rises in the sea levels were interpreted to be sudden based on the vertical proportion curve. Tectonic activity can be responsible for the sudden sea-level rises. Sequence boundaries that represent surfaces along which sediment is bypassed during a relative sea-level fall are interpreted to cap the intervals where conglomerate is present with high proportion and that transition stratigraphically

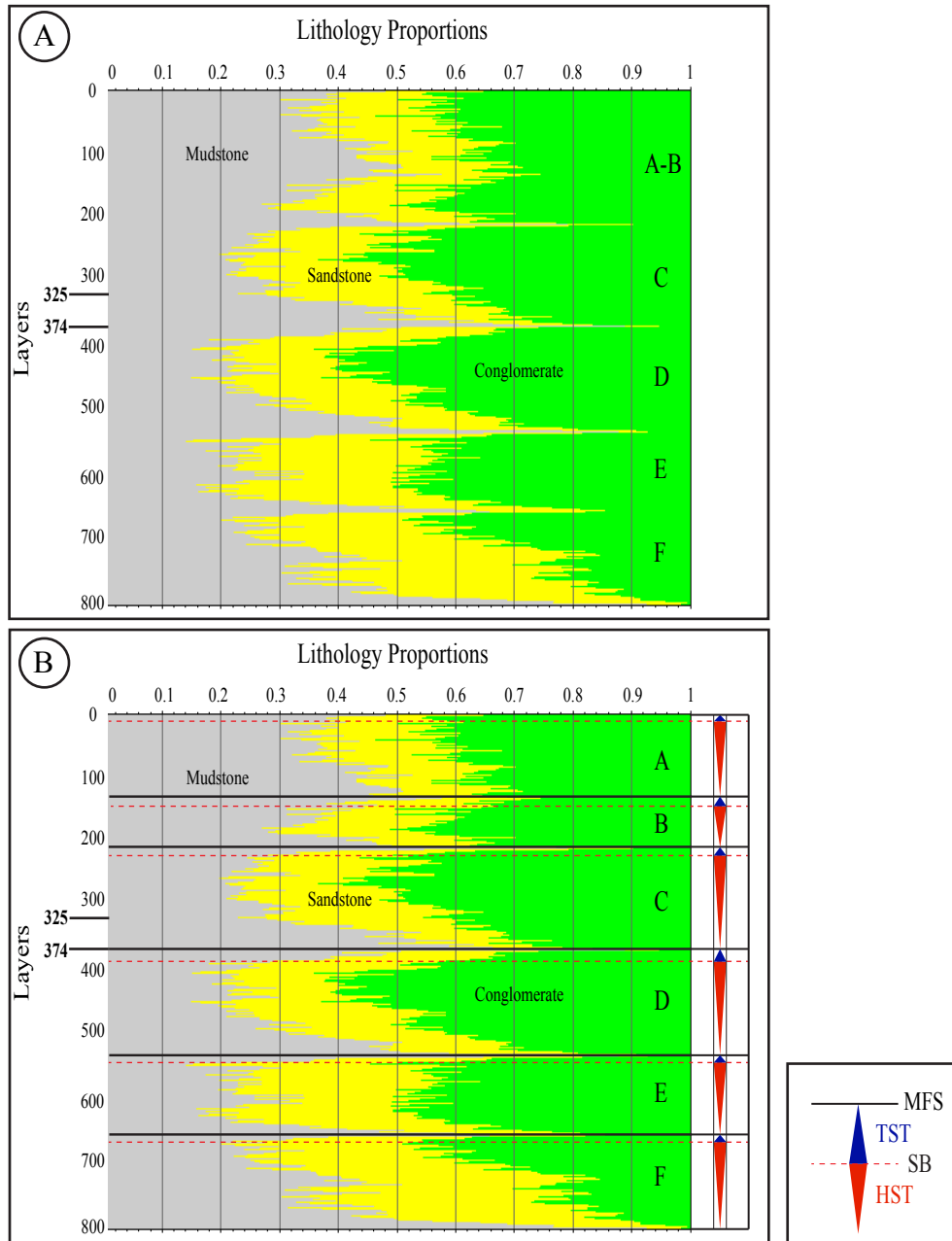


Figure 15. A) Lithology proportion curve showing the vertical proportion of three lithologies from the upscaled lithology logs and the wash zones from Marmaton A to F. B) Transgressive and highstand system tracts interpreted from the vertical proportion curve. The zones can be interpreted as 3<sup>rd</sup> order regressive-transgressive cycles. MFS: Maximum flooding surface; SB: Sequence boundary; TST: Transgressive system tract; HST: Highstand system tract. Zones with highest mudstone proportion are associated with the maximum flooding surfaces. Between the maximum flooding surfaces, sequence boundaries are interpreted where the proportion of conglomerate is greatest and the mudstone proportion starts increasing above it. The highstand system tracts show shallowing-upward sequence while the transgressive system tracts show deepening-upward sequence. Lowstand system tracts are not observable because of the proximal location. See Appendix H-2 for example two layers during maximum flooding (374) and highstand system tract (325). A-F correspond to Marmaton A-F zones.

upward into mudstone. The stratigraphic variability in lithology most likely reflects periods of uplift and erosion of the nearby Amarillo-Wichita Uplift. Smaller scale cycles within the zones can be interpreted as parasequences bounded by flooding surfaces indicating relative changes in sea level.

## **Spatial Distribution, Continuity and Connectivity of Fan-Delta**

### **Deposits**

In this study, sequential-indicator simulation (SIS) was used to model spatial distribution of lithologies (conglomerates, sandstones, and mudstones) in the Elk City Field. Four different lithology models were created in this study (Appendix J-1). The first model consists of 3 lithologies and 5 zones defined by the maximum flooding surfaces and is called the “sequence lithology model” considering the definition of the sequence based on maximum flooding surfaces (Galloway, 1989). The second model, which is called the “system tract lithology model”, has 12 zones that define the transgressive and highstand system tracts (Figure 15). This model was created by generating additional sequence boundary surfaces and it has 3 lithologies (conglomerate, sandstone, mudstone). The third and the fourth models, “sequence reservoir models”, have only two classes that are reservoir and non-reservoir, and have the same zones as the sequence lithology model. These two models were created to understand the utility of using the neural network and porosity-lithology relation in lithology estimation in terms of the resulting static connectivity and pore volume. In the third model, the lithology logs created by using only gamma-ray cut-off values were honored (Appendix E-4). In the fourth model, the lithology logs using the neural

network, gamma-ray cut-off, and lithology-porosity relation were honored. Previously estimated sandstones and conglomerates are combined under reservoir class for the fourth model.

### **Continuity of Conglomerates and Sandstones**

The three-dimensional stratigraphic and structural framework, upscaled lithology logs, vertical lithology percentages, and vertical and horizontal variograms were all honored in the lithology modeling. Azimuth values necessary in the determination of major and minor anisotropy ranges were determined for each lithology by zone from horizontal variogram maps (polar plots). Vertical and horizontal variograms were created by zone and for each lithology. From the experimental variograms, ranges for each lithology were determined (Appendix K). For the sequence lithology model and system tract lithology model the same azimuth angles and variogram parameters were used for the same stratigraphic intervals. For the third and the fourth models, azimuth angles, horizontal and vertical anisotropy values were determined separately by analyzing the horizontal variogram maps and variograms. In sequence model and system tract model azimuth angles of major anisotropy ranges for conglomerate range between 90° and 145° while for sandstone they range between 135° and 150°. This suggests that both conglomerates and sandstones exhibit greater continuity parallel to the trend of the Mountain Front Fault (Figure 1). This is consistent with a fan-delta environment sourced from the uplifted area to the south (Figures 1, 13). Sandstones have greater major and minor horizontal ranges than conglomerates which suggests that they are more laterally continuous than conglomerates (Appendix K-16). Sandstones are most continuous in the Marmaton D interval (sandstone range 4,868 ft;

1,484 m), and conglomerates exhibit the greatest continuity in the Marmaton A-B interval (conglomerate range 4,028 ft; 1,228 m). The vertical continuity of conglomerate and sandstone beds are similar (conglomerate vertical range 28-39 ft; 9-12 m, and sandstone vertical range 26-32 ft; 8-10 m), indicating that the general thickness of these deposits are similar.

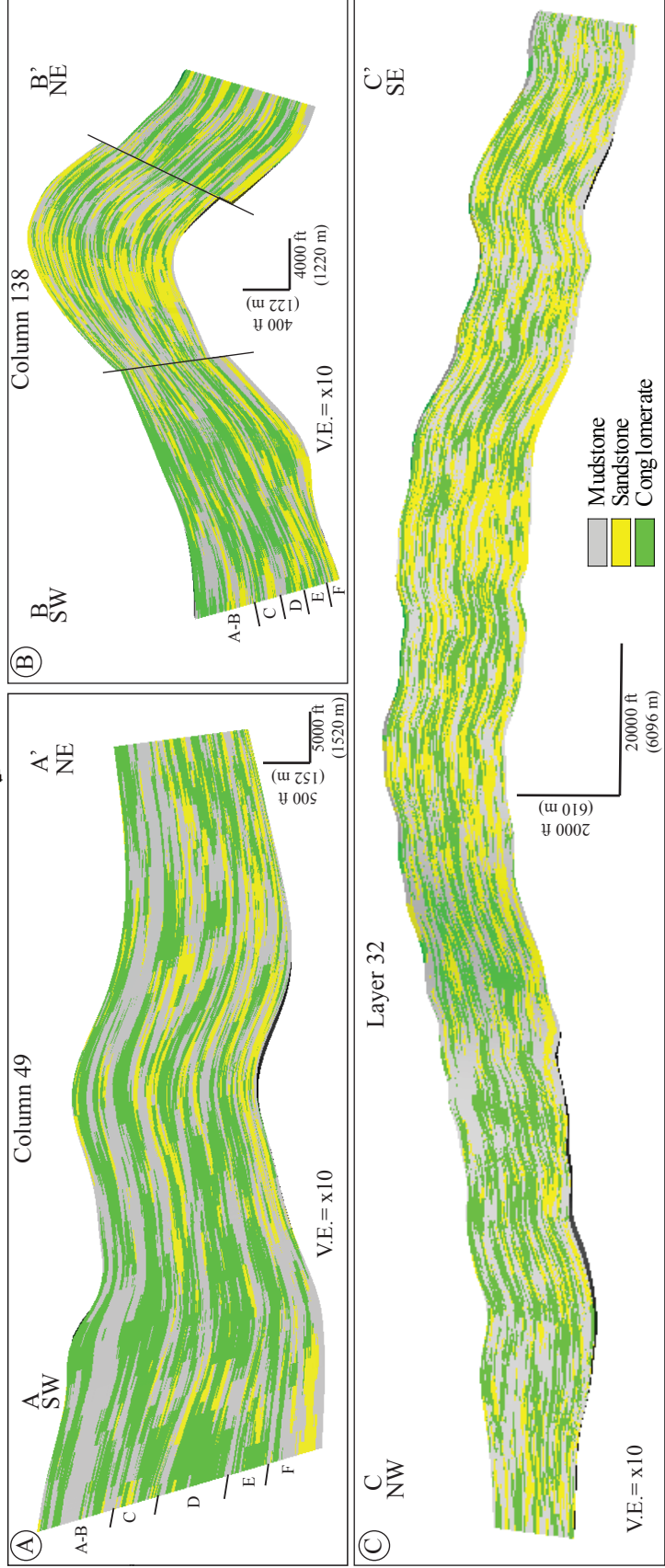
### **Lithology Distribution**

The resulting sequence lithology model and system tract lithology model have 36% mudstone, 27% sandstone and 37% conglomerate. Three-dimensional lithology models and 2-D lithology percentage maps demonstrate the distribution of these lithologies in the study area (Figures 16, 17; appendix J-2). The northwest side of the study area is more conglomeratic, and the proportion of sandstone increases toward southeast (Figures 16C; appendix J-2). The interpretation that the southeast side of the study area is relatively more distal than the northwest side of the study area is supported by the lower amount of conglomerate on the southeast side of the study area. The amount of conglomerate decreases and the amount of sandstone increases toward southeast, away from the source area on the northwest side of the study area (Figures 16, 17). Because a greater amount of coarse-grained sediments is deposited to the proximal areas and the grain-size decreases away from the source in fan-delta environments, it is expected to observe more conglomerate on the northwest side of the field (Brown; 1979; Ethridge and Wescott, 1984). The extensive mudstones associated with flooding surfaces are apparent with their high lateral continuity in the model (Appendix J-3). The mudstones lithology in the model also includes the sandy mudstones and pebbly mudstones associated with the debris flows in the proximal fan





Figure 16. 3-D lithology model with cross-sectional views. Note the greater amount of conglomerate on the northwest side of the study area, and increase in the amount of sandstone toward southeast side. Flooding mudstones can be recognized with their long lateral continuity. Toward northeast (away from source site) the amount of conglomerate decreases while the amount of sandstone increases.



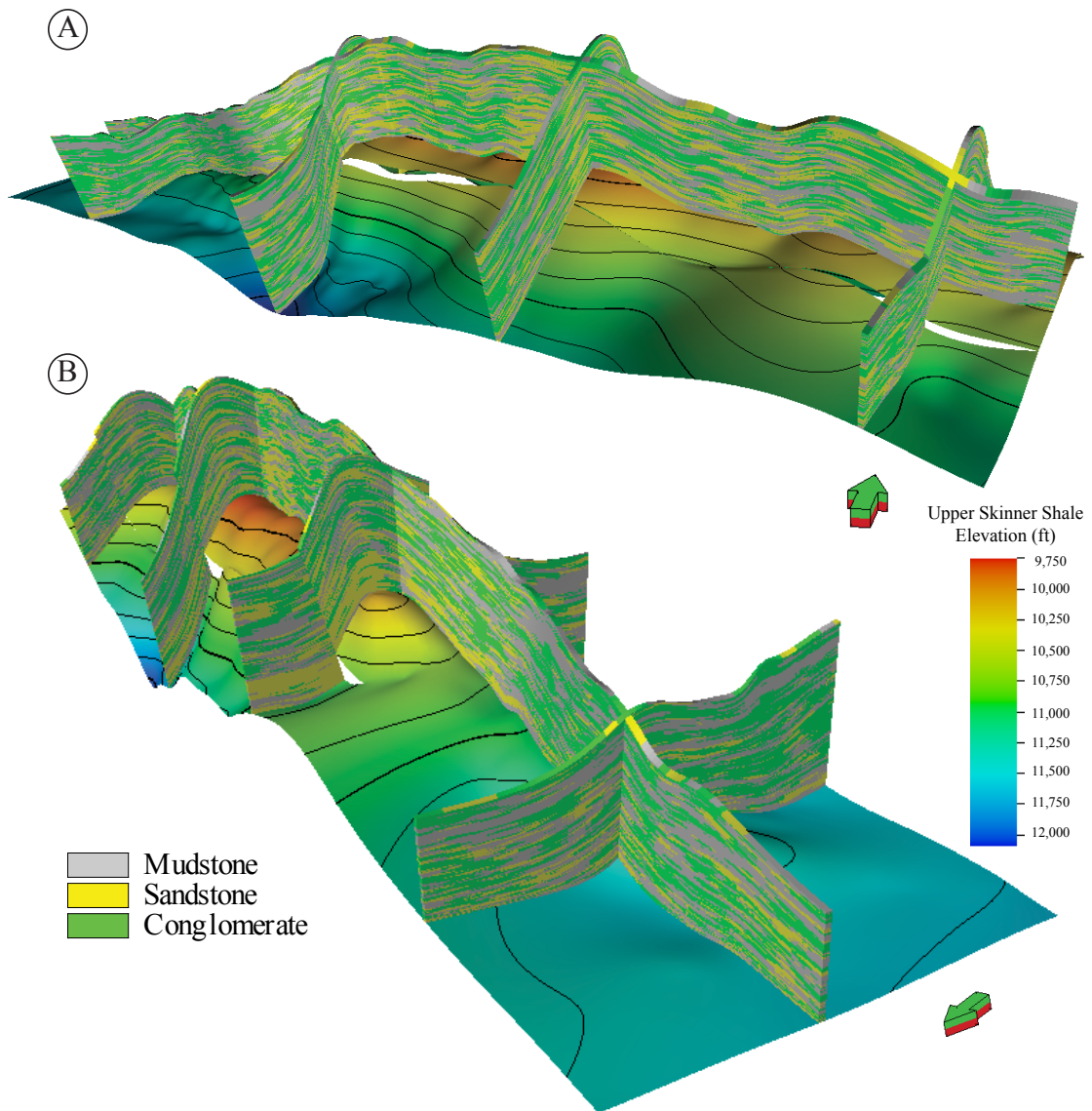


Figure 17. 3-D view of the lithology model A) from the southeast, B) from the northwest with slices along I and J directions with ten times vertical exaggeration. The model overlies the top of the Upper Skinner shale surface. Northwest trending anticline bounded by two faults on its flanks is the major structure in the field. Mudstones can be observed with their high lateral continuity. The amount of conglomerates is greater on the northwest side of the field, and sandstone amount increases toward southeast side of the field. Proximity to the source can be the most significant factor in the distribution of sandstone and conglomerate in a fan-delta depositional environment.

area (Figure 8; Appendix F). Therefore, mudstones are not limited to the transgressive cycles. The system tract lithology model has more conglomerates and sandstones in the highstand system tracts (Appendix M-1). There are more conglomerates than sandstones in all system tracts except the highstand system tract of Marmaton F interval. This interval has relatively distal deposits where fewer conglomerates were deposited considering the decreasing grain size away from the source area in a fan-delta setting (Figure 13).

### **Porosity Distribution**

Effective porosity calculation from the well logs requires the calculation of shale volume ( $V_{shale}$ ). For the formations with radioactive minerals, calculating the  $V_{shale}$  from gamma-ray logs result in overestimated  $V_{shale}$  because of the high gamma-ray in reservoirs (Asquith et al., 2004). Using the thorium component of the spectral gamma-ray in the equation can differentiate the radioactive reservoirs from shales. However, lack of enough spectral gamma-ray log data prevents using this approach. Another way of calculating  $V_{shale}$  under these circumstances is to use the separation between the neutron porosity (NPHI) and density porosity (DPHI) as an indicator of the relative amount of shale. However, using this equation is successful only for formations without gas, because cross-over ( $DPHI > NPHI$ ) of porosity logs gives negative values of  $V_{shale}$  in the calculation. Because of these limitations, only total porosity was calculated in this research.

Sequential-Gaussian Simulation (SGS) was utilized to generate total porosity ( $\phi_t$ ) models for each lithology models created. Total porosity ( $\phi_t$ ) logs were calculated for each well by taking the root-mean-square of neutron porosity (NPHI) and density

porosity (DPHI). Using this equation is more proper for gas-bearing reservoirs because it can compensate for the effect of gas in the result (Bassiouni, 1994). Calculated total porosity logs were upscaled by using the arithmetic average method in which the average of the values corresponding to each cell was assigned as the upscaled porosity value. The three-dimensional grid and lithology model constrained the porosity model and the upscaled porosity logs and variograms were honored. Vertical and horizontal ranges were determined from the variograms (Appendix L-1). Considering the internal heterogeneities within each lithology, smaller vertical and horizontal ranges exist for porosity as compared to the ranges for lithologies. The relationship between the lithology and total porosity can be observed in the lithology percent maps and average porosity maps for the reservoirs (Appendices J-2, L-2). Porosity increases upward and Marmaton A-B interval has the highest average porosity. Areas where sandstone is abundant exhibit less than 5% for average porosity values. Laterally, there is an observable increase in porosity from east to west that can be related with the increasing amount of conglomerates that show larger dissolution porosity than sandstones (Appendix C). Also, regarding the relative distance from the source area and the environmental setting, more interaction with mudstones and the bioturbation in the sandstones can have effect on lower amount of porosity on the southeast side of the study area. Muddy sandstones grouped under sandstone in the lithology model can be another contributor for the lower porosity in sandstone lithology. Another possibility can be that the reservoirs on the northwest side of the study area might have more preserved primary intergranular porosity than the reservoirs on the southeast side which show mainly secondary dissolution type of porosity.

## **Static Connectivity and Pore Volume**

Static connectivity is a significant reservoir property that affects recovery directly. Static connectivity of a reservoir can be defined as the percentage of the reservoir that is connected to a certain group of wells and calculated by dividing the connected volume of the reservoirs to total volume of reservoirs. In this study, for the sequence and system tract models, static connectivity and pore volume analyses were conducted for sandstones and conglomerates separately. In the third and fourth models, connectivity and pore volume were calculated for the reservoir rock that is composed of sandstone and conglomerate together. All the wells were defined as index wells in the connectivity analyses meaning that volumes that did not intersect at least one of these wells were not counted as connected volumes. Also, 5% and 10% porosity values were used as filters in the connectivity in order to determine the connected volume of reservoirs with porosity greater than these certain amounts (Figure 18).

In the sequence lithology model, static connectivity results show that there is not a significant connectivity difference between the zones except the Marmaton F interval which has the lowest connectivity both for sandstones and conglomerates (Table 2). Marmaton C interval has the greatest connectivity for the reservoirs. Connectivity of sandstones is found lower than connectivity of conglomerates. This is primarily because of the porosity constraints for the connectivity. Because sandstones have lower porosity than conglomerates in the model, and sandstones with porosities lower than certain porosity amounts are not considered. Higher interaction of the sandstones with the wave processes due to their relatively more distal location and their finer grain size compared to the conglomerates can be another contributor for their lower connectivity (Figure 13).

Table 2. Total volumes, pore volumes, and connected volumes for conglomerates and sandstones at each zone. For connectivity, 5% and 10% porosity cut-off values were used as constraints. Marmaton C interval has the greatest connectivity for both conglomerates and sandstones, followed by the Marmaton A-B interval which has the greatest pore volume. Conglomerates have higher connectivity than sandstones in all zones. They have also higher amount of pore volume than sandstones in all zones except Marmaton F interval.

CONGLOMERATE						
ZONES	Total volume in BCF (x10 <sup>9</sup> ft <sup>3</sup> )	Pore volume (x10 <sup>6</sup> RB)	Porosity > 5%		Porosity > 10%	
			Connected volume in BCF	Connectivity (%)	Connected volume in BCF	Connectivity (%)
Marmaton A-B	656	9,138	555	84.5	114	17.3
Marmaton C	487	6,866	429	88.1	85	17.5
Marmaton D	540	7,132	437	80.9	79	14.6
Marmaton E	387	5,145	315	81.6	51	13.3
Marmaton F	273	3,012	158	57.9	18	6.8

SANDSTONE						
ZONES	Total volume in BCF (x10 <sup>9</sup> ft <sup>3</sup> )	Pore volume (x10 <sup>6</sup> RB)	Porosity > 5%		Porosity > 10%	
			Connected volume in BCF	Connectivity (%)	Connected volume in BCF	Connectivity (%)
Marmaton A-B	350	3,767	221	63.1	16	4.6
Marmaton C	325	3,570	218	67.1	16	4.9
Marmaton D	312	3,009	170	54.5	5	1.7
Marmaton E	300	3,037	175	58.4	11	3.6
Marmaton F	404	3,716	206	51.0	5	1.4

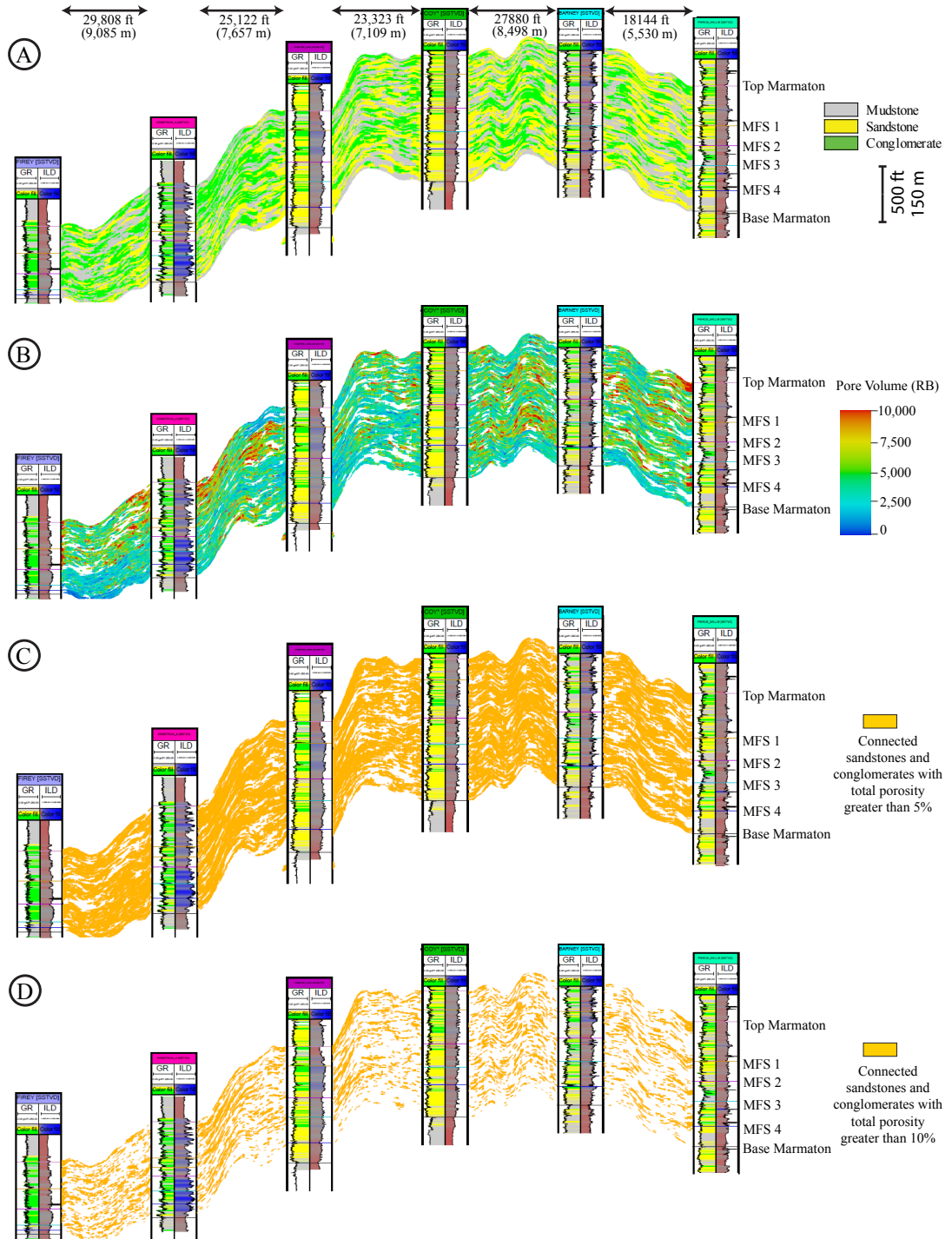


Figure 18. Structural cross section E-E' with the modeled properties between the wells (Figure 2). A) lithologies, B) total pore volume for sandstones and conglomerates, C) connected volume of reservoirs with total porosity greater than 5%, and D) connected volume of reservoirs with total porosity greater than 10%. Cyclic deposition results in similar connectivity in each zones. Conglomerates have greater pore volume than sandstones in general. This can be because of more amount of intergranular porosity, more dissolution porosity, or combination of both.

Conglomerates have greater pore volume than sandstone except the Marmaton F interval (Table 2). This interval has the highest amount of sandstone and lowest sandstone connectivity compared to the other zones and has relatively more distal lithofacies.

Static connectivity analysis and pore volume calculations were also conducted for the system tract model to see the relationship between the pore volume, connectivity, and system tracts (Figures 18, 19; appendix M-1 – 4). Highstand system tracts in each zone showed greater amount of connectivity for both conglomerates and sandstones than the transgressive system tracts. The amount of total pore volume in reservoirs is greater in highstand system tracts, and conglomerate have more total pore volume than sandstones except the Marmaton F interval (Figure 19). Higher amount of pore volume in reservoirs in highstand system tracts is directly related to the higher amount of reservoir present in these zones. Higher pore volume in conglomerates can be explained with greater secondary porosity in coarser grained samples observed (Appendix C).

Connectivity and pore volume in each zone were also calculated for two reservoir models honoring different lithology logs; one including neural network and porosity-lithology relation in addition to the gamma-ray cut-off values in estimation, and the other one based on only gamma-ray cut-off values (Appendix E-4). Connectivity and the amount of pore volume of the reservoirs is less in the model which is based on only the gamma-ray cut-off (Appendix M-5). Less pore volume is a result of the underestimated reservoirs with the gamma-ray cut-off method (Appendix E-4). This can also have some effect for the lower connectivity in the zones. Similar pore volume



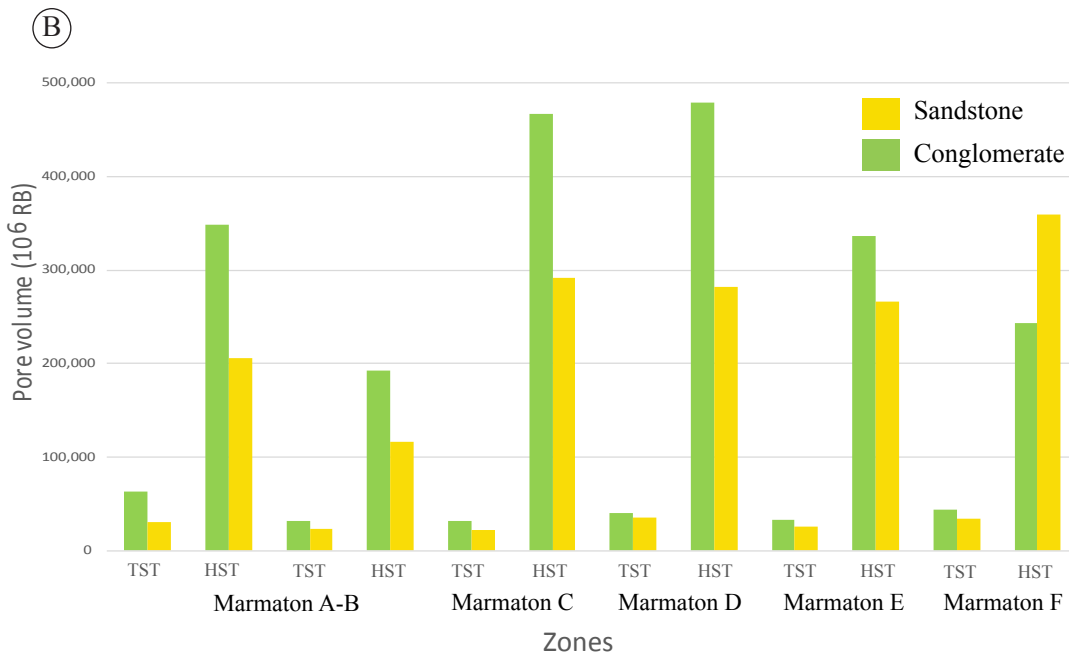
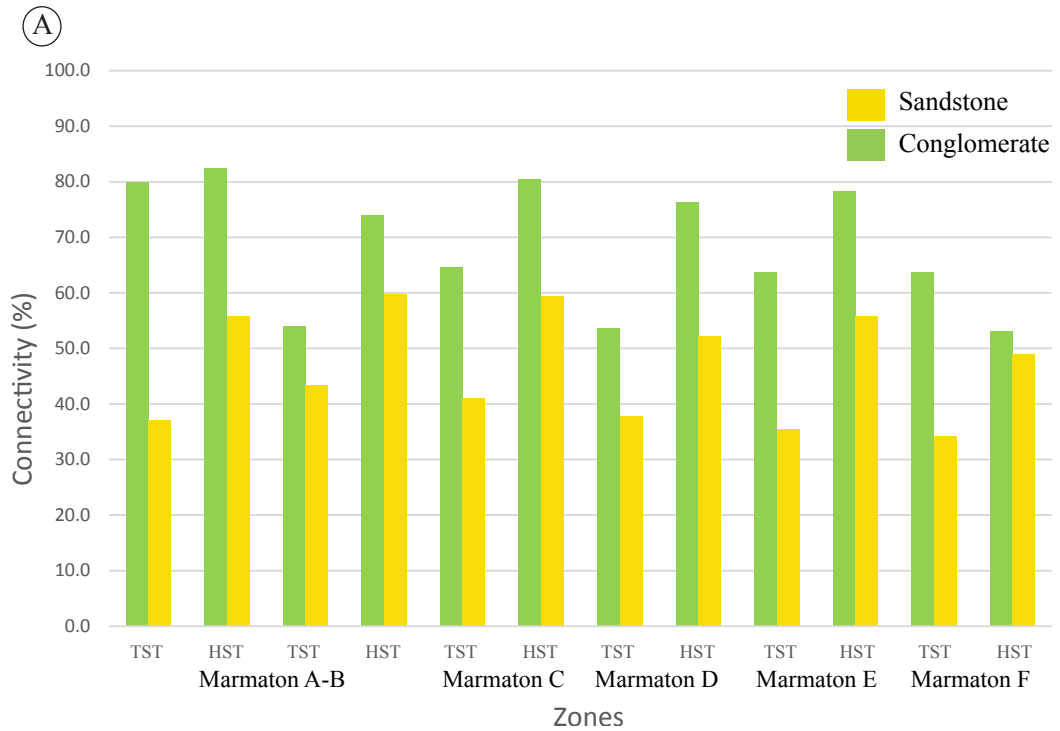


Figure 19. Histograms showing A) the connectivities of conglomerates and sandstones with greater than 5% porosity, B) the amount of pore volumes in conglomerates and sandstones in each highstand system tract and transgressive system tract. Reservoirs in the highstand system tracts have greater connectivities than those in transgressive system tracts. Conglomerates mostly have higher connectivities than sandstones. Highstand system tracts have greater pore volume than transgressive system tracts both for conglomerates and sandstones. Conglomerates have greater pore volume than sandstones except Marmaton F interval.

amounts between the two models for the Marmaton F interval is because reservoir rock is not underestimated as much for this zone (Appendix E-4). These results reveal the significance of using the porosity-lithology relation and Artificial Neural Network in lithology estimation for the reservoirs with potassium feldspar and the extent that reservoir rock, pore volume, and connectivity can be underestimated by using only gamma-ray cut-off values.

## **Conclusion**

Desmoinesian-age Marmaton Group Granite Wash deposits in the Elk City Field have five lithologies which are conglomerates, sandstones, muddy sandstones, sandy mudstones and mudstones. The dominant lithofacies observed in two cores are orthoconglomerates, paraconglomerates; parallel-stratified, cross-stratified, bioturbated, granule-pebble-bearing, and structureless sandstones; bioturbated, slumped muddy sandstones and sandy mudstones; and bioturbated, fossiliferous, pebbly and massive mudstones. Sedimentary structures and the relations of lithologies and lithofacies with each other in the cores, thin section observations, similarity between the well-log patterns of the cored interval and the non-cored wells, the depositional environment was interpreted to be shelf-type fan delta. Porosity observed in thin sections are mainly secondary and related with feldspar and chert dissolution. Total pore volume in conglomerates is greater than in sandstones.

Using an Artificial Neural Network, estimation of five lithologies within the cored interval resulted in 66% accuracy. Although the neural network was able to differentiate sandstones, conglomerates, and mudstone, it encountered difficulty in

differentiating muddy sandstones and sandy mudstones. When sandy mudstones and muddy sandstones are merged with mudstones and sandstones, respectively, estimation of three lithologies resulted in 83% total accuracy. Conglomerates, sandstones, and mudstones match with the original lithology log 88%, 84%, and 79% of the time, respectively. By constraining the resulting neural-network estimation in the non-cored wells by gamma-ray cut-off values and the relation between the lithologies and neutron and density porosities, more accurate estimations were achieved.

Well logs indicate that the different sandstone and conglomerate lithologies are separated by at least four distinct and laterally extensive shales. Based on cores, well logs, vertical proportion curve, and sea level cycles, these shales are interpreted to be capped by condensed sections separating 3<sup>rd</sup> order cycles. Correlation suggests that structurally, Elk City field is composed of a northwest trending post-depositional anticline with possible faulting on both sides. Based on the well-log responses, there are more flooding surfaces on the southeast side of the study area suggesting a relatively more distal environment of deposition.

By using Sequential Gaussian Simulation several lithology models were created to understand the continuity, spatial distribution, and connectivity of the lithologies, as well as their relation with the sequence stratigraphy and two different methods used in reservoir estimation. Sandstones were found more continuous than conglomerates laterally while conglomerates show greater vertical continuity. The amount of sandstone was found to increase toward southeast side while more conglomerates dominate on the northwest side of the study area. Porosity models show that generally conglomerates tend to have higher porosity than sandstones. The Marmaton C interval has the highest

connectivity for conglomerates and sandstones while Marmaton A-B interval has the highest amount of pore volume. Pore volume in conglomerates is greater than sandstones except for the Marmaton F interval which has the highest amount of sandstone and lowest connectivity. Highstand system tracts exhibit greater connectivity and pore volume for both conglomerates and sandstones than the transgressive system tracts. Reservoir models honoring lithology estimation based on only gamma-ray cut-off values result in underestimation in the amount of reservoirs, their connectivity, and pore volume compared to the reservoir models honoring lithology logs calculated by using a neural network, gamma-ray cut-off values, and lithology porosity relation.

## References

- Anggraini, J., and M. Puspa, 2008, Supervised and unsupervised neural networks technique in facies classification and interpretation, *in* Indonesian Petroleum Association Thirty-Second Annual Convention & Exhibition: p. 1 – 8.
- Asquith, G., D. Krygowski, S. Henderson, and N. Hurley, 2004, Basic well log analysis, 2d ed.: AAPG Methods in Exploration Series 16, 244 p.
- Bassiouni, Z., 1994, Theory, measurement, and interpretation of well logs in: Doherty, H. L. (ed.), Memorial Fund of AIME. SPE, New York, 372 p.
- Blakey, R., 2011, Paleogeography and geologic evolution of North America, <http://cpgeosystems.com/paleomaps.html>, (accessed July, 2016).
- Boyd, D. T., 2002, Map of Oklahoma oil and gas fields: Oklahoma Geological Survey Map GM-36, scale 1: 500,000, 1 sheet.
- Brown, L.F., Jr., 1979, Deltaic sandstone facies of the Midcontinent, in N.J. Hyne, ed., Pennsylvanian sandstones of the Mid-Continent: Tulsa Geological Society, p. 35 – 63.
- Duggins, W. T., 2013, Facies architecture and sequence stratigraphy of part of the Desmoinesian Granite Wash, Texas Panhandle and western Oklahoma: The University of Tulsa, 1 – 162 p.
- Dutton, S. P., 1985, Fan-delta Granite Wash of the Texas Panhandle: Oklahoma City Geological Society Short Course, p. 1–144.
- Dutton, S. P., 1979, Pennsylvanian fan delta sandstones of the Palo Duro Basin, Texas: Pennsylvanian Sandstones of the Mid-Continent, p. 235 – 245.
- Ethridge, F. G., and W. A. Wescott, 1984, Tectonic setting, recognition and hydrocarbon reservoir potential of fan-delta deposits: Canadian Society of Petroleum Geologists, v. 10, p. 217 – 235.
- Gelphman, N. R., 1961, West Sentinel Oil Field, Washita County, Oklahoma: sedimentology of the “Granite Wash” and structural geology: The Shale Shaker, v. 10, no. 2, p. 234 – 247.
- Gilbert, M. C., 1992, Speculations on the origin of the Anadarko Basin: Basement Tectonics 7, v. 1, p. 195 – 208.
- Ham, W. E., R. E. Denison, and A. C. Merritt, 1965, Basement rocks and structural evolution of southern Oklahoma - A Summary: Bulletin of the American Association of Petroleum Geologists, v. 49, no. 7, p. 927 – 934.

- Haq, B. U., and S. R. Schutter, 2008, A chronology of Paleozoic sea-level changes: *Science*, v. 322, October 2008, p. 64 – 68.
- Henry, M. E., and T. C. Hester, 1995, Anadarko Basin Province (058): US Geological Survey National Oil and Gas Assessment, U.S. Geological Survey, Central Energy Resources Team, p. 1 – 47.
- Holmes, C. D., 2015, Stratigraphic architecture, facies characteristics, and distribution of deepwater deposits, Colony Granite Wash, Anadarko Basin, Oklahoma: University of Oklahoma, 1 – 166 p.
- Iloghalu, E. M., and N. Azikiwe, 2003, Application of neural networks technique in lithofacies classifications used for 3-D reservoir geological modelling and exploration studies. - A novel computer-based methodology for depositional environment interpretation, *in* AAPG Annual Convention Salt Lake City, Utah: p. 1 – 7.
- Johnson, K. S., 1989, Geologic evolution of the Anadarko Basin: Oklahoma Geological Survey Circular, v. 90, p. 3 – 12.
- Karis, A. M., 2015, Stratigraphy and reservoir characteristics of the Desmoinesian Granite Wash (Marmaton Group), Southern Anadarko Basin: University of Oklahoma, 1 – 87 p.
- Locricchio, E., 2012, Granite Wash play overview, Anadarko Basin: stratigraphic framework and controls on Pennsylvanian Granite Wash production, Anadarko Basin, Texas and Oklahoma, *in* Granite Wash and Pennsylvanian Sand Forum, Oklahoma City, Oklahoma: p. 1 – 30.
- Lyday, J. R., 1985, Atokan (Pennsylvanian) Berlin Field: genesis of recycled detrital dolomite reservoir, deep Anadarko Basin, Oklahoma: *American Association of Petroleum Geologists Bulletin*, v. 69, no. 11, p. 1931 – 1949.
- McConnell, D. A., M. J. Goydas, G. N. Smith, and J. P. Chitwood, 1990, Morphology of the frontal fault zone, southwest Oklahoma: Implications for deformation and deposition in the Wichita uplift and Anadarko basin: *Geology*, v. 18, no. 7, p. 634 – 637.
- Mitchell, J., 2011, Horizontal drilling of deep Granite Wash reservoirs, Anadarko Basin, Oklahoma and Texas: *Shale Shaker*, v. 62, no. October, p. 118 – 167.
- Nemec W. and R. J. Steel, 1988, What is a fan delta and how do we recognize it? *in* W. Nemec and R. J. Steel., eds., *Fan Deltas: Sedimentology and Tectonic Setting*: London, Brackie and Son, p. 3 – 13.

- Northcutt, R. A. and J. A. Campbell, 1995, Geologic provinces of Oklahoma: Oklahoma Geological Survey Open-File Report 5-95, 1 sheet, scale 1: 750,000, 6-page explanation and bibliography.
- Perry, W. J., 1989, Tectonic evolution of the Anadarko Basin region, Oklahoma: US Geological Survey Bulletin 1866-A, p. A1 – A19.
- Reineck, H. E., I. B. Singh, 1975, Depositional Sedimentary Environments. With Reference to Terrigenous Clastics: New York, Springer Verlag, 439 p.
- Richards, B.C. 2013, Current status of the International Carboniferous Time Scale: The Carboniferous-Permian Transition, Bulletin 60. Edited by S.G. Lucas, et al. New Mexico Museum of Natural History and Science, p. 348 – 353.
- Ross, C. A., and Ross, J. R. P., 1988, Late Paleozoic transgressive-regressive deposition: Society of Economic Paleontologists and Mineralogists Special Publication 42, p. 227 – 247.
- Sahl, H. L., 1970, Mobeetie Field, Wheeler County, Texas: The Shale Shaker, v. 19, p. 300 – 307.
- Sneider, R. M., F. H. Richardson, D. D. Paynter, R. E. Eddy, and I. A. Wyant, 1977, Predicting reservoir rock geometry and continuity in Pennsylvanian reservoirs, Elk City Field, Oklahoma: Journal of Petroleum Technology, v. 29, p. 851 – 866.
- Verma, A. K., B. A. Cheadle, A. Routray, W. K. Mohanty, and L. Mansinha, 2014, Porosity and permeability estimation using neural network approach from well log data: Search and Discovery, p. 1 – 9.

## Appendix A: Paleogeographic Maps

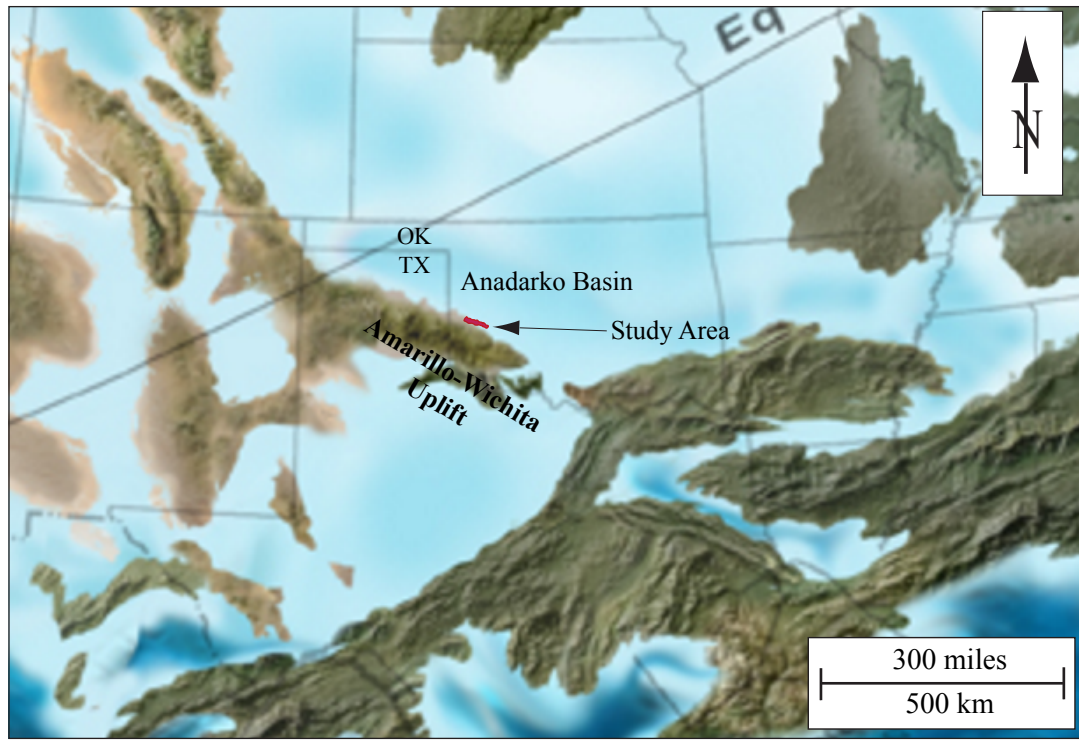


Figure A-1. Middle Pennsylvanian (308 Ma) paleogeographic map (modified from Blakey, 2013). The Amarillo-Wichita Uplift started to form in Early Pennsylvanian with the onset of the compressional regime while the Anadarko Basin started to subside. The study area is shown by red color. It is located in the southern Anadarko Basin, just in front of the Amarillo-Wichita Uplift. Sediments eroded from the Amarillo-Wichita Uplift were transported to the basin as alluvial fan, fan-delta, debris flow and turbidite deposits.



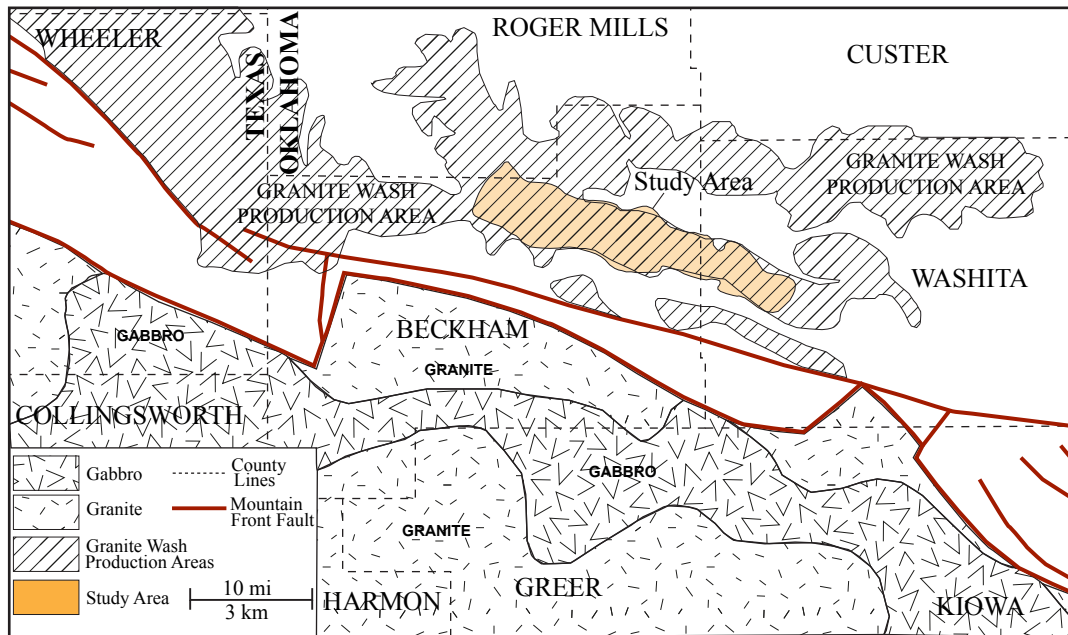


Figure A-2. Middle Desmoinesian paleogeographic map showing the Mountain Front Fault, granite wash production areas, and the basement rock type that are the source of the granite wash deposits (modified from Mitchell, 2011; Ham et.al., 1964; McConnell 1989). The proportion of the gabbroic rocks within the source rock region in the south of the study area increases toward east. The source rock composition can be responsible for the different well-log responses, especially gamma-ray, in the northwest and southeast sides of the study area. See Figure 9 for the well-log responses across the study area from northwest to southeast.

## Appendix B: Core Descriptions

Two cores, GHK 1-34 Finnell and GHK 1-27 Niece were described in terms of lithology, grain size, sorting, roundness, color, and sedimentary structures. Totally, 15 lithofacies were observed. The legend for the core description is as follows.

LEGEND					
	Muddy matrix		Convoluted bedding		Conglomerate
	Pebble sized clasts		Fluidization		Sandstone
	Granule sized clasts		Bioturbation		Muddy sandstone
	Parallel stratification		Fossils		Sandy mudstone
	Cross stratification		Scoured surface		Mudstone
	Distorted bedding		Rip-up clasts		

## **GHK 1-34 Finnell**





Depth (ft)	Gravel		Sand					Mud		Sorting			Lithology	Color	Structures	Remarks/Description	Lithofacies	
	Cobble	Pebble	Gravel	VC	C	M	F	VF	Silt	Clay	P	M						G
11108													Sst	Grey	Bioturbation. Fluidization Bioturbation. Parallel lamination Bioturbation. Wavy bedding Bioturbation	Fine grained, massive, occasionally parallel bedded, well sorted, well rounded sst. Partly, there are some mudstone layers disturbed due to bioturbation. Occasionally, there are structures that are evidence for fluidization.	Massive sst Parallel stratified sst Parallel stratified sst Bioturbated sst Bioturbated sst Bioturbated sst Bioturbated sst	
11109													Muddy sst		Bioturbation. Parallel lamination		Bioturbated muddy sst Bioturbated sst Bioturbated sst Bioturbated sst Bioturbated sst	
11110													Sst		Bioturbation	Fine grained, well sorted, well rounded sst and mudstone alternation. Bedding is disturbed due to bioturbation.	Bioturbated sst Bioturbated sst Bioturbated sst Bioturbated sst Bioturbated sst	
													Muddy sst	Grey and dark grey	Bioturbation. Parallel bedding		Bioturbated muddy sst Bioturbated muddy sst	
11111															Bioturbation		Bioturbated sst	
															Massive. Bioturbation		Massive sst	
															Massive. Bioturbation. Fluidization		Massive sst	
11112															Massive. Bioturbation		Bioturbated sst	
															Bioturbation. Parallel lamination		Bioturbated sst Parallel stratified sst Parallel stratified sst	
11113																Fine grained, massive to bioturbated, well sorted, well rounded sst.	Bioturbated sst Bioturbated sst Bioturbated sst Bioturbated sst Bioturbated sst Bioturbated sst Bioturbated sst Bioturbated sst Bioturbated sst Bioturbated sst	
11114															Massive. Bioturbation		Bioturbated sst Bioturbated sst Bioturbated sst Bioturbated sst Bioturbated sst Bioturbated sst Bioturbated sst Bioturbated sst Bioturbated sst Bioturbated sst	
11115															Cross lamination	Medium grained, cross laminated, well sorted, well rounded sst.	Cross stratified sst	
															Massive. Bioturbation. Fluidization		Bioturbated sst	
															Massive. Bioturbation		Bioturbated sst	
11116															Massive. Bioturbation. Fluidization		Bioturbated sst	
																	Bioturbated sst	
																	Bioturbated sst	
11117															Massive. Bioturbation; small muddy parts		Bioturbated sst Bioturbated sst Bioturbated sst Bioturbated sst Bioturbated sst Bioturbated sst Bioturbated sst Bioturbated sst Bioturbated sst	
																		Bioturbated sst
11118																Fine grained, massive, bioturbated, well sorted, well rounded sst. Occasionally there are some water escape structures.	Bioturbated sst Bioturbated sst Bioturbated sst Bioturbated sst Bioturbated sst Bioturbated sst Bioturbated sst Bioturbated sst	
															Massive. Bioturbation		Bioturbated sst Bioturbated sst Bioturbated sst Bioturbated sst Bioturbated sst Bioturbated sst Bioturbated sst Bioturbated sst	
11119															Bioturbation. Dish structures		Bioturbated sst	
															Massive. Bioturbation		Bioturbated sst	
															Bioturbation. Dish structures		Bioturbated sst	
																	Bioturbated sst	
															Massive. Bioturbation		Bioturbated sst	



Depth (ft)	Gravel			Sand					Mud			Sorting			Lithology	Color	Structures	Remarks/Description	Lithofacies
	Cobble	Pebble	Gravel	VC	C	M	F	VF	Silt	Clay	P	M	G						
11132														Sst	Grey and dark grey	Bioturbation. Fluidization		Massive sst	
																Bioturbation		Bioturbated muddy sst	
														Muddy sst	Grey and dark grey	Parallel bedding. Bioturbation		Bioturbated muddy sst	
																		Bioturbated muddy sst	
														Sst	Grey and dark grey			Parallel stratified sst	
11133																Bioturbation		Bioturbated muddy sst	
																		Bioturbated muddy sst	
														Muddy sst	Grey and dark grey			Bioturbated muddy sst	
																		Bioturbated muddy sst	
11134																Bioturbation. Sand filled burrows		Bioturbated muddy sst	
																Bioturbation		Bioturbated muddy sst	
																		Bioturbated muddy sst	
														Sst	Grey	Bioturbation. Massive	Fine grained, massive, well sorted, well rounded sst.	Massive sst	
11135															Grey			Massive sst	
																		Bioturbated muddy sst	
														Muddy sst	Grey and dark grey	Bioturbation	Very fine grained, well sorted, well rounded sst and mudstone alternation. Bioturbation gives rise to wavy to lenticular bedding.	Bioturbated muddy sst	
11136																		Bioturbated muddy sst	
																		Bioturbated muddy sst	
																		Bioturbated muddy sst	
																		Bioturbated muddy sst	
																		Bioturbated sst	
11137														Sst	Grey	Parallel lamination. Flaser bedding	Fine grained, cross to parallel laminated, well sorted, well rounded sst. There are some mud drapes leading to flaser bedding.	Parallel stratified sst	
																Cross lamination. Flaser bedding		Cross stratified sst	
																		Cross stratified sst	
																Cross lamination	Fine grained, cross laminated, well sorted, well rounded sst.	Cross stratified sst	
11138																		Cross stratified sst	
														Muddy sst	Grey and dark grey	Bioturbation. Wavy bedding	Very fine grained, well sorted, well rounded sst and mudstone alternation.	Bioturbated muddy sst	
																		Cross stratified sst	
														Sst	Grey and dark grey	Cross lamination	Fine grained, cross laminated, well sorted, well rounded sst.	Cross stratified sst	
																		Bioturbated muddy sst	
11139																		Bioturbated muddy sst	
																		Bioturbated muddy sst	
																		Bioturbated muddy sst	
																		Bioturbated muddy sst	
11140																		Bioturbated muddy sst	
																		Bioturbated muddy sst	
																		Bioturbated muddy sst	
																		Bioturbated muddy sst	
11141																		Bioturbated muddy sst	
																		Bioturbated muddy sst	
																		Bioturbated muddy sst	
																		Bioturbated muddy sst	
11142														Muddy sst	Grey and dark grey	Bioturbation		Bioturbated muddy sst	
																		Bioturbated muddy sst	
																		Bioturbated muddy sst	
																		Bioturbated muddy sst	
																		Bioturbated muddy sst	
11143																		Bioturbated muddy sst	
																		Bioturbated muddy sst	
																		Bioturbated muddy sst	
																		Bioturbated muddy sst	
11144																		Very fine grained, well sorted, well rounded sst and mudstone alternation. Lamination/bedding is disturbed due intense bioturbation. In some parts, bioturbation gives rise to wavy to lenticular bedding	











Depth (ft)	Gravel		Sand						Mud	Sorting			Lithology	Color	Structures	Remarks/Description	Lithofacies	
	Cobble	Pebbles	Gravel	VC	C	M	F	VF	Silt	Clay	P	M						G
													Sst	Grey	Massive	Fine grained, massive, well sorted, well rounded sst including some mud rip-up clasts. There is a scour	Massive sst	
													Sst	Dark grey and grey	Bioturbation. Fossils		Bioturbated sandy mud	
													Sst	Grey	Massive	Fine grained, massive, well sorted, well rounded sst including some mud rip-up clasts.	Massive sst	
11194													Mudstone	Dark grey	Bioturbation. Fossils	Bioturbated, fossiliferous mudstone	Bioturbated mudstone	
													Mudstone	Dark grey	Bioturbation. Fossils		Bioturbated mudstone	
													Mudstone	Dark grey	Bioturbation. Fossils		Bioturbated mudstone	
11195													Sst	Grey	Massive	Fine grained, massive, well sorted well rounded sandstone. There is a scour surface at the bottom of the sst. There are some rip-up clasts at the top section	Massive sst	
													Sst	Grey	Massive		Massive sst	
													Mudstone	Dark grey	Bioturbation. Fossils		Bioturbated mudstone	
													Mudstone	Dark grey	Bioturbation. Fossils		Bioturbated mudstone	
11196													Mudstone	Dark grey	Bioturbation. Fossils	Bioturbated, fossiliferous mudstone.	Bioturbated mudstone	
													Mudstone	Dark grey	Bioturbation		Bioturbated mudstone	
													Mudstone	Dark grey	Bioturbation. Fossils		Bioturbated mudstone	
11197													Sandstone	Grey and dark grey	Bioturbation. Parallel bedding. Fossils	Parallel bedded mudstone sandstone alternation. Due to high degree of bioturbation the lamination is disturbed at some sections.	Bioturbated sandy mud	
													Sandstone	Grey and dark grey	Bioturbation		Bioturbated sandy mud	
													Sandstone	Grey and dark grey	Bioturbation		Bioturbated sandy mud	
11198													Sandstone	Grey and dark grey	Bioturbation. Parallel bedding	There is a large sand inclusion	Bioturbated sandy mud	
													Sandstone	Grey and dark grey	Bioturbation. Parallel bedding	Laminated mudstone sandstone alternation. Due to high degree of bioturbation the lamination is disturbed at some sections.	Bioturbated sandy mud	
													Mudstone	Black	Bioturbation		Bioturbated mudstone	
													Mudstone	Black	Bioturbation. Fossils		Bioturbated mudstone	
													Mudstone	Black	Bioturbation	Laminated mudstone. Due to high degree of bioturbation the lamination is disturbed at some sections. Some parts are fossiliferous.	Bioturbated mudstone	
													Mudstone	Black	Bioturbation. Fossils		Bioturbated mudstone	
11200													Mudstone	Black	Lamination. Bioturbation. Fossils		Bioturbated mudstone	
													Sandy mud	Dark grey and grey	Bioturbation. Lamination	Laminated, bioturbated mudstone. Sandstone filled burrow.	Bioturbated sandy mud	
													Mudstone	Black	Bioturbation. Lamination	Laminated, bioturbated mudstone.	Bioturbated mudstone	
													Sandy mud	Dark grey and grey	Bioturbation. Lamination	Mudstone. Includes 2 cm thick sandstone base of which is scoured.	Bioturbated sandy mud	
													Mudstone	Black	Bioturbation		Bioturbated mudstone	
11201													Mudstone	Black	Bioturbation		Bioturbated mudstone	
													Sst	Grey and dark grey	Massive. Mud drapes	Fine grained, massive, well sorted well rounded sandstone and mudstone. There are a few mud drapes at the upper section. Transition from mudstone to sandstone is abrupt.	Massive sst	
													Sst	Grey	Massive		Massive sst	
													Mudstone	Black	Bioturbation		Bioturbated mudstone	
11202													Mudstone	Black	Bioturbation		Bioturbated mudstone	
													Sandy mud	Grey and dark grey	Scour surface, rip-up clasts	Very fine grained, massive, well sorted, well rounded sandstone and mudstone. There are a few rip-up clasts.	Bioturbated mudstone	
													Mudstone	Black	Bioturbation		Bioturbated mudstone	
													Mudstone	Black	Bioturbation		Bioturbated mudstone	
11203													Sst	Grey	Massive. Some rip-up clasts	Fine grained, massive, well sorted well rounded sst. There are a few rip-up clasts.	Massive sst	
													Mudstone	Black	Bioturbation		Bioturbated mudstone	
													Mudstone	Black	Fossils. Bioturbation	Mudstone. Occasionally fossiliferous.	Bioturbated mudstone	
11204													Mudstone	Black	Bioturbation		Bioturbated mudstone	
													Sst	Grey	Massive. Scour surface	Fine grained, massive, well sorted well rounded sandstone. There is a scoured surface at the bottom of	Massive sst	
													Mudstone	Black	Bioturbation, lamination		Bioturbated mudstone	
11205													Mudstone	Black	Bioturbation, lamination		Bioturbated mudstone	
													Mudstone	Black	Bioturbation, lamination		Bioturbated mudstone	

**GHK 1-27 Niece**

Depth (ft)	Gravel			Sand					Mud		Sorting			Lithology	Color	Structures	Remarks/Description	Lithofacies
	Co	Peb	Gra	VC	C	M	L	VF	S	Cl	P	M	G					
11678																		
11679														Muddy sst	Dark grey to grey	Bioturbation		Bioturbated muddy sand
																		Bioturbated muddy sand
														Sst	Grey	Parallel lamination	Fine grained, well sorted, well rounded parallel laminated sst	Parallel stratified sst
																		Parallel stratified sst
11680																		Bioturbated muddy sand
																		Bioturbated muddy sand
																		Bioturbated muddy sand
																		Bioturbated muddy sand
																		Bioturbated muddy sand
11681																		Bioturbated muddy sand
														Muddy sst	Dark grey to grey	Bioturbation		Bioturbated muddy sand
																		Bioturbated muddy sand
																		Bioturbated muddy sand
																		Bioturbated muddy sand
11682																		Bioturbated muddy sand
																		Bioturbated muddy sand
																		Bioturbated muddy sand
																		Bioturbated muddy sand
11683	MISSING SECTION																	
11684																		
11685																		
11686														Muddy sst	Dark grey to grey	Bioturbation		Bioturbated muddy sand
																		Bioturbated muddy sand
	MISSING SECTION																	
																		Bioturbation
																		Bioturbation, parallel lamination
11687																		Fine grained, well sorted, well rounded parallel laminated sst
																		Bioturbated muddy sand
																		Bioturbated muddy sand
																		Bioturbated muddy sand
																		Bioturbated muddy sand
																		Bioturbated muddy sand
11688																		Bioturbated muddy sand
																		Bioturbated muddy sand
																		Bioturbated muddy sand
																		Bioturbated muddy sand
																		Bioturbated muddy sand
																		Bioturbated muddy sand





Depth (ft)	Gravel			Sand				Mud		Sorting			Lithology	Color	Structures	Remarks/Description	Lithofacies	
	Co	Peb	Gra	VC	C	M	LF	VF	S	Cl	P	M						G
11700											X			Mudstone	Black	Massive	Massive mudstone with small amount of fine grains	Massive mudstone
											X			Muddy sand	Dark grey to grey	Bioturbation	Bioturbated sandy mudstone. Sandy parts are medium to fine grained.	Bioturbated muddy sand
											X							Bioturbated muddy sand
											X							Bioturbated muddy sand
11701											X			Sst	Grey		Medium to fine grained, moderately sorted bioturbated sst.	Biourbated sst
											X							Biourbated sst
11702	MISSING SECTION																	
11703	MISSING SECTION																	
11704											X							Orthoconglomerate
											X							Orthoconglomerate
											X							Orthoconglomerate
											X							Orthoconglomerate
11705											X			Congl.	Beige	Massive, occasionally coarsening upward		Orthoconglomerate
											X							Orthoconglomerate
											X							Orthoconglomerate
											X							Orthoconglomerate
											X							Orthoconglomerate
											X							Orthoconglomerate
											X							Orthoconglomerate
11706											X							Orthoconglomerate
											X							Orthoconglomerate
											X							Orthoconglomerate
											X							Orthoconglomerate
											X							Orthoconglomerate
											X							Orthoconglomerate
											X							Orthoconglomerate
											X							Orthoconglomerate
11707											X							Orthoconglomerate
											X							Orthoconglomerate
											X							Orthoconglomerate
											X							Orthoconglomerate
11708											X							Orthoconglomerate
											X							Paraconglomerate
											X							Paraconglomerate
											X							Paraconglomerate
											X							Paraconglomerate
11709											X							Massive sst
											X							Massive sst
											X							Massive sst
											X							Massive sst
11710	MISSING SECTION																	

Depth (ft)	Gravel			Sand					Mud			Sorting			Lithology	Color	Structures	Remarks/Description	Lithofacies
	Co	Peb	Gra	VC	C	M	L	VF	S	Cla	P	M	G						
11711	MISSING SECTION																		
11712													X	Sst	Grey	Massive	Coarse to very coarse grained, rounded to subangular, well to moderately sorted, massive sst.	Massive sst	
													X					Massive sst	
													X				Granule to pebble sized conglomerate. No matrix.	Orthoconglomerate	
													X	Congl.	Beige, greenish, grey, etc.	No structure		Orthoconglomerate	
11713													X				Bioturbation	Orthoconglomerate	
													X	Sandy mud	Grey to dark grey			Bioturbated sandy mud	
													X		Black to grey			Bioturbated sandy mud	
													X					Bioturbated sandy mud	
11714													X			Cross lamination	Grey	Cross stratified sst	
													X					Massive sst	
													X	Sst	Massive			Massive sst	
													X		Dish structures			Massive sst	
11715													X	Muddy sand	Grey to dark grey	No structure	Very coarse to coarse grained sst, poorly sorted, rounded to subrounded grains. Granular grains	Slumped muddy sand	
MISSING SECTION																			
11716													X				Medium to very coarse grained sst poorly sorted, rounded to subrounded grains. Granular grains float in the matrix.	Slumped muddy sand	
													X	Muddy sand	Grey to dark grey	No structure		Slumped muddy sand	
													X					Slumped muddy sand	
													X					Slumped muddy sand	
11717													X				Massive mudstone with small amount of grains	Massive mudstone	
													X	Mudstone	Black			Massive mudstone	
													X					Massive mudstone	
													X					Massive mudstone	
11718													X				Massive. Few granules	Slumped sandy mudstone	
													X					Slumped sandy mudstone	
													X	Sandy mud	Grey to black			Slumped sandy mudstone	
													X					Slumped sandy mudstone	
11719													X				Granules and pebbles	Slumped sandy mudstone	
													X	Mudstone				Pebbly mudstone	
													X					Pebbly mudstone	
													X					Pebbly mudstone	
11720													X	Sandy mud	Black to dark grey	Granules and pebbles	Slumped sandy mudstone		
													X					Slumped sandy mudstone	
													X	Mudstone				Pebbly mudstone	
													X					Pebbly mudstone	
11721													X					Slumped sandy mudstone	
													X					Slumped sandy mudstone	
													X					Slumped sandy mudstone	
													X					Slumped sandy mudstone	



Depth (ft)	Gravel			Sand				Mud		Sorting			Lithology	Color	Structures	Remarks/Description	Lithofacies	
	Co	Peb	Gra	VC	C	M	LF	VF	S	Cla	P	M						G
11734																		
11735																		
11736																		
11737																		
11738										X			Muddy sand	Dark grey	Massive		Slumped muddy sand	
									X									Slumped muddy sand
									X									Slumped muddy sand
									X									Slumped muddy sand
									X									Slumped muddy sand
11739										X			Sst	Grey			Massive sandstone	
										X							Massive sandstone	
										X							Massive sandstone	
11740										X							Slumped sandy mud	
										X							Slumped sandy mud	
										X							Slumped sandy mud	
										X							Slumped sandy mud	
										X							Slumped sandy mud	
11741										X			Sandy mud	Blackish, dark grey to grey	Bioturbation, distorted bedding		Slumped sandy mud	
										X								Slumped sandy mud
										X								Slumped sandy mud
										X								Slumped sandy mud
										X								Slumped sandy mud
11742										X							Slumped sandy mud	
										X							Slumped sandy mud	
										X							Slumped sandy mud	
11743										X							Slumped sandy mud	
										X							Slumped sandy mud	
										X							Slumped sandy mud	
										X							Slumped sandy mud	
11744										X			Sandy mud	Grey, black. Pebbles are white	Massive. Pebbles		Slumped sandy mud	
										X								Slumped sandy mud
										X								Slumped sandy mud

Depth (ft)	Gravel			Sand				Mud		Sorting			Lithology	Color	Structures	Remarks/Description	Lithofacies	
	Co	Peb	Gra	VC	C	M	L	VF	S	Cl	P	M						G
											X							Slumped sandy mud
											X							Slumped sandy mud
											X							Slumped sandy mud
11745											X							Pebbly mudstone
											X							Pebbly mudstone
MISSING SECTION																		
11746											X			Conglomerate	Beige, grey, greenish		Pebble sized, poorly sorted, subangular to subrounded grains floating in coarse grained matrix.	Paraconglomerate
MISSING SECTION																		
11747																		
											X			Conglomerate	Beige, grey, greenish	No structure	Pebble to granular sized, poorly sorted, angular to rounded grains in contact with each other. Generally floating in granular matrix.	Orthoconglomerate
											X			Conglomerate	Beige, grey, greenish	No structure	Pebble to granular sized, poorly sorted, angular to rounded grains in contact with each other. Generally floating in granular matrix.	Orthoconglomerate
											X			Conglomerate	Beige, grey, greenish	No structure	Pebble to granular sized, poorly sorted, angular to rounded grains in contact with each other. Generally floating in granular matrix.	Orthoconglomerate
MISSING SECTION																		
11749																		
11750																		
											X			Conglomerate	Beige, grey, greenish	No structure	Pebble sized, poorly sorted, subrounded grains floating in coarse grained matrix.	Paraconglomerate
											X			Conglomerate	Beige, grey, greenish	No structure	Pebble sized, poorly sorted, subrounded grains floating in coarse grained matrix.	Paraconglomerate
11751																		
MISSING SECTION																		
11752											X			Conglomerate	Beige, grey, greenish	No structure	Pebble sized, poorly sorted, subrounded grains floating in coarse grained matrix.	Paraconglomerate
MISSING SECTION																		
11753											X			Conglomerate	Beige, grey, greenish	No structure	Pebble sized, poorly sorted, subangular to rounded grains floating in medium grained matrix.	Paraconglomerate
											X			Conglomerate	Beige, grey, greenish	No structure	Pebble sized, poorly sorted, subangular to rounded grains floating in medium grained matrix.	Paraconglomerate
											X			Conglomerate	Beige, grey, greenish	No structure	Pebble sized, poorly sorted, subangular to rounded grains floating in medium grained matrix.	Paraconglomerate
MISSING SECTION																		
11754																		
											X			Conglomerate	Beige, grey, greenish	No structure	Pebble sized, poorly sorted, subangular to subrounded grains	Paraconglomerate
11755											X			Conglomerate	Beige, grey, greenish	No structure	Pebble sized, poorly sorted, subangular to subrounded grains	Paraconglomerate

Depth (ft)	Gravel			Sand					Mud		Sorting			Lithology	Color	Structures	Remarks/Description	Lithofacies																		
	Co	Peb	Gra	VC	C	M	F	VF	Sz	Cla	P	M	G																							
														ate	grey, greenish	No structure	floating in coarse to very coarse grained matrix.	Paraconglomerate Paraconglomerate																		
MISSING SECTION																																				
11756														Sst	Grey	Parallel bedding	Medium grained, well sorted well rounded, parallel bedded sst.	Parallel stratified sst Parallel stratified sst Parallel stratified sst Parallel stratified sst Parallel stratified sst																		
11757	MISSING SECTION																																			
11758																			MISSING SECTION																	
11759																																				
11760														Grey	Massive		Massive sst Massive sst Massive sst Massive sst Massive sst																			
11761																		Massive. Dish structures	Massive sst Massive sst																	
11762														Grey dark grey	Parallel bedding		Parallel stratified sst Parallel stratified sst Parallel stratified sst																			
															Massive		Massive sst Massive sst Massive sst																			
11763	MISSING SECTION																																			
11764														Sst	Grey	Massive	Coarse grained, well sorted, well rounded	Massive sst Massive sst Massive sst Massive sst																		
11765	MISSING SECTION																																			
11766	MISSING SECTION																																			

Depth (ft)	Gravel			Sand					Mud		Sorting			Lithology	Color	Structures	Remarks/Description	Lithofacies
	Co	Peb	Gra	VC	C	M	L	VF	S	Cl	P	M	G					
												X	Sst	Grey	Cross bedding Parallel bedding	Medium grained, well sorted well rounded, parallel to low angle cross bedded sst.	Cross stratified sst Parallel stratified sst	
11767	MISSING SECTION																	
												X	Sst	Grey	Massive	Medium grained, well sorted well rounded, massive sst.	Massive sst	
11768											X	Sst	Grey	Massive	Medium grained, well sorted well rounded, massive sst.	Massive sst		
											X	Sst	Grey	Massive	Medium grained, well sorted well rounded, massive sst.	Massive sst		
											X	Sst	Grey	Massive	Medium grained, well sorted well rounded, massive sst.	Massive sst		
11769	MISSING SECTION																	
11770	MISSING SECTION																	
11771	MISSING SECTION																	
11772											X	Sst	Grey	Massive			Massive sst	
											X	Sst	Grey	Massive			Massive sst	
											X	Sst	Grey to beige	Bioturbation			Bioturbated sst	
											X	Sst	Grey to beige	Bioturbation			Bioturbated sst	
											X	Sst	Grey to beige	Bioturbation			Bioturbated sst	
11773	MISSING SECTION																	
11774	MISSING SECTION																	
11775											X	Sst	Light to dark grey	Bioturbation	Very fine grained, highly bioturbated sand		Bioturbated sst	
											X	Sst	Light to dark grey	Bioturbation	Very fine grained, highly bioturbated sand		Bioturbated sst	
											X	Sst	Light to dark grey	Bioturbation	Very fine grained, highly bioturbated sand		Bioturbated sst	
											X	Sst	Light to dark grey	Bioturbation	Very fine grained, highly bioturbated sand		Bioturbated sst	
											X	Sst	Light to dark grey	Bioturbation	Very fine grained, highly bioturbated sand		Bioturbated sst	
11776											X	Sst	Light to dark grey	Bioturbation	Very fine grained, highly bioturbated sand		Bioturbated sst	
											X	Sst	Light to dark grey	Bioturbation	Very fine grained, highly bioturbated sand		Bioturbated sst	
11777	MISSING SECTION																	

Depth (ft)	Gravel			Sand					Mud		Sorting		Lithology	Color	Structures	Remarks/Description	Lithofacies
	Co	Peb	Gra	VC	C	M	L	VF	S	Cl	P	M					
11778											X		Sst	Light to dark grey	Bioturbation	Very fine grained, highly bioturbated sand	Bioturbated sst
										X		Bioturbated sst					
										X		Bioturbated sst					
										X		Bioturbated sst					
										X		Bioturbated sst					
11779											X						Bioturbated sst
11780																	
11781																	
11782																	
11783																	
11784											X		Muddy sand	Grey to black	Bioturbation	Highly bioturbated, muddy sand	Bioturbated muddy sand
										X		Bioturbated muddy sand					
										X		Bioturbated muddy sand					
										X		Bioturbated muddy sand					
										X		Bioturbated muddy sand					
										X		Bioturbated muddy sand					
										X		Bioturbated muddy sand					
										X		Bioturbated muddy sand					
11785											X						Bioturbated muddy sand
											X						Bioturbated muddy sand
											X						Bioturbated muddy sand
11786																	
11787											X		Muddy sand	Grey to black	Bioturbation	Original paralel stratification (sand-mud intercalation) is distorted by the intense bioturbation.	Bioturbated muddy sand
										X		Bioturbated muddy sand					
										X		Bioturbated muddy sand					
										X		Bioturbated muddy sand					
										X		Bioturbated muddy sand					
										X		Bioturbated muddy sand					
										X		Bioturbated muddy sand					
										X		Bioturbated muddy sand					
11788											X						Bioturbated muddy sand
											X						Bioturbated muddy sand
											X						Bioturbated muddy sand
											X						Bioturbated muddy sand



Depth (ft)	Gravel			Sand				Mud			Sorting			Lithology	Color	Structures	Remarks/Description	Lithofacies
	Co	Peb	Gra	VC	C	M	L	VF	S	Cl	P	M	G					
11789												X	X			Bioturbation. Parallel bedded		Bioturbated muddy sand
												X	X					Bioturbated muddy sand
	MISSING SECTION																	
11790																		
												X	X	Sst	Grey	Massive. Fluid escape structures		Massive sst
												X	X					Massive sst
11791																		
	MISSING SECTION																	
													X					Bioturbated sst
													X	Sst	Grey	Bioturbation. Fluid escape structures		Bioturbated sst
11792													X					Bioturbated sst
													X					Bioturbated sst
													X					Bioturbated sst
													X					Bioturbated sst
11793																		
	MISSING SECTION																	
												X	X	Muddy sand	Grey to black	Bioturbation		Bioturbated muddy sand
11794												X	X					Bioturbated muddy sand
	MISSING SECTION																	
												X	X	Sst	Grey	Massive		Massive sst
	MISSING SECTION																	
11795												X	X	Sst	Grey	Massive		Massive sst
												X	X					Massive sst
	MISSING SECTION																	
11796																		
												X	X	Sst	Grey	Massive		Massive sst
												X	X					Massive sst
11797																		
	MISSING SECTION																	
												X	X	Sst	Grey	Massive		Massive sst

### Appendix C: Thin-Section Photomicrographs

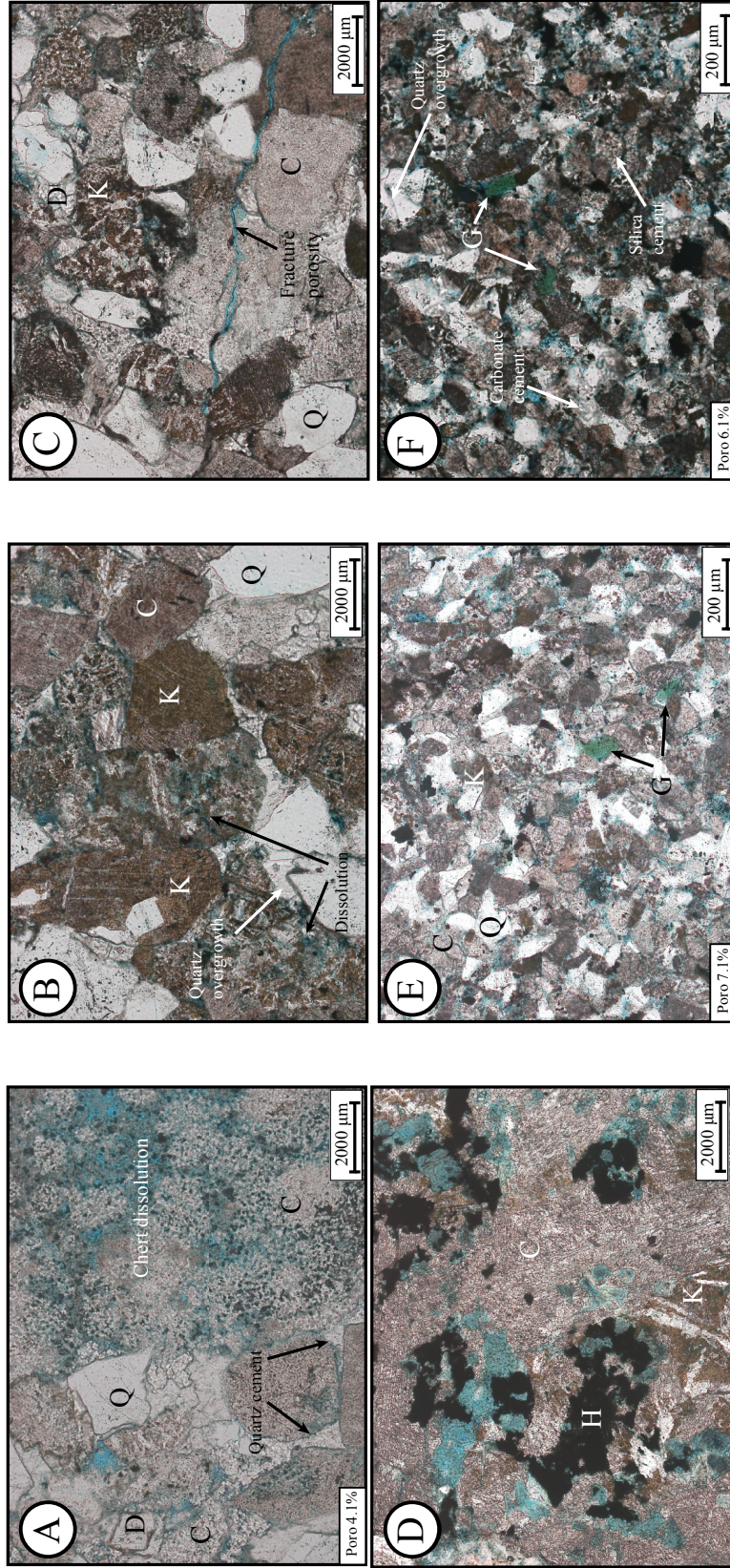


Figure C-1. Conglomerate (A-D) and sandstone (E, F) samples under thin section. Conglomerate consists mostly of rounded to sub-angular quartz, feldspar, biotite, chert, glauconite clasts, and granitic rock fragments. Sandstones have the same mineralogy with less rock fragments. Clasts composing sandstones are more angular. Feldspars are highly altered and occasionally replaced by carbonate cement. Potassium feldspars are stained to dark yellow. Most of the porosity is secondary. Quartz overgrowths are common. A) Chert dissolution, B) K- feldspar dissolution, C) Fracture porosity, D) Secondary porosity partly filled with hematite, E) Medium-grained sandstone with smaller pore spaces mostly developed by dissolution of feldspars. F) Fine-grained slightly bioturbated sandstone with less porosity. Q: Quartz, K: Potassium feldspar, C: Chert, H: Hematite, D: Dolomite, G: Glauconite.

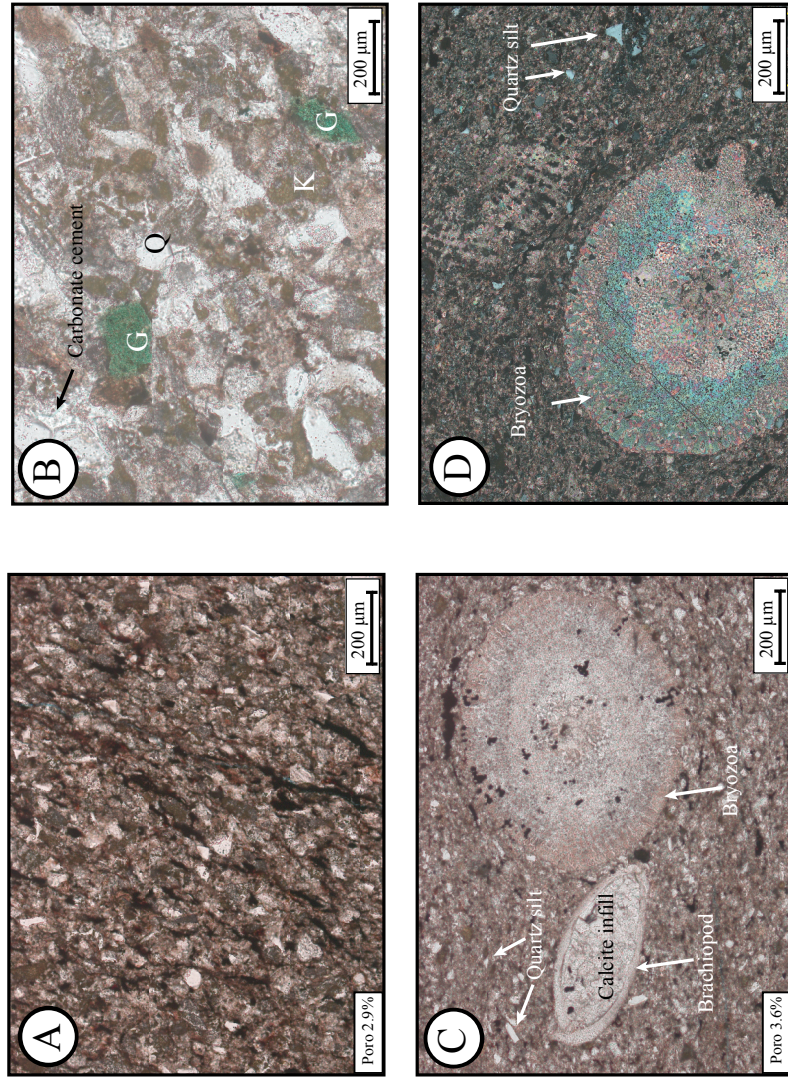


Figure C-2. A, B) Thin section from bioturbated muddy sandstone lithofacies. Bioturbated muddy sandstone is composed of angular to sub-angular quartz, feldspar, glauconite clasts with abundant clay minerals. Q: Quartz, K: Potassium feldspar, G: Glauconite. C) Thin section from bioturbated mudstone lithofacies. Bioturbated mudstone has silt-sized quartz clasts and fossil shells. D) Thin section from the same bioturbated mudstone under cross-polarized light.

## Appendix D: Spectral Gamma-Ray Data

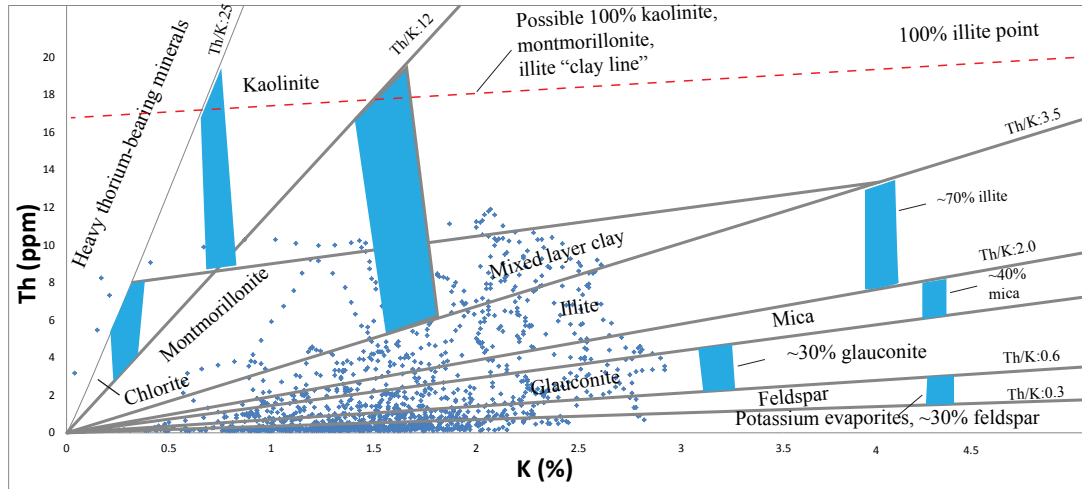


Figure D-1. Thorium (Th) vs. potassium (K) cross plot for mineral identification using spectral gamma-ray data for the cored interval (GHK 1-34 Finnell). Notice the high abundance of data within the feldspar and glauconite region. Data points within the illite and mixed clay layer region belong to mudstone (chart is by Schlumberger).

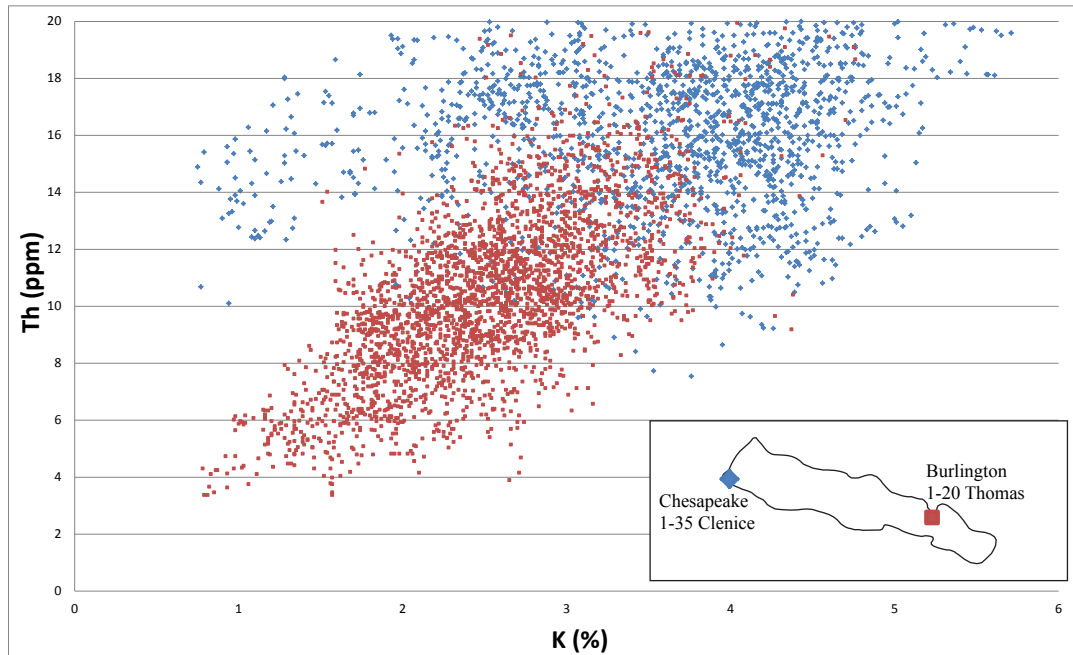


Figure D-2. Thorium (Th) vs. potassium (K) cross-plot for two wells located in Beckham County (blue) and Washita County (red). Th and K values are from spectral gamma ray log. On the west side potassium content is found to be higher than on the east side.

## Appendix E. Artificial Neural Network Analysis

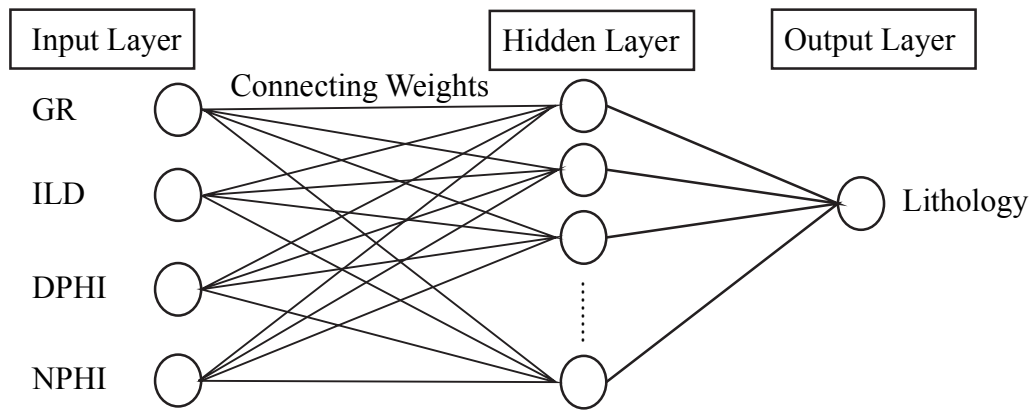


Figure E-1. Schematic diagram showing the architecture of the Artificial Neural Network. Modified from Kumar and Kisra, 2006; Verma et. al., 2014.

The standard workflow of back propagation method used in this work consists of the following steps:

- 1) Initialize the network synaptic weights to small random values.
- 2) From the set of training input/output pairs, present an input pattern and calculate the network response.
- 3) The desired network response is compared with the actual and using the equations, the local errors are computed.
- 4) The weights of the network are updated.
- 5) Step 2 to step 4 are repeated until a minimum overall error is obtained.

In general, suppose there are “n” number of inputs ( $x_1, x_2, x_3, \dots, x_n$ ) and one output, then the output ( $y$ ) can be presented by following relationship:

$$y = f(\text{net}) = f\left(\sum_{i=1}^n w_i x_i\right)$$

$$\text{net} = w^T x = w_1 x_1 + w_2 x_2 + \dots + w_n x_n$$

where “ $f(\text{net})$ ” refers to activation or transfer function and, “ $w_i$ ” is the weight vector.

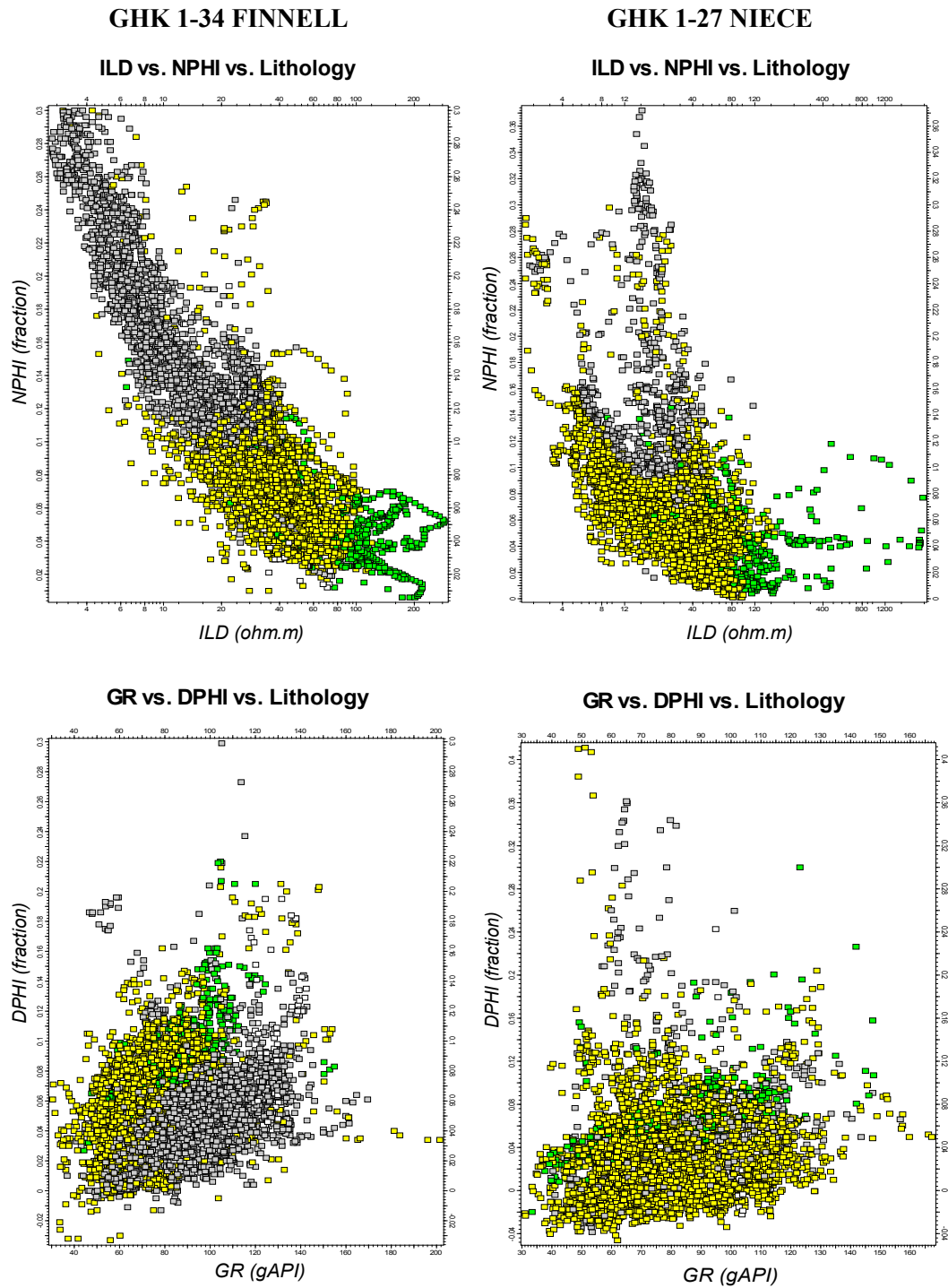


Figure E-2. Cross plots of deep-resistivity vs. neutron-porosity and gamma-ray vs. density-porosity color coded by lithology for the cored wells. Lithologies are estimated from Artificial Neural Network (ANN). Although the lithologies clustered somehow there is still unrealistic estimations.

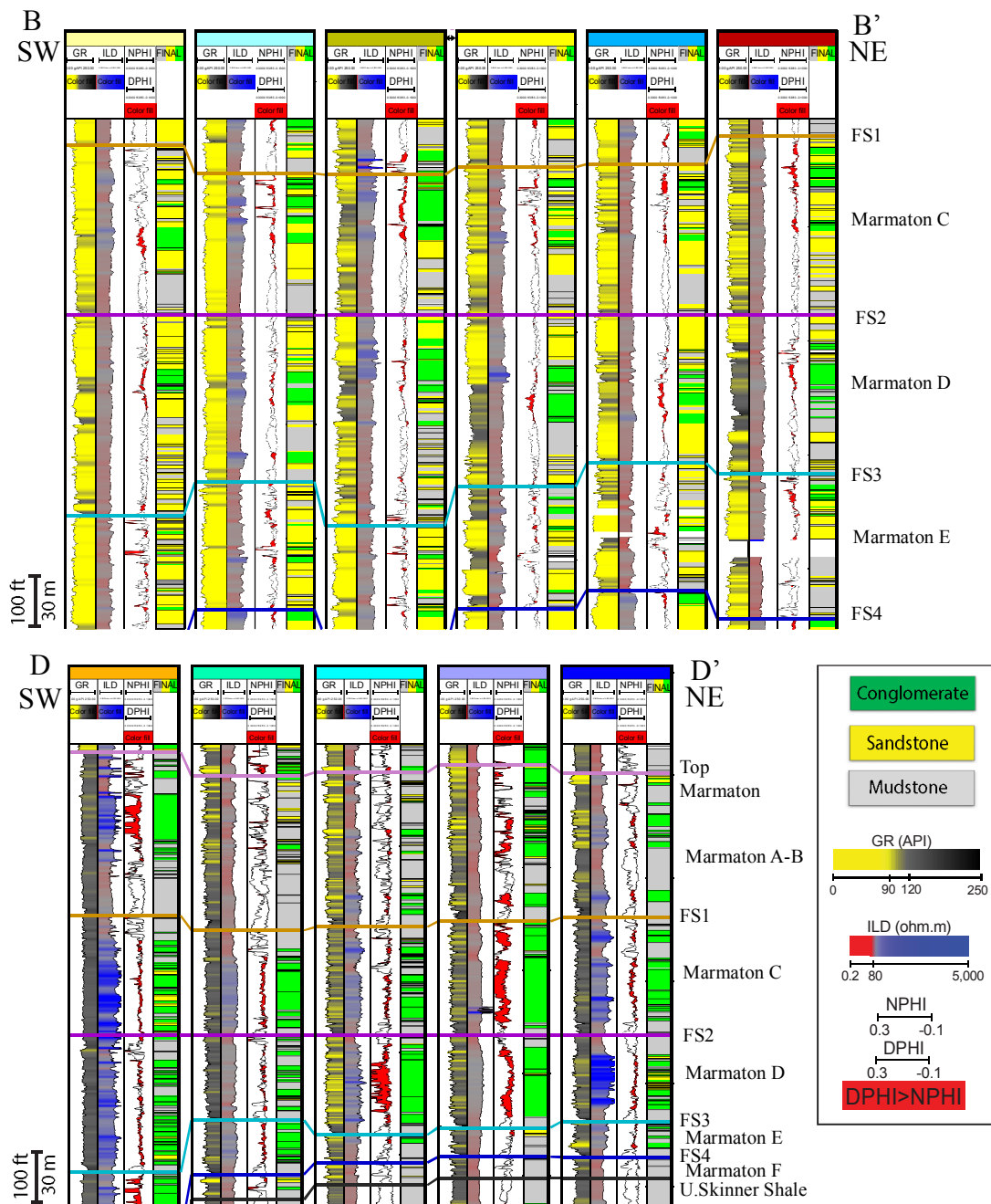


Figure E-3. Stratigraphic cross sections with estimated lithologies using the combination of ANN and gamma-ray cut-off values, and porosity-lithology relation. GR: Gamma-ray; ILD: Deep-resistivity; NPHI: Neutron-porosity; DPHI: Density-porosity. Refer to figure 2 for the location of the cross sections. Sections are flattened on the 2nd Marmaton flooding surface. Note that intervals with high gamma-ray values accompanied by the separation of porosity logs and low resistivity are classified as mudstones while those with high gamma-ray values accompanied by cross-over of porosity logs and high resistivity are classified as conglomerates. Intervals with relatively lower gamma-ray and lower resistivity with cross-over or low separation are classified as sandstones. The west side of the study area (cross section D-D') includes more conglomerate than the east side (cross section C-C'). This could be the effect of proximity to the source area.



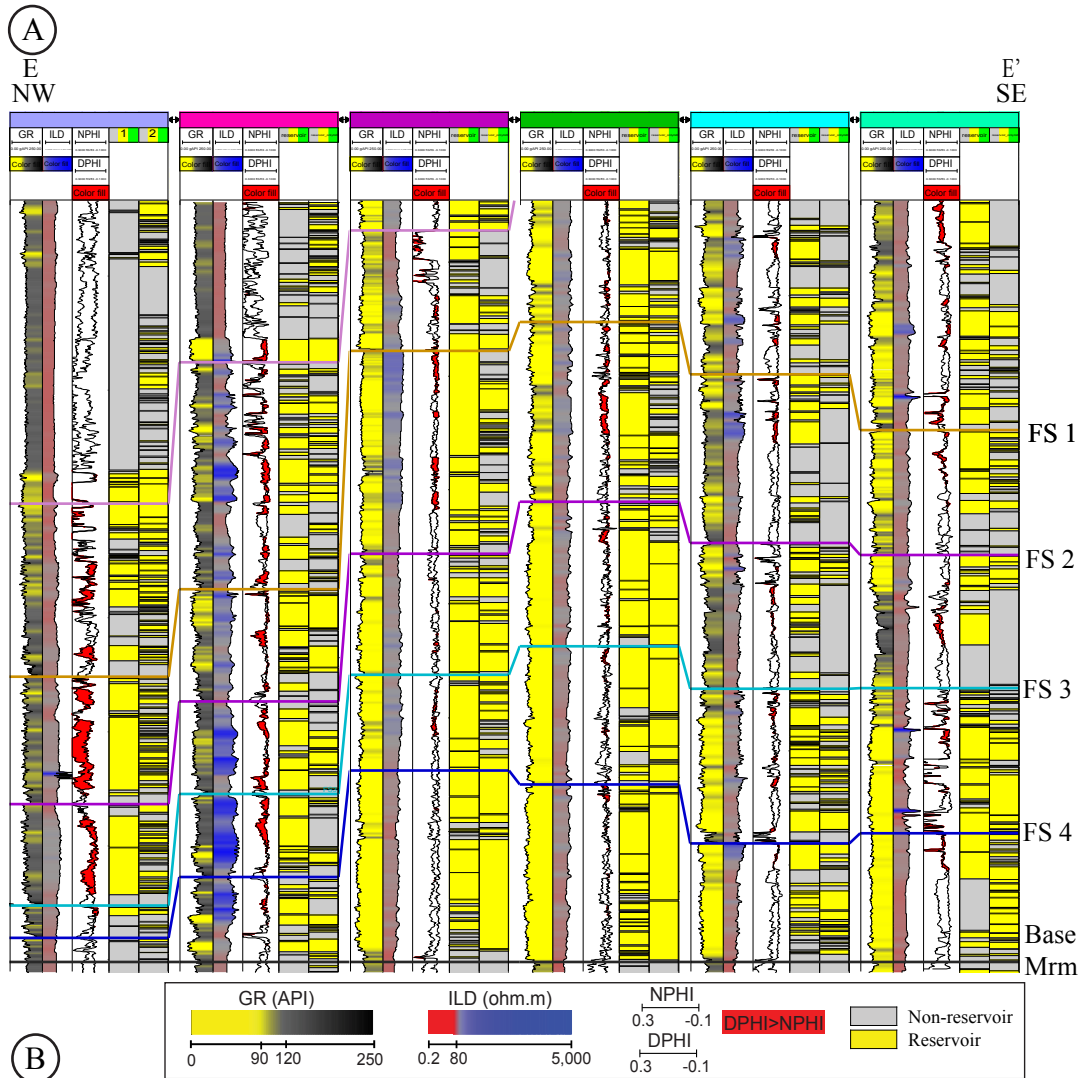


Figure E-4. A) Stratigraphic cross-section flattened on the Upper Skinner shale (Base Marmaton). Refer to figure 2 for the location of the cross section. GR: gamma-ray, ILD: deep-resistivity, NPHI: neutron-porosity, DPHI: density-porosity, Mrm: Marmaton. 1) estimated lithology logs by combining Artificial Neural Network, GR cut-off values and the relation between lithology and porosity. Conglomerates and sandstones are merged under reservoir group. 2) Estimated lithology logs by only using GR cut-off values. 120 API and 105 API cut-off values are used on the northwest and southeast side of the study area, respectively. Note the underestimated reservoir intervals by the GR cut-off values analysis. B) Histogram showing the percent of reservoirs and non-reservoirs in the well-logs for each zone estimated by combining Artificial Neural Network (ANN), GR cut-off values and the relation between lithology and porosity (blue), and by only using GR cut-off values (red). There is significant amount of underestimation of reservoirs in the GR cut-off value analysis.

## Appendix F. Lithofacies and Interpretation of Depositional Setting

Lithology	Lithofacies	Description	Depositional Setting	%
CONGLOMERATES	Orthoconglomerate (C1)	Pebble-to granule-sized, poorly sorted, rounded to sub-angular clasts mostly granitic with different colors. Clast supported. They are in contact with each other	Sub-aerial proximal fan (channelized)	3.6
	Paraconglomerate (C2)	Pebble sized, poorly sorted, rounded to subangular granitic clasts floating in fine to medium grained sandstone matrix. Abundant matrix separating the clasts from each other	Sub-aerial proximal fan debris flow (unchannelized)	4.8
SANDSTONES	Parallel-stratified (S1)	Grey to beige, fine-to medium-grained, well sorted, well rounded. Transitional with the cross-stratified sandstones. Occasionally have burrows.	Proximal to medial fan	4.6
	Cross-stratified (S2)	Grey to beige, fine-to coarse-grained, well to moderately sorted, low angle cross-bedded. Mostly underlying the conglomerates with sharp scoured surfaces and overlying muddy sand intervals	Proximal to medial fan	4.5
	Structureless (S3)	Grey, medium-to very coarse-grained, well sorted, well rounded. Occasionally show convoluted bedding indicating slump. Sometimes overlying shelf mudstones with scoured surfaces	Medial to distal fan; shelf	10.4
	Granule-pebble bearing (S4)	Grey, medium-to coarse-grained, well sorted, rounded to sub-rounded sand with well-oriented granule sized clasts. Sands are parallel or cross-stratified	Proximal to medial fan; fluctuations between upper and lower flow regimes	0.4
	Bioturbated (S5)	Light to dark grey, fine-to medium-grained, well sorted	Medial to distal fan	11.0

Lithology	Lithofacies	Description	Depositional Setting	%
MUDDY SANDSTONES	Bioturbated (MS1)	Intercalated fine-to very fine-grained sandstone/siltstone and mudstone layers distorted with bioturbation. Occasionally, primary bedding structures can be observed	Distal fan; low energy conditions	18.4
	Slumped (MS2)	Medium-to coarse-grained, moderately to poorly sorted, sub-rounded to sub-angular sandstone and black mudstone with deformed structure that might indicate slump. Occasionally, there are light grey granule to pebble-sized clasts floating in sandstone-mudstone matrix. Poorly sorted, chaotic structure as a whole	Proximal fan	3.5
SANDY MUDSTONES	Bioturbated (SM1)	Intercalated very fine-grained sandstone and mudstone layers distorted with bioturbation. Occasionally with fossil shells	Transitional to marine, prodelta	12.8
	Slumped (SM2)	Dark grey to black mudstones intercalated with grey to beige sandstones. Lots of distorted bedding; poorly sorted, chaotic structure	Proximal fan	0.8
MUDSTONES	Bioturbated (M1)	Dark grey, carbonate rich mudstone with various degree of bioturbation. Lamination is preserved occasionally where the degree of bioturbation is less	Prodelta and shelf	12.3
	Fossiliferous (M2)	Dark grey, carbonate rich mudstone with abundant fossils, mostly crinoid and bivalves	Prodelta and shelf	7.5
	Pebbly (M3)	Light grey, pebble-sized, subangular to subrounded clasts floating in black mudstone matrix	Proximal to medial fan	2.7
	Massive (MS4)	Black, massive mudstone with abundant fractures	Prodelta and shelf	2.7

## Appendix G: Structural and Stratigraphic Framework

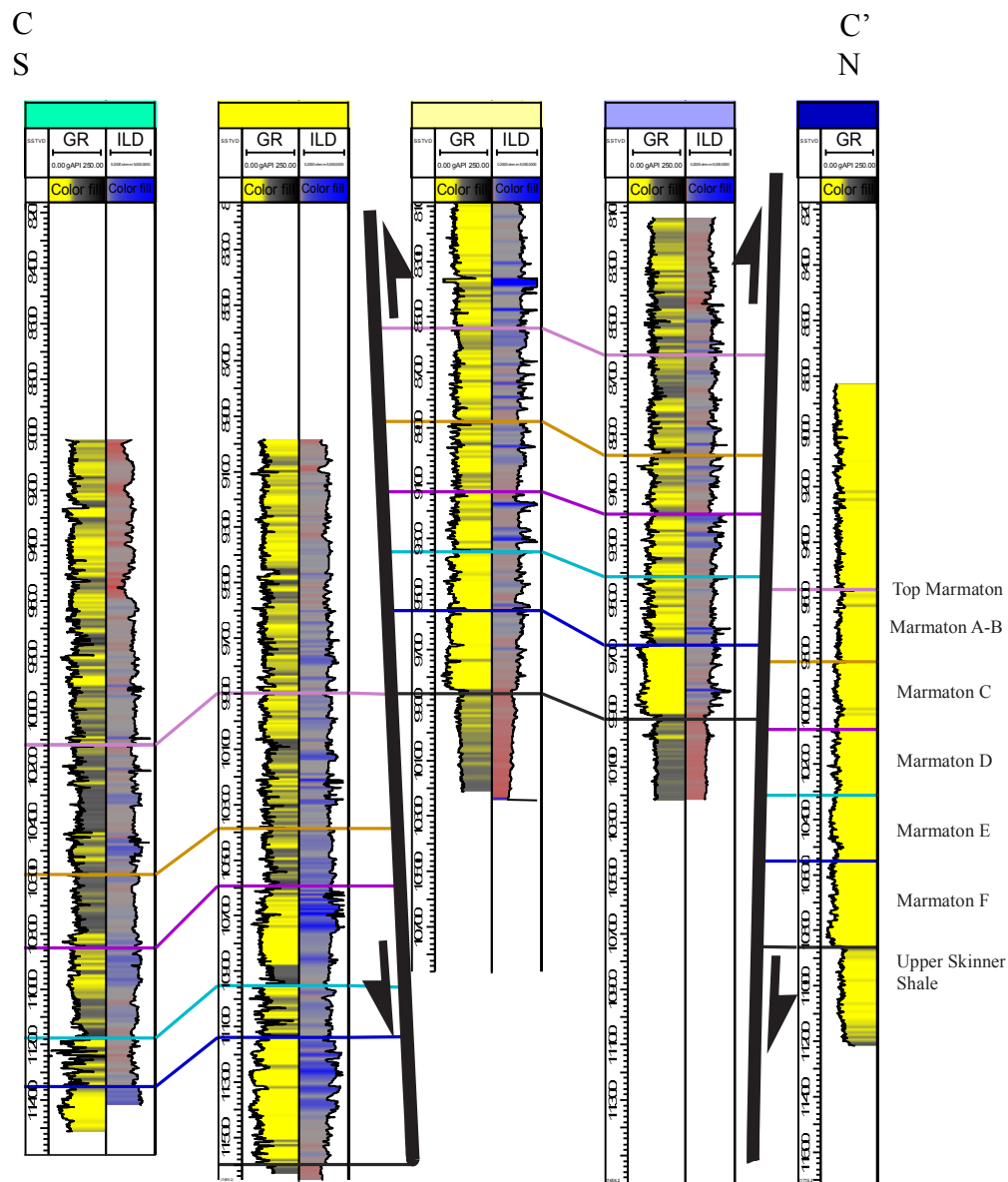


Figure G-1. Structural cross section with wireline logs and formation tops. Refer to figure 2 for the location of the cross section. The wells are equally spaced. Significant changes in the structural elevation of the formation tops are interpreted as a faulted anticline.

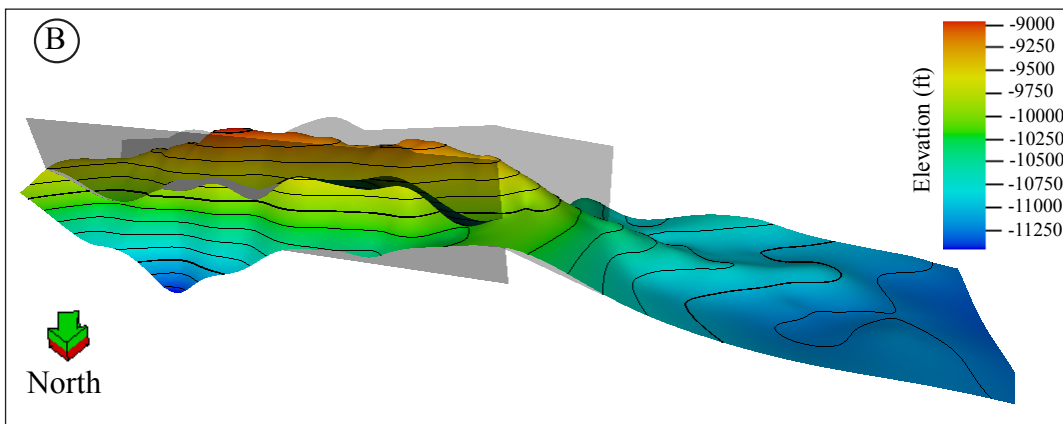
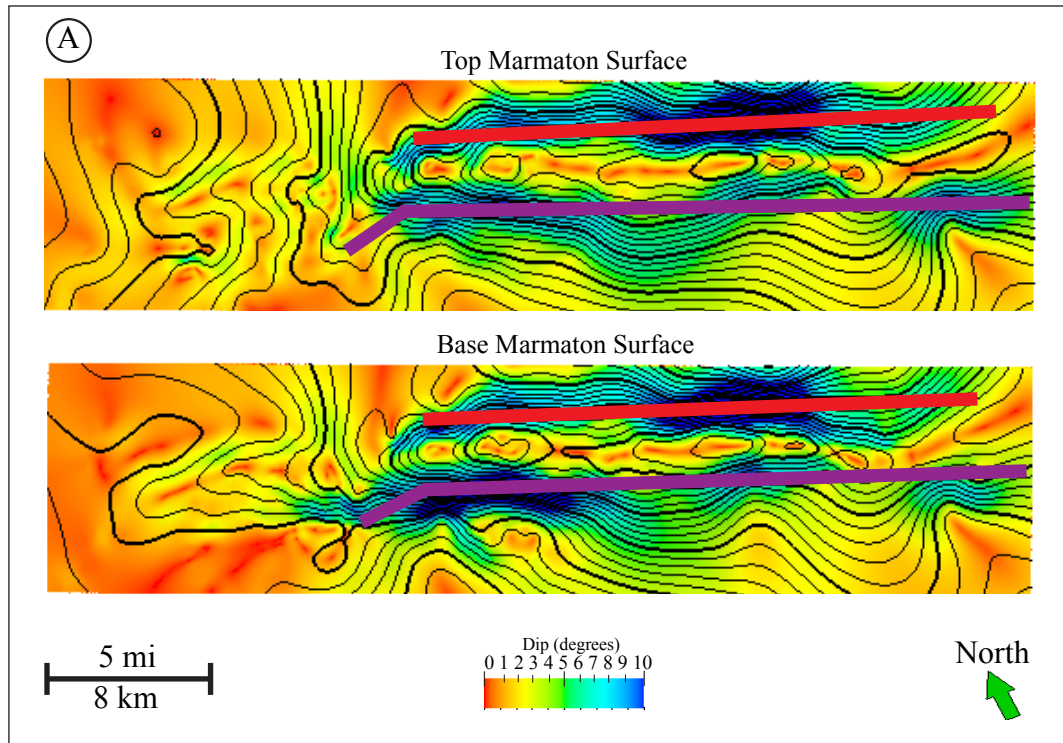


Figure G-2. A) Structural contour map for the top and base Marmaton Group. Colors indicate the dip magnitude. Two fault traces are picked along the structural contours with high dip magnitude. According to the location of the fault traces the faults were interpreted to have reverse movements although the available data is not enough for making a confident interpretation on the type of the fault. B) 3-D view of the faulted 2<sup>nd</sup> Marmaton flooding surface with the interpreted fault planes on both sides of the anticline.

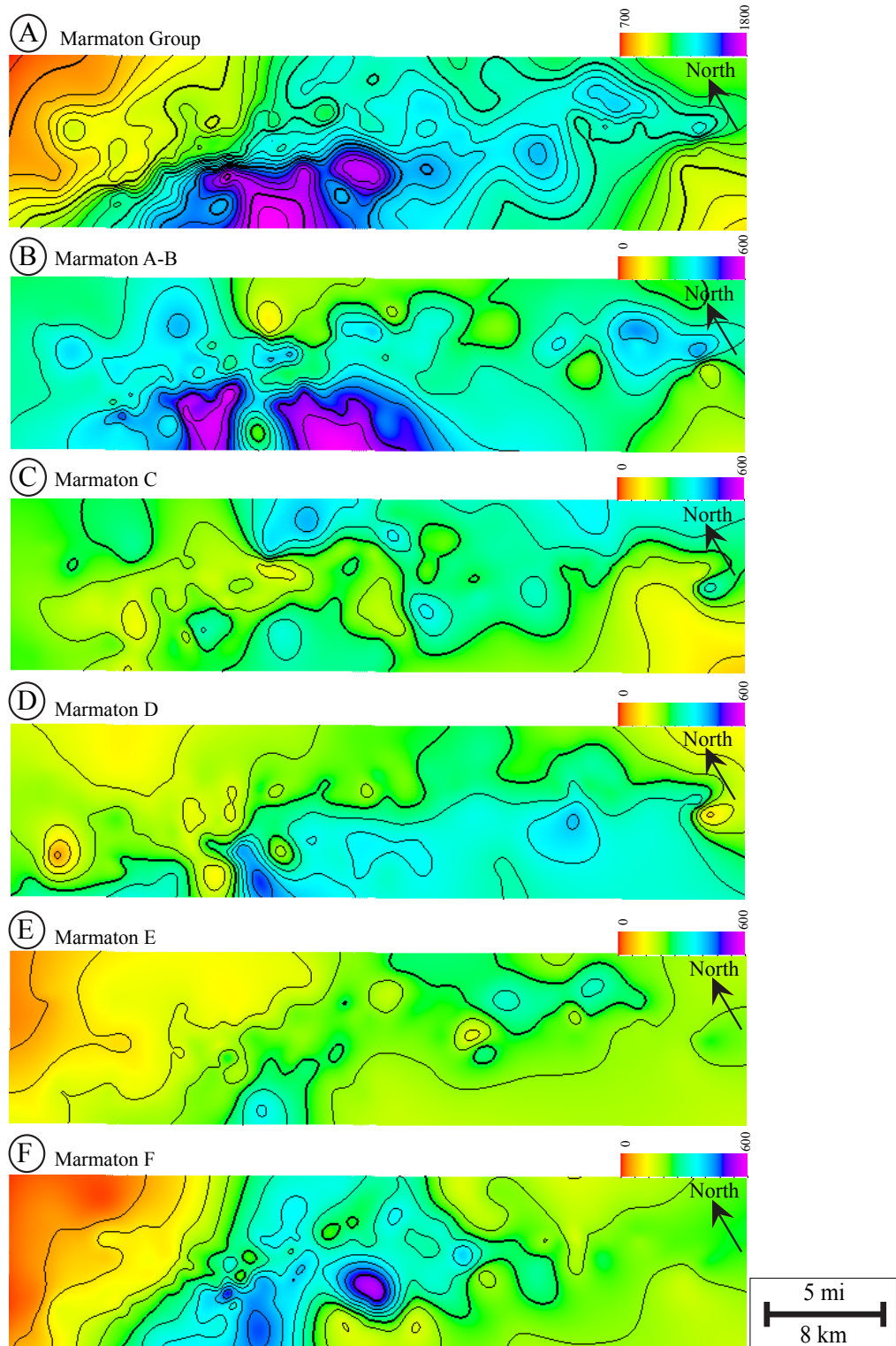


Figure G-3. Isopach maps for the Marmaton Group and the Marmaton Wash zones. A) Marmaton Group is thickest on the south-central part and thins away from here in all direction. B-F) Thickness changes across the field is likely associated with the different accommodation space at the time of deposition. They thin toward north. Marmaton E and Marmaton F zones thicken toward east.

## Appendix H. Upscaled Lithology Logs

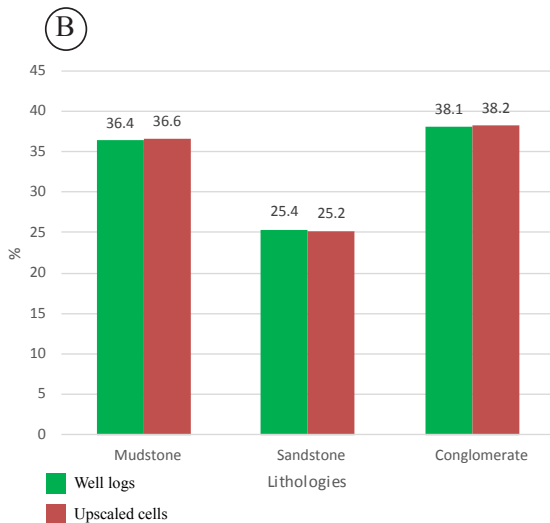
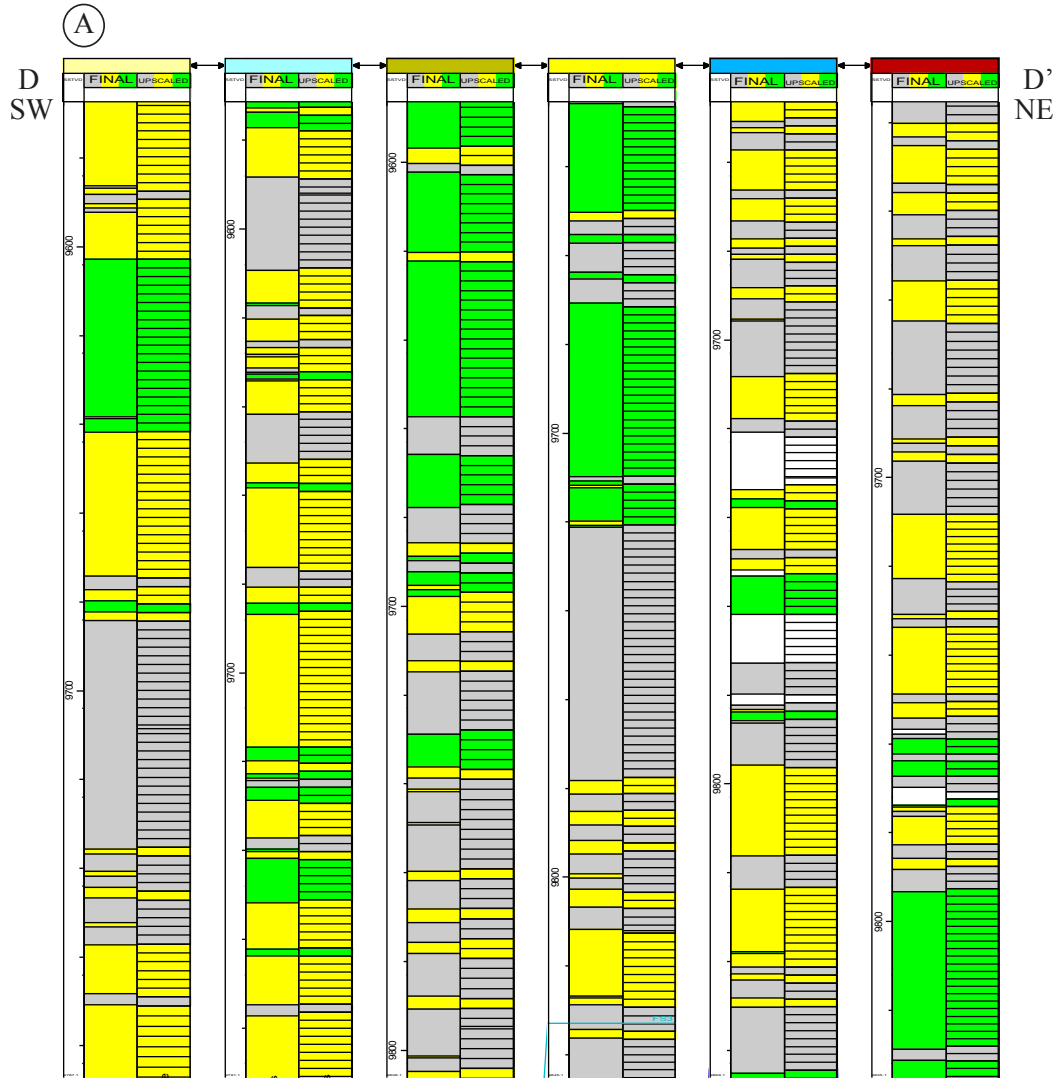
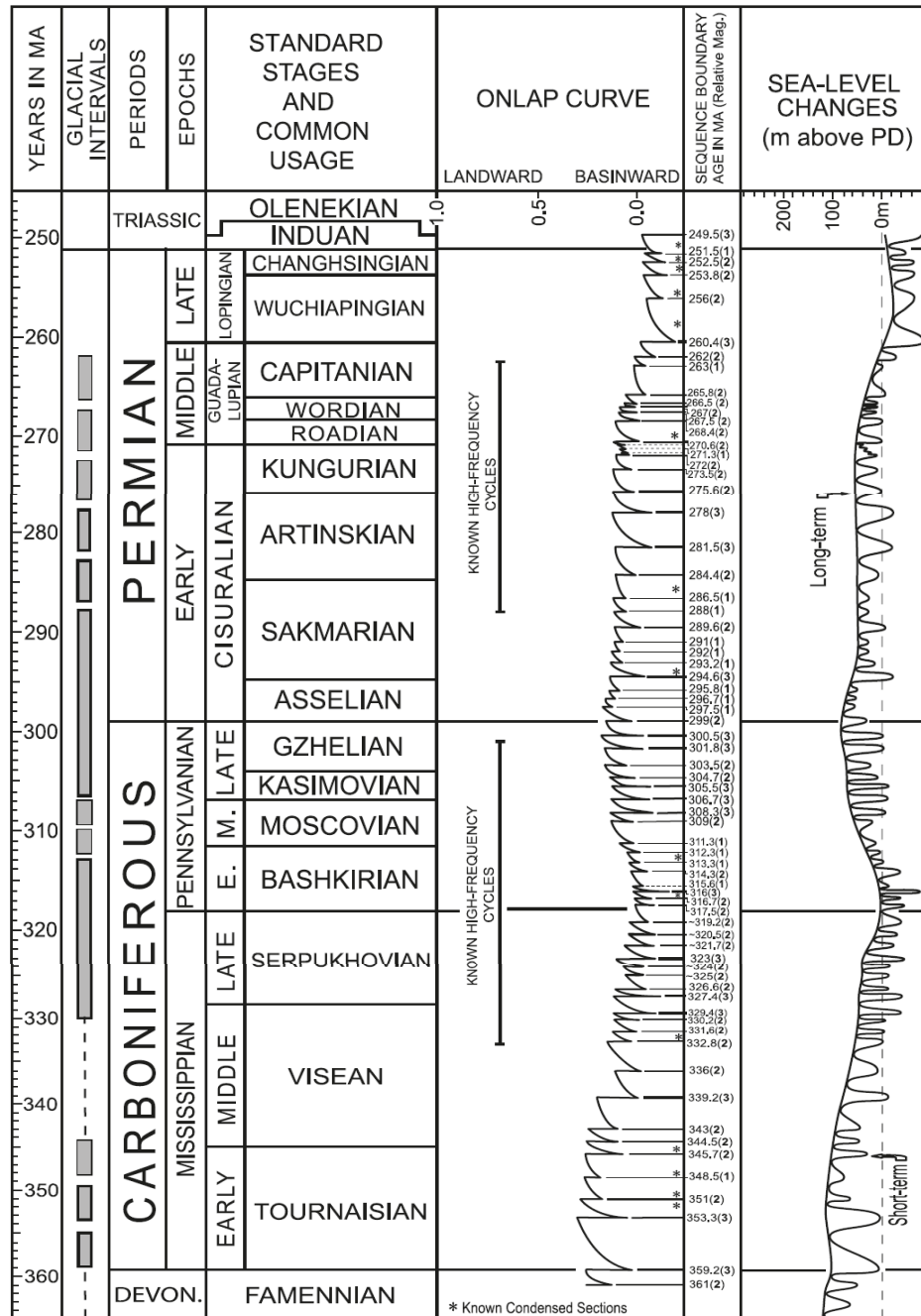


Figure H. A) Structural cross section D-D' showing the estimated lithology logs and the upscaled lithology logs. Refer to figure 2 for location of the cross section. Average 1.5 ft of layering thickness is adequate for capturing the lithologies satisfactorily. B) Histogram showing the percent of lithologies in the original estimated lithology logs and the upscaled lithology logs. They are almost the same which means that the upscaling is satisfactory and the upscaled logs can be used in the modeling confidently.

## Appendix I. Sea Level Curve for Carboniferous-Permian



Carboniferous-Permian sea-level changes. Modified from Haq and Schutter, 2008.



## Appendix J: Lithology Models and Maps

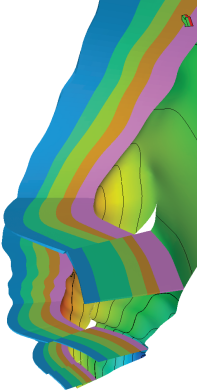
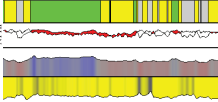
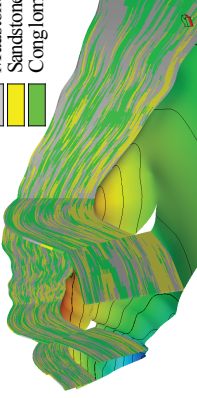
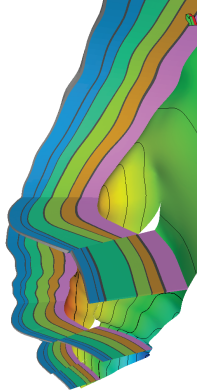
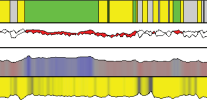
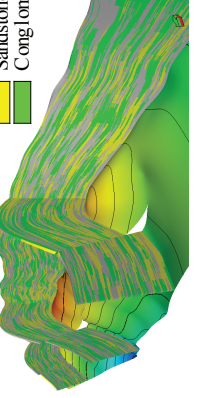
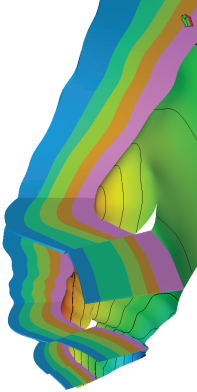
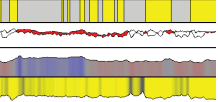
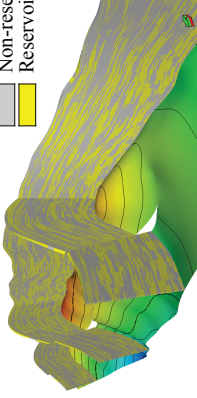
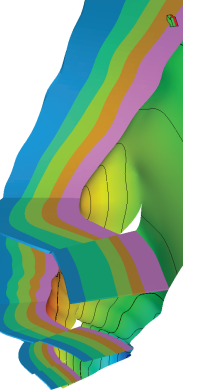
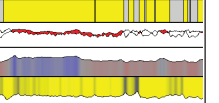
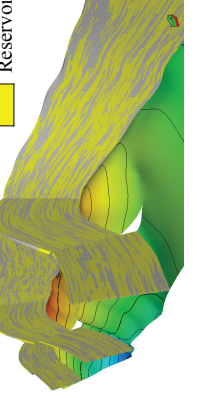
	3-D Grid	Lithology Log	Lithology Model
Sequence Lithology Model	 <p>Stratigraphic Zones Marmaton A-B Marmaton C Marmaton D Marmaton E Marmaton F</p>	 <p>GR I.D. Lithology logs estimated by using ANN+ GR cut-off + Porosity-lithology relation</p>	 <p>Mudstone Sandstone Conglomerate</p>
System Tract Lithology Model	 <p>Stratigraphic Zones Marmaton A (TST) Marmaton A (HST) Marmaton B (TST) Marmaton B (HST) Marmaton C (TST) Marmaton C (HST) Marmaton D (TST) Marmaton D (HST) Marmaton E (TST) Marmaton E (HST) Marmaton F (TST) Marmaton F (HST)</p>	 <p>GR I.D. Lithology logs estimated by using ANN+ GR cut-off + Porosity-lithology relation</p>	 <p>Mudstone Sandstone Conglomerate</p>
Sequence Reservoir Model - 1	 <p>Stratigraphic Zones Marmaton A-B Marmaton C Marmaton D Marmaton E Marmaton F</p>	 <p>GR I.D. Lithology logs estimated by using only GR cut-off</p>	 <p>Non-reservoir Reservoir</p>
Sequence Reservoir Model - 2	 <p>Stratigraphic Zones Marmaton A-B Marmaton C Marmaton D Marmaton E Marmaton F</p>	 <p>GR I.D. Lithology logs estimated by using ANN+ GR cut-off + Porosity-lithology relation</p>	 <p>Non-reservoir Reservoir</p>

Figure J-1. Four lithology models with the 3-D grids and lithology logs honoring them. Sequence models consist of 5 stratigraphic zones separated by maximum flooding surfaces. System tract lithology model has 12 zones that define the interpreted transgressive and highstand system tracts. Sequence reservoir models have only two types of rocks which are reservoir and non-reservoir rocks. Reservoir rocks include sandstones and conglomerates. Sequence reservoir model is honored by the lithology logs calculated by using only gamma-ray (GR) cut-off value while sequence reservoir model 2 is honored by the lithology logs estimated by using Artificial Neural Network (ANN), gamma-ray cut-off value, and porosity-lithology relation. Sequence reservoir model-1 has less reservoir than sequence reservoir model-2.

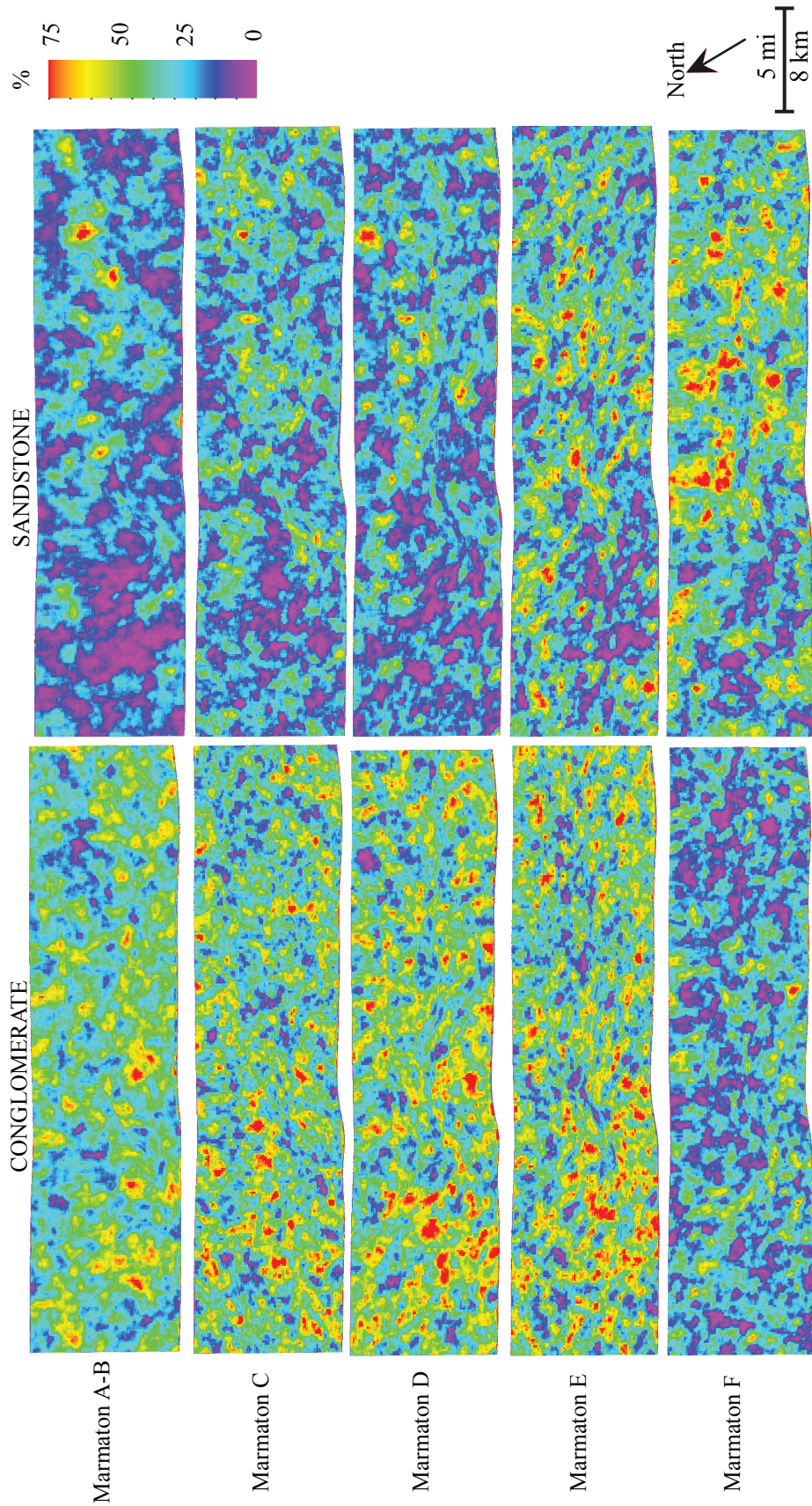


Figure J-2. Conglomerate and sandstone percent maps for each zone. Sandstone proportion decreases upward from Marmaton F through Marmaton A-B while conglomerate proportion increases up to Marmaton D and then starts to decrease (honoring the vertical proportion curve in figure 15). These can be related with the relative fall and rise in sea level. Laterally, on the northwest side of the study area proportion of conglomerate is greater than sandstone. This can be interpreted to be the result of relative proximity to the source area.

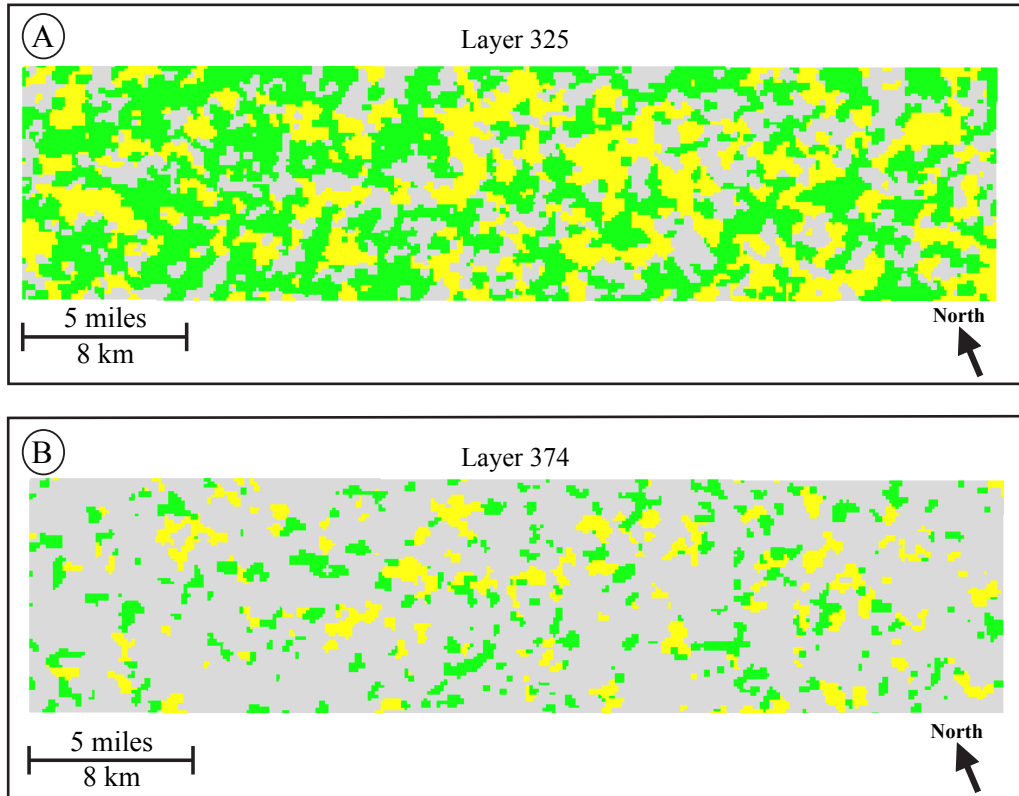


Figure J-3) A) Layer 325 in the sequence lithology model. This layer is within the highstand system tract according to the interpretations based on the vertical proportion curve, and rich in conglomerate and sandstone. B) Layer 375 in the sequence lithology model. This layer overlies the interpreted flooding surface 2. Correlated flooding surfaces correspond to the layers with highest mudstone proportion in the vertical proportion curve, and they can be considered as maximum flooding surfaces. Refer to figure 15 for the location of the layers in the vertical proportion curve.

## Appendix K: Variograms

Figure K-1. Variogram models and horizontal variogram map for mudstone in Top Marmaton Wash zone.

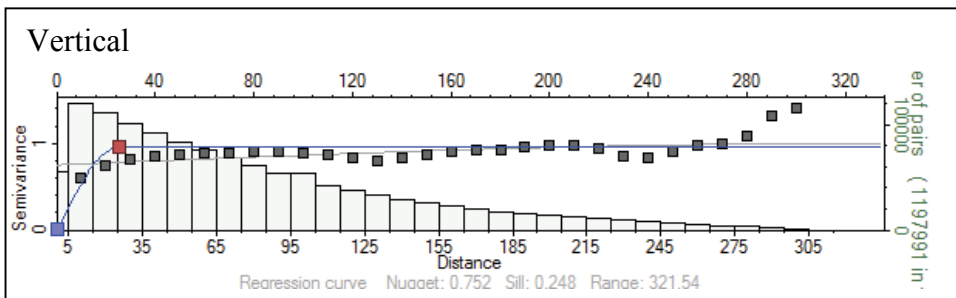
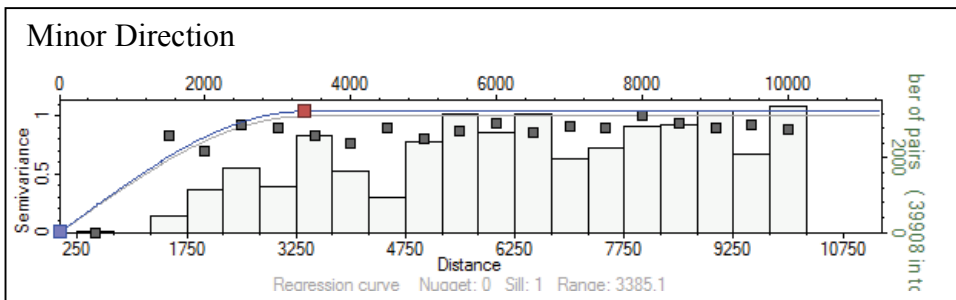
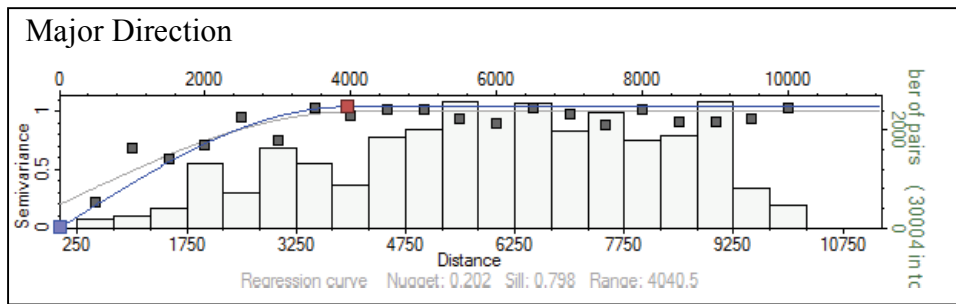
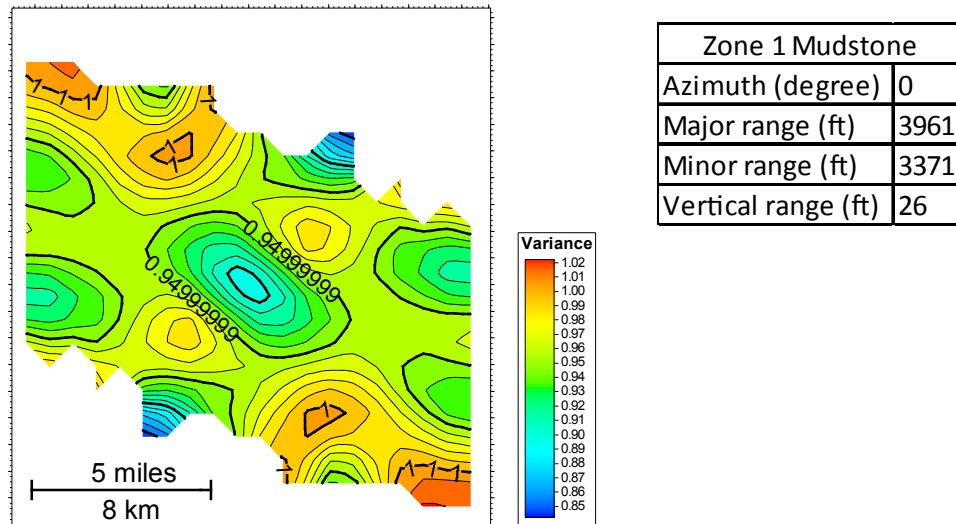


Figure K-2. Variogram models and horizontal variogram map for sandstone in Top Marmaton Wash zone.

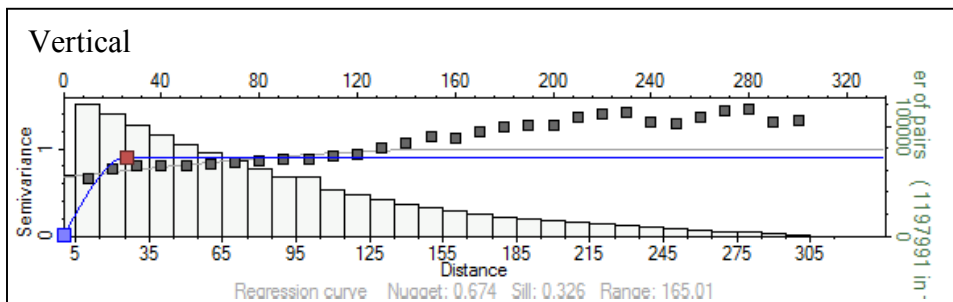
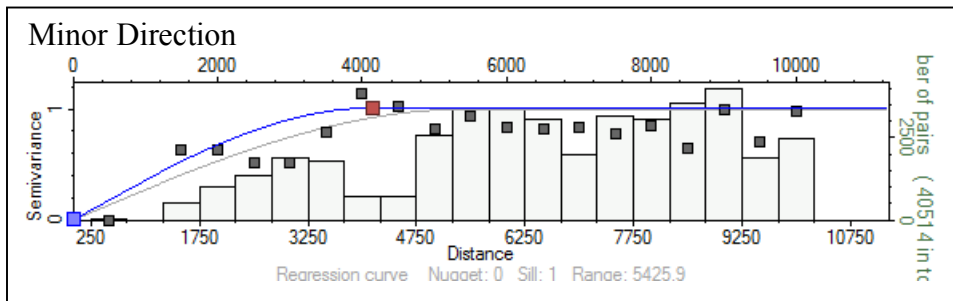
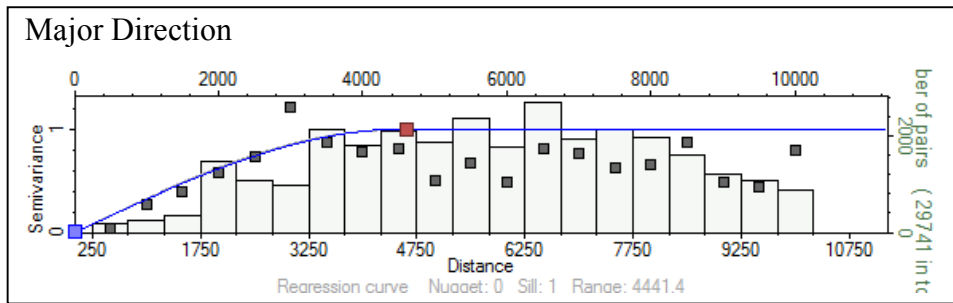
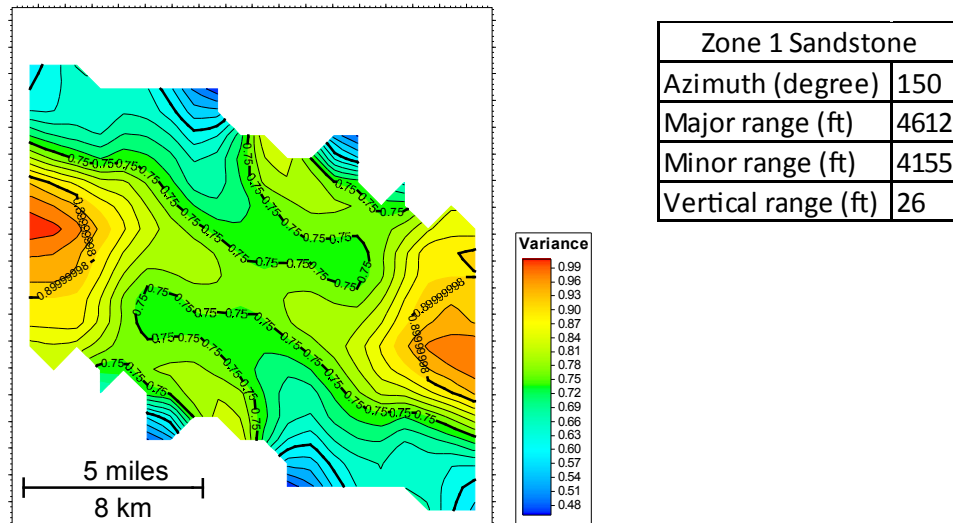


Figure K-3. Variogram models and horizontal variogram map for conglomerate in Top Marmaton Wash zone.

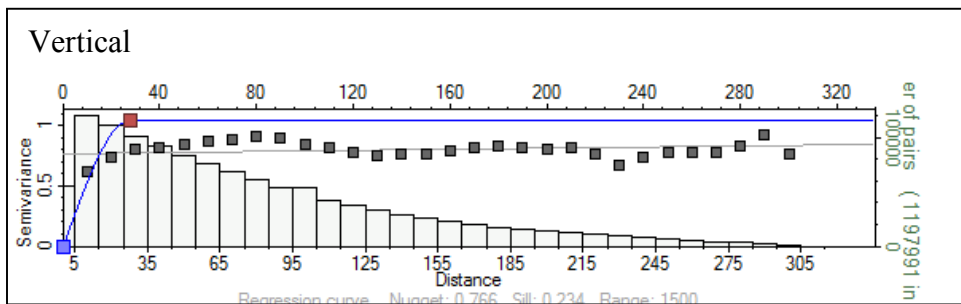
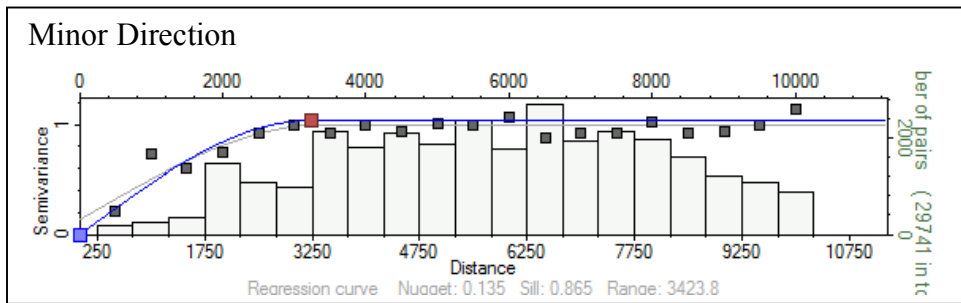
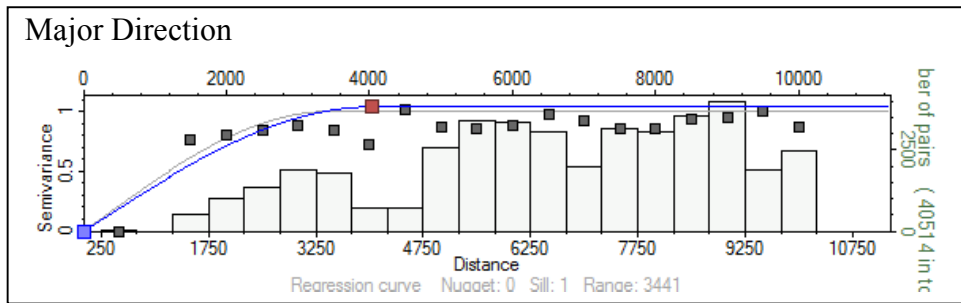
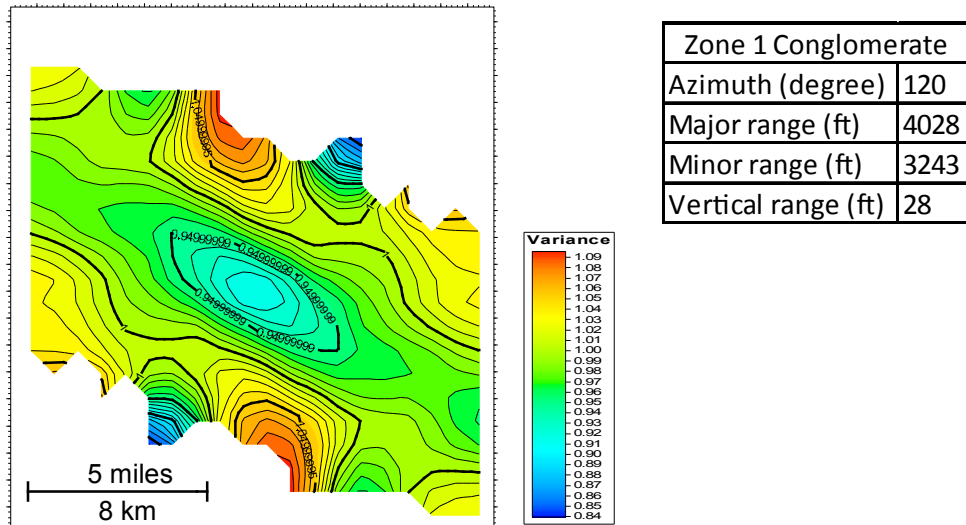


Figure K-4. Variogram models and horizontal variogram map for mudstone in Marmaton C Wash zone.

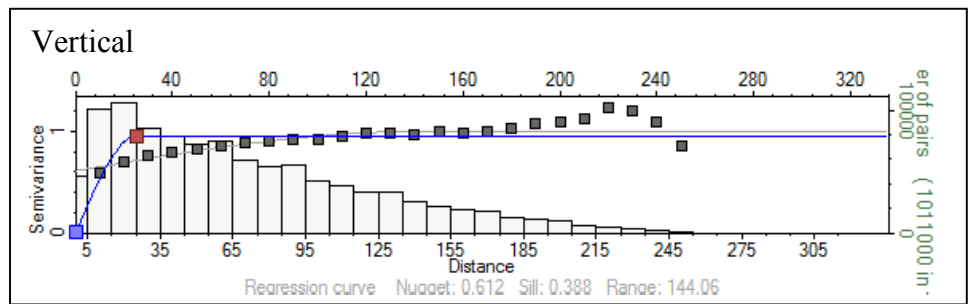
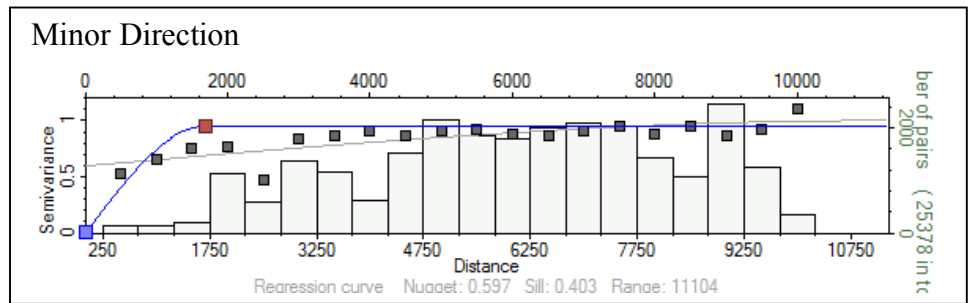
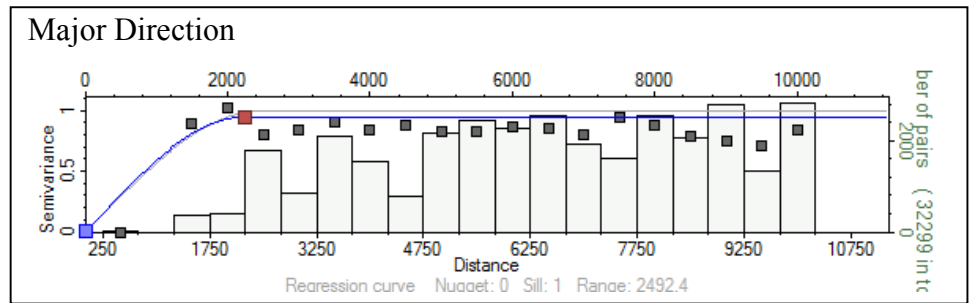
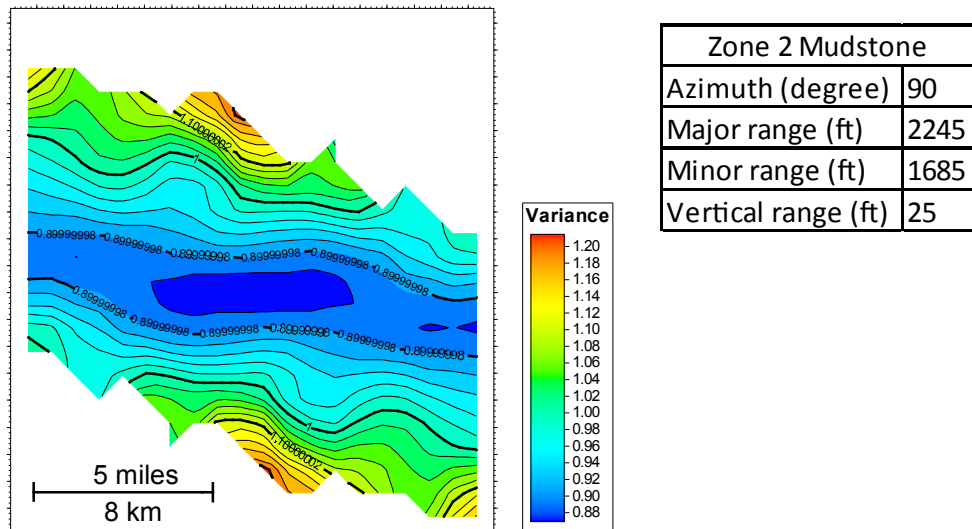


Figure K-5. Variogram models and horizontal variogram map for sandstone in Marmaton C Wash zone.

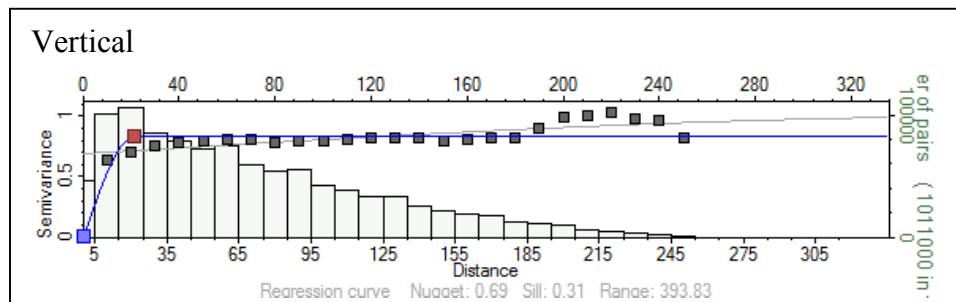
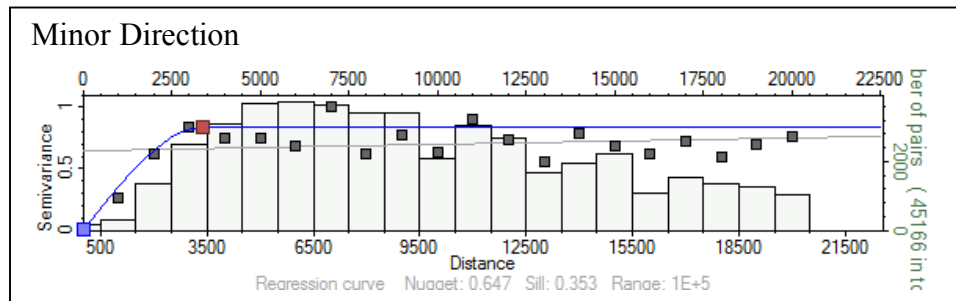
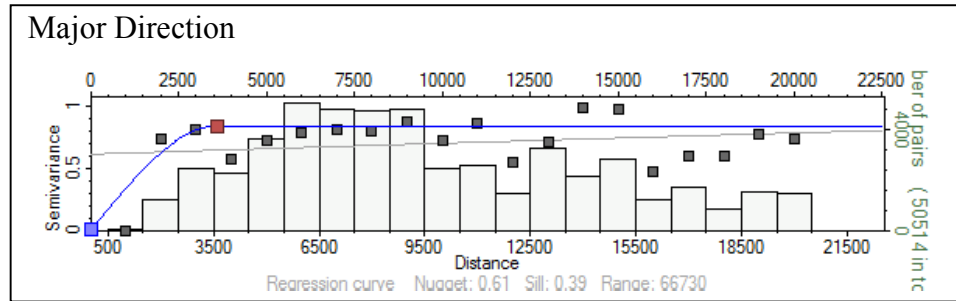
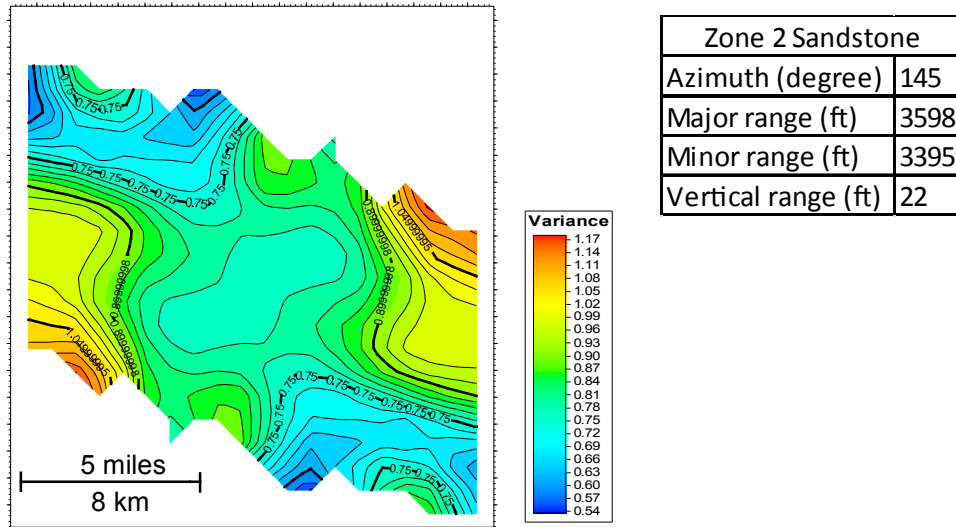




Figure K-6. Variogram models and horizontal variogram map for conglomerate in Marmaton C Wash zone.

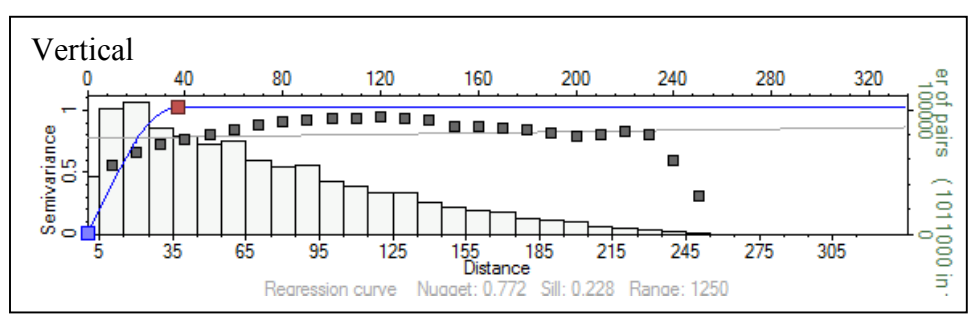
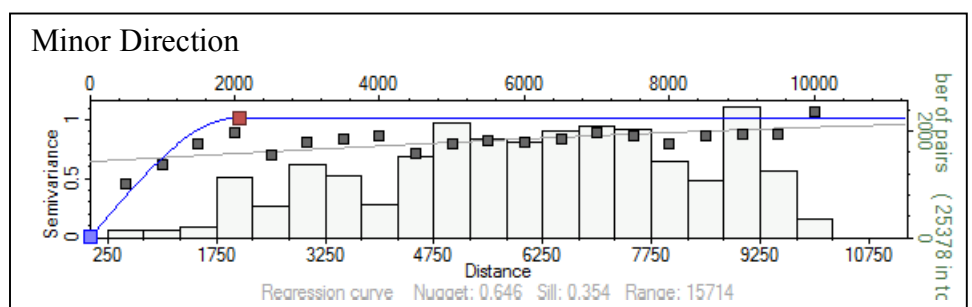
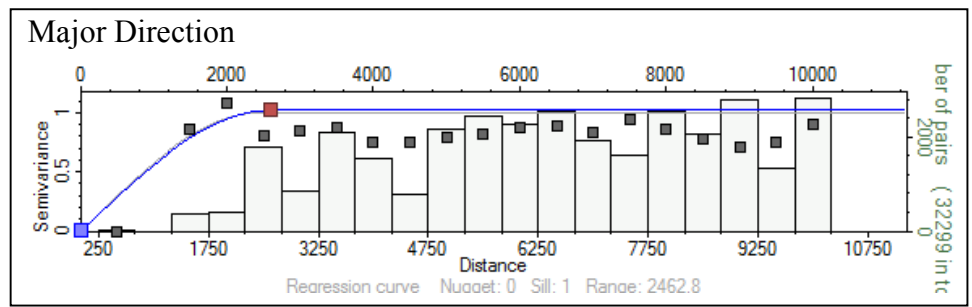
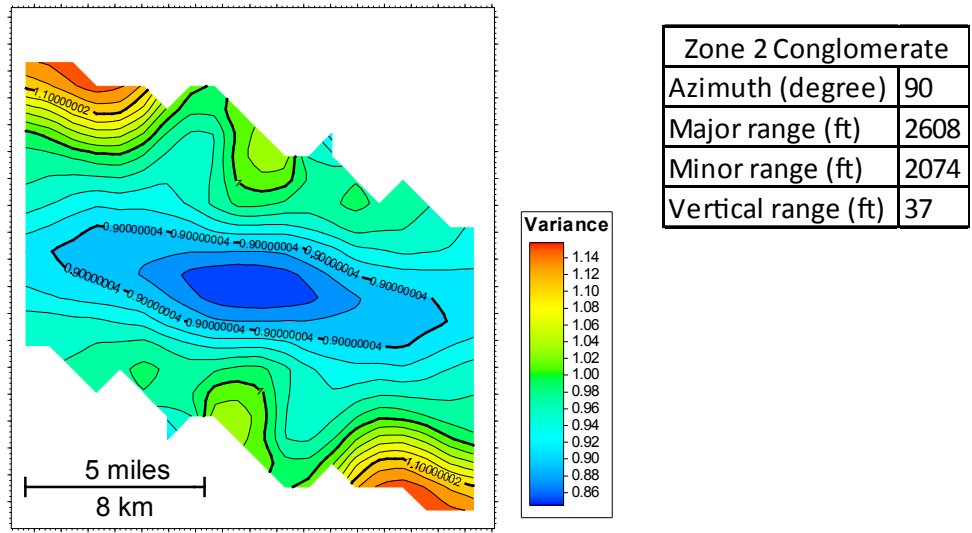


Figure K-7. Variogram models and horizontal variogram map for mudstone in Marmaton D Wash zone.

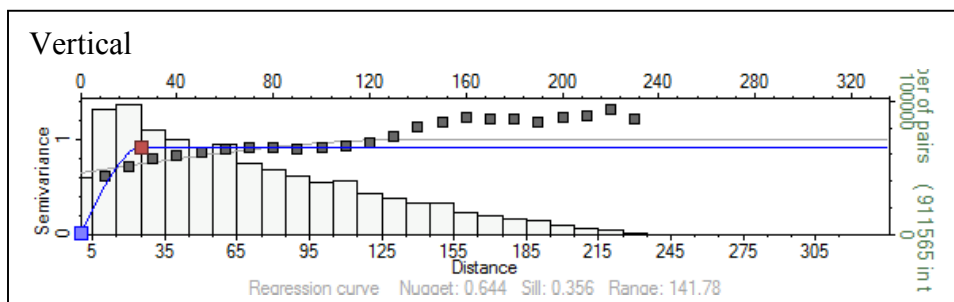
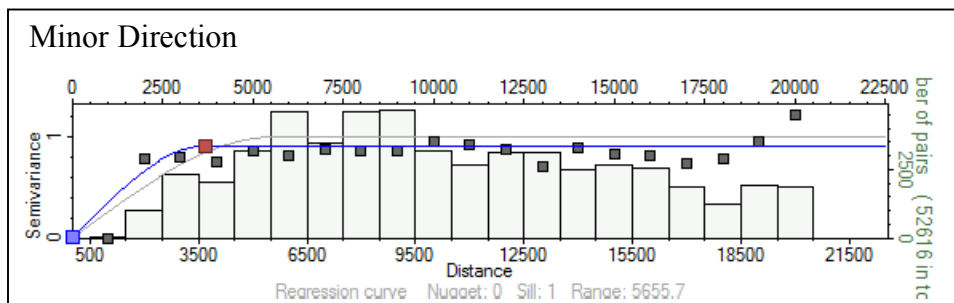
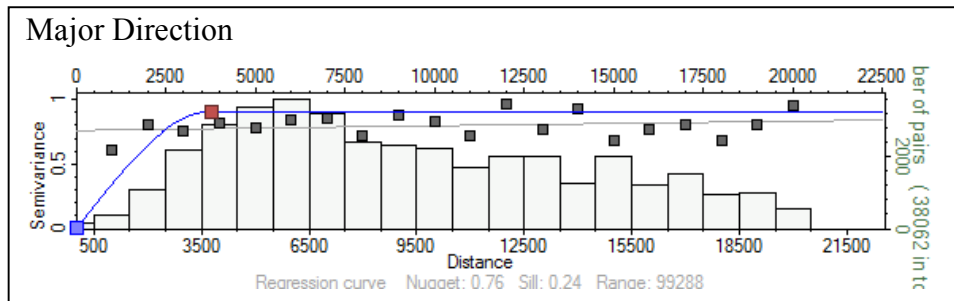
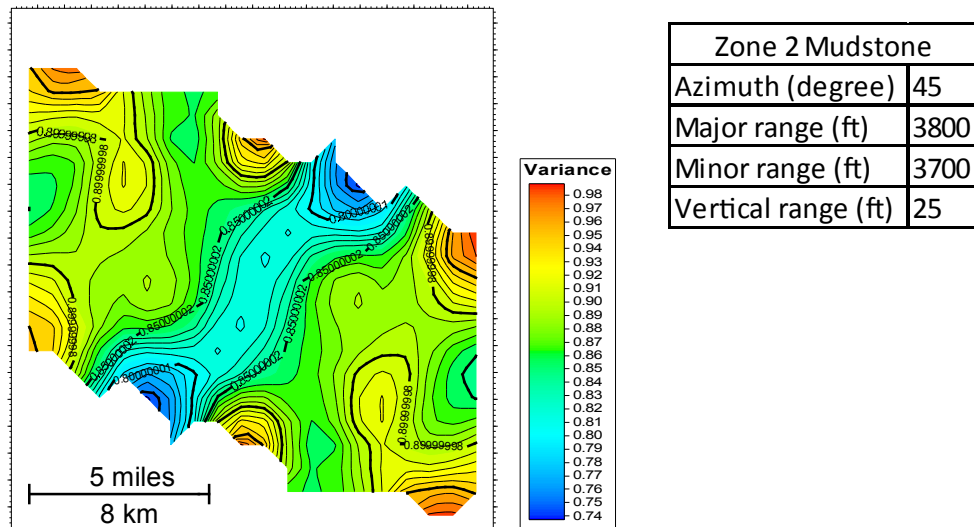


Figure K-8. Variogram models and horizontal variogram map for sandstone in Marmaton D Wash zone.

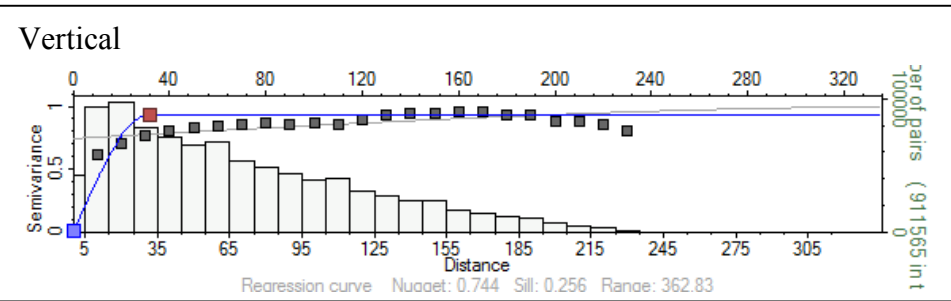
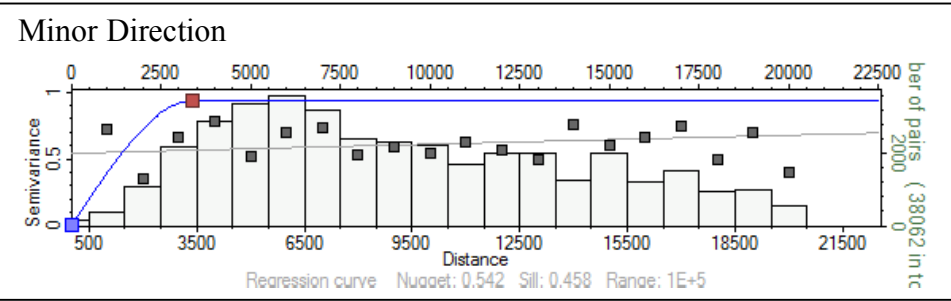
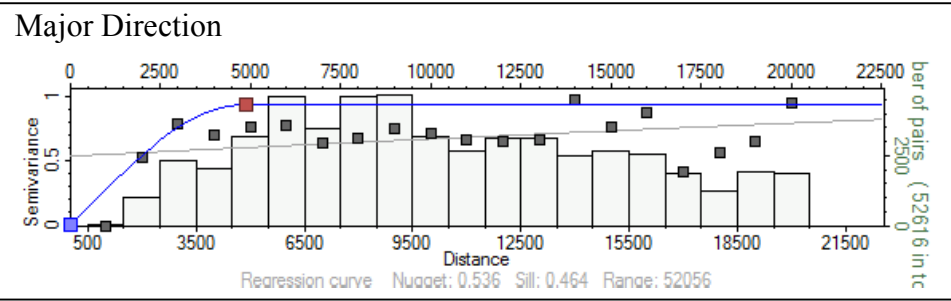
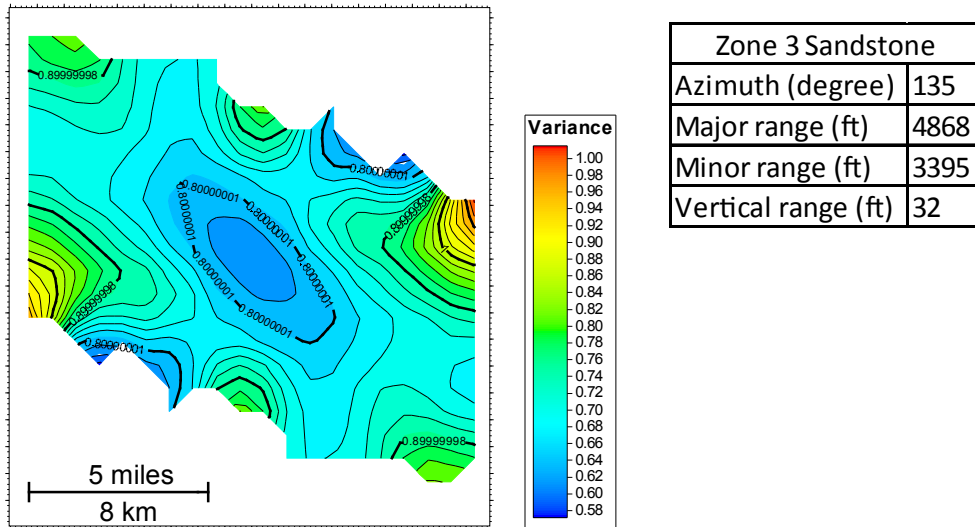


Figure K-9. Variogram models and horizontal variogram map for conglomerate in Marmaton D Wash zone.

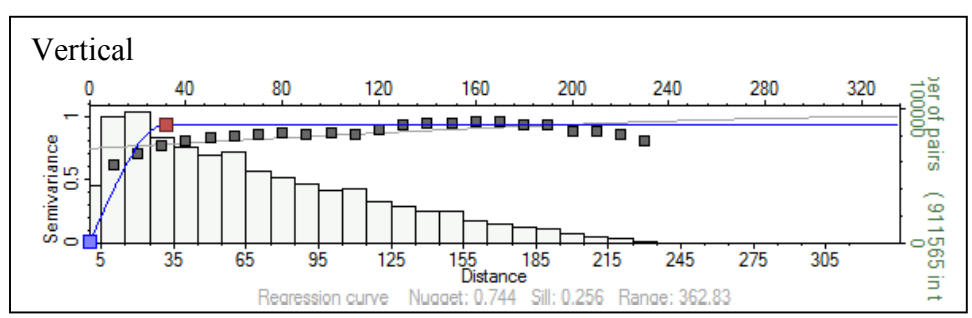
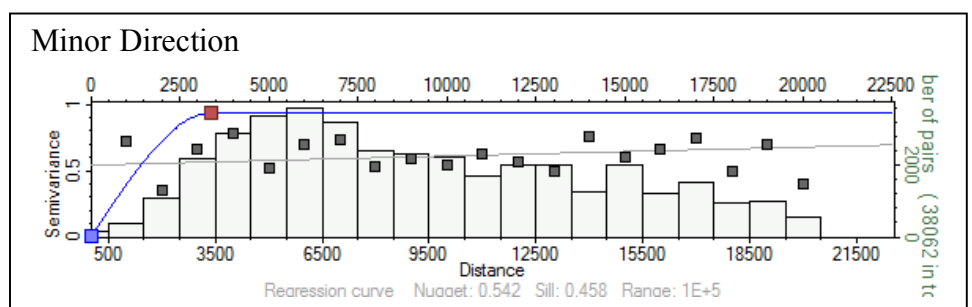
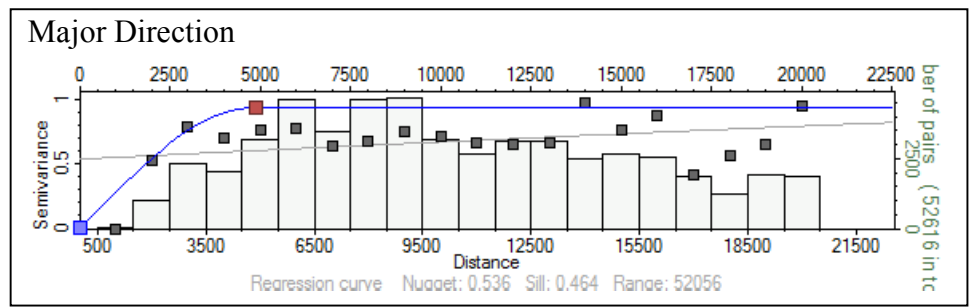
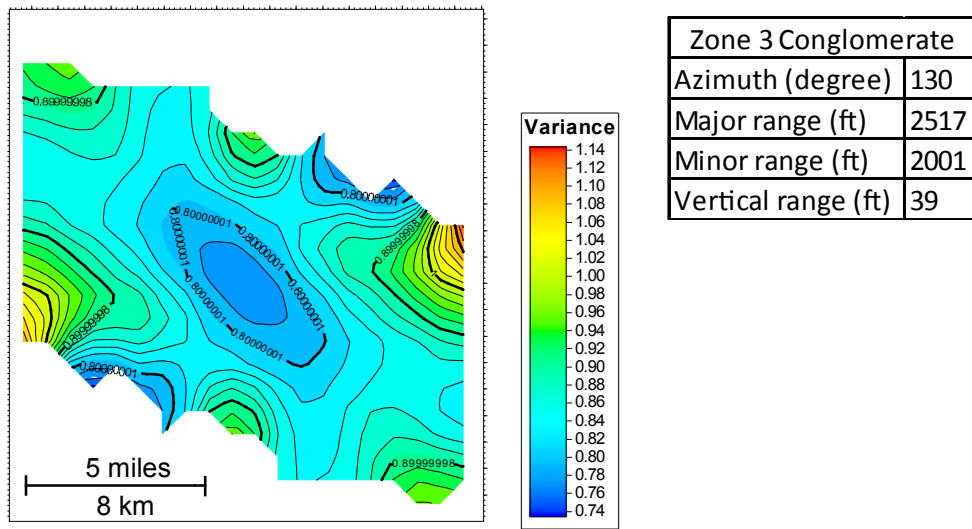


Figure K-10. Variogram models and horizontal variogram map for mudstone in Marmaton E Wash zone.

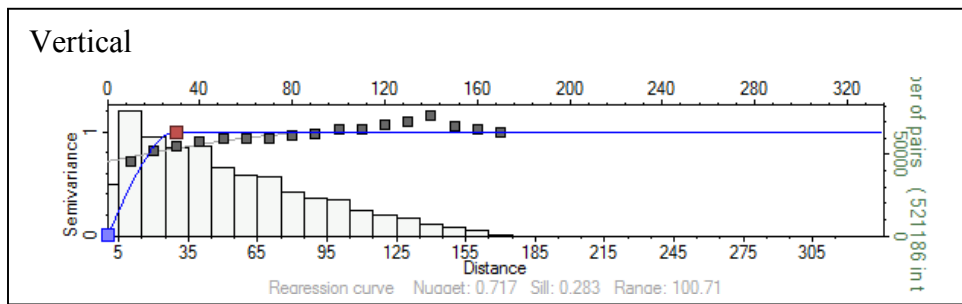
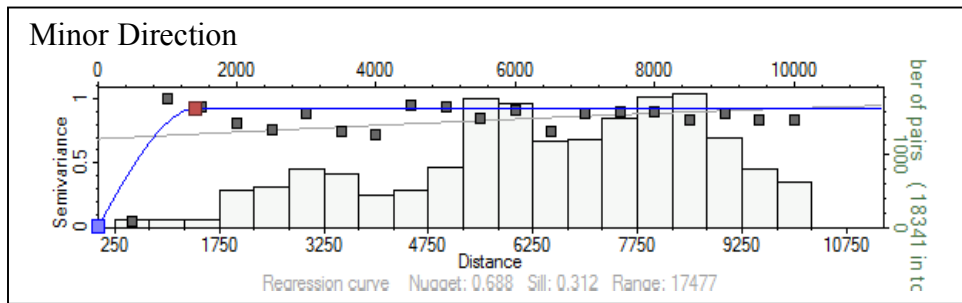
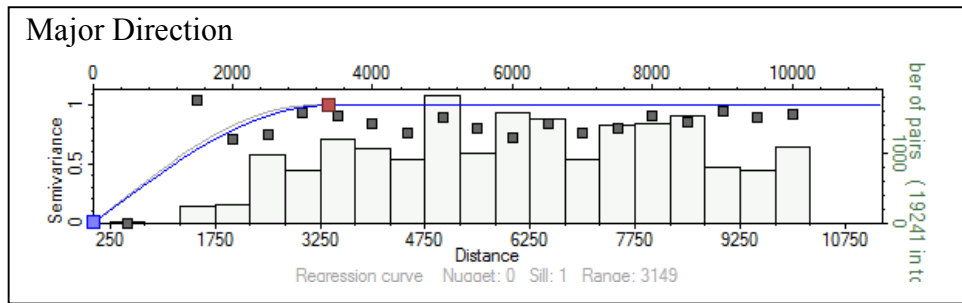
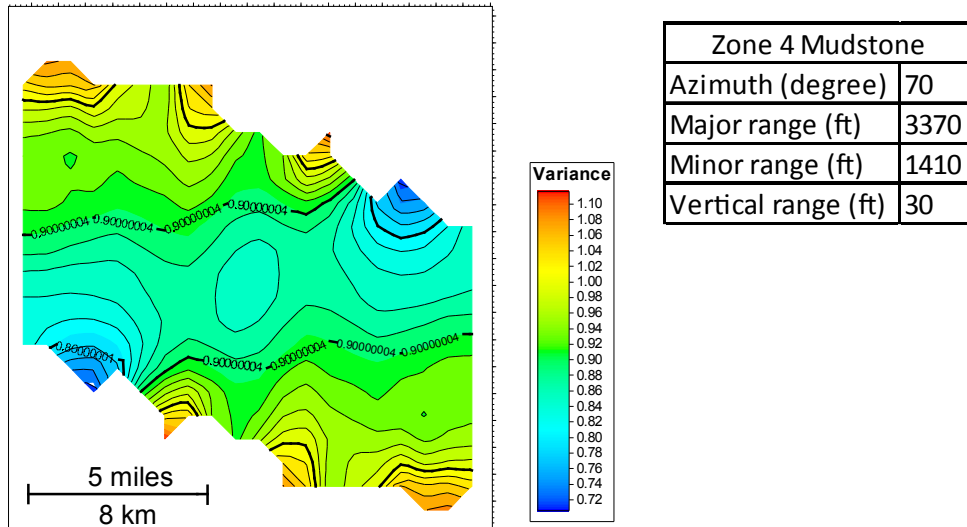


Figure K-11. Variogram models and horizontal variogram map for sandstone in Marmaton E Wash zone.

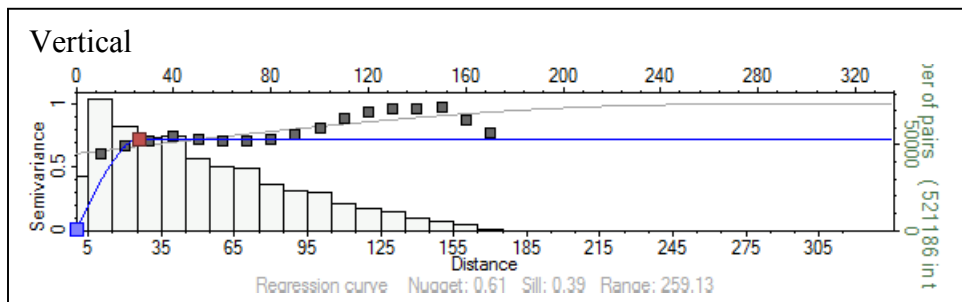
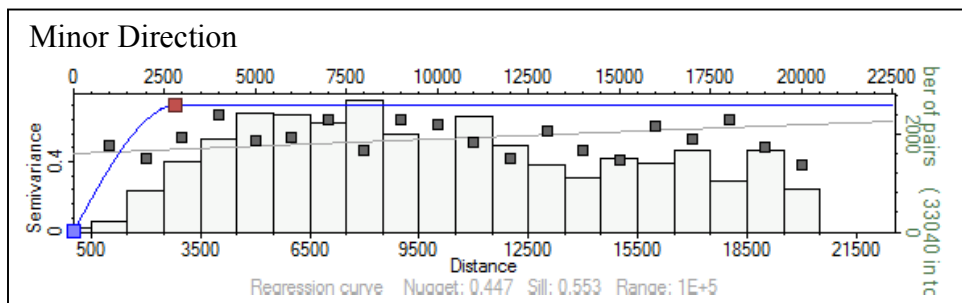
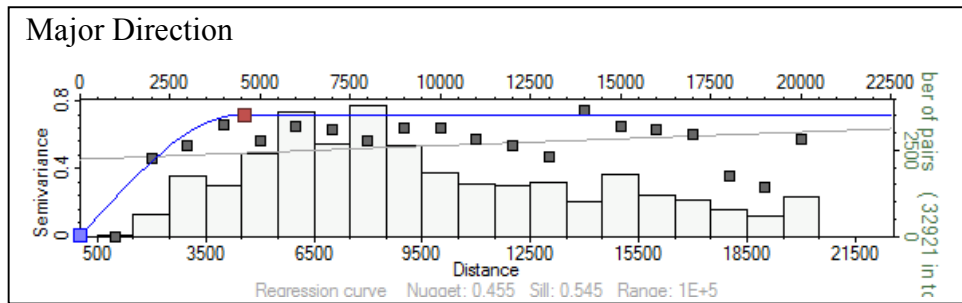
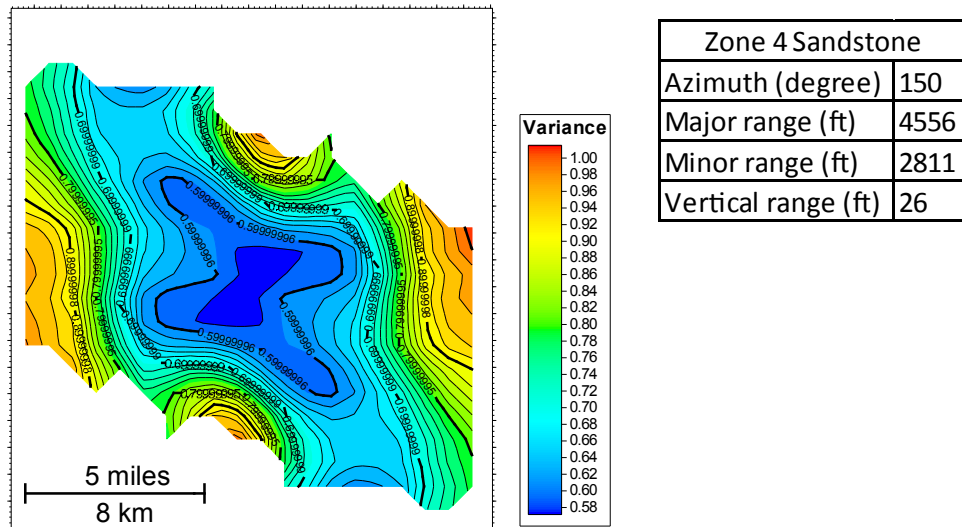
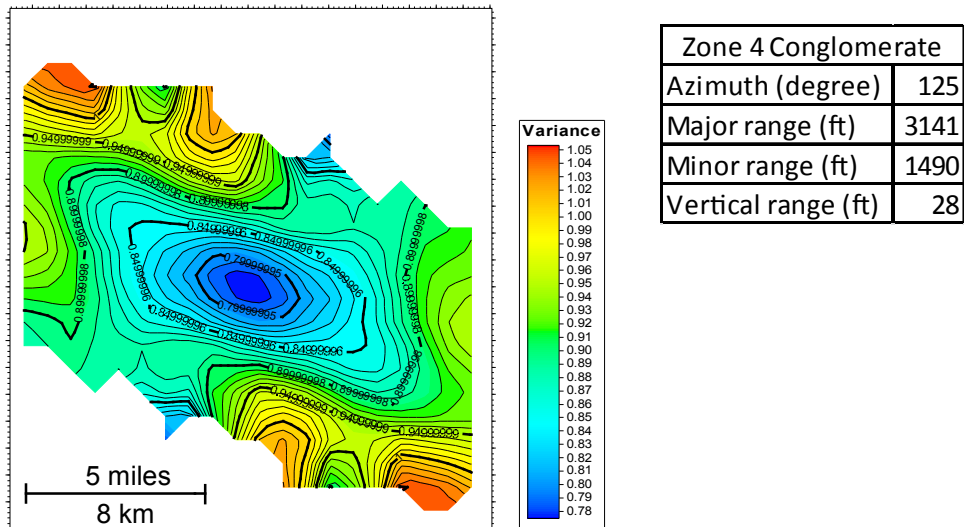


Figure K-12. Variogram models and horizontal variogram map for conglomerate in Marmaton E Wash zone.



Zone 4 Conglomerate	
Azimuth (degree)	125
Major range (ft)	3141
Minor range (ft)	1490
Vertical range (ft)	28

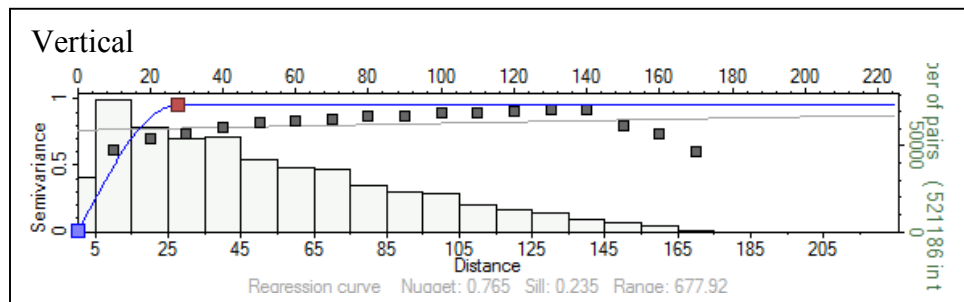
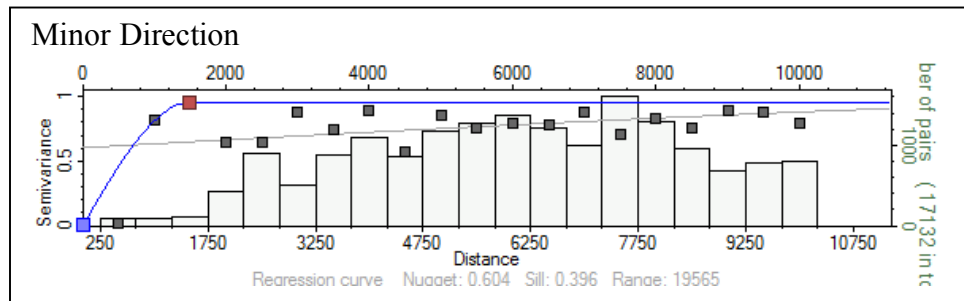
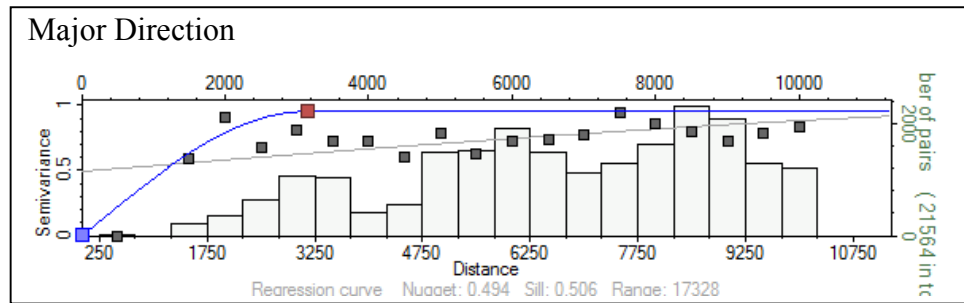


Figure K-13. Variogram models and horizontal variogram map for mudstone in Marmaton F Wash zone.

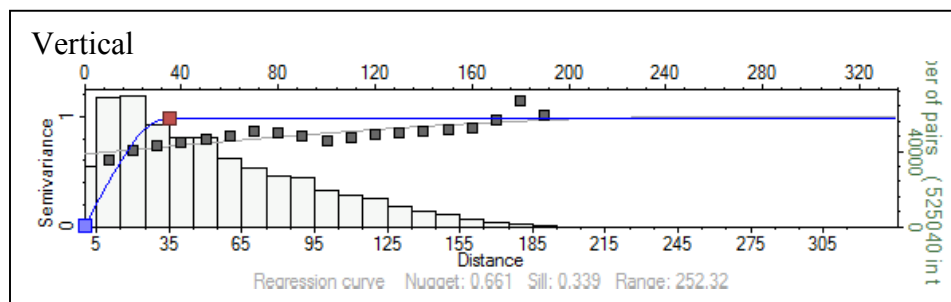
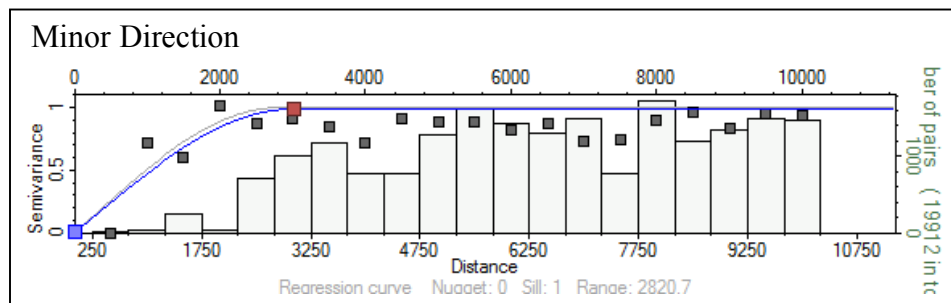
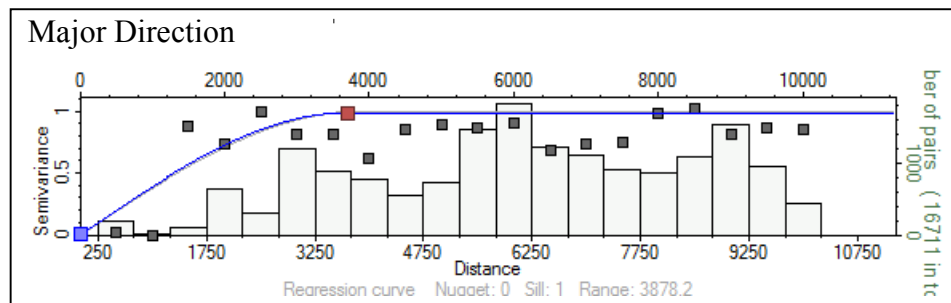
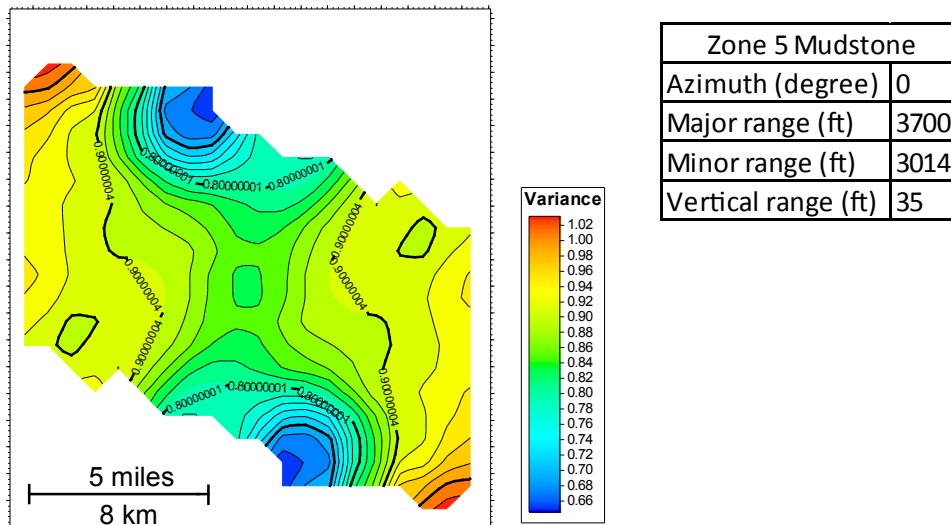




Figure K-14. Variogram models and horizontal variogram map for sandstone in Marmaton F Wash zone.

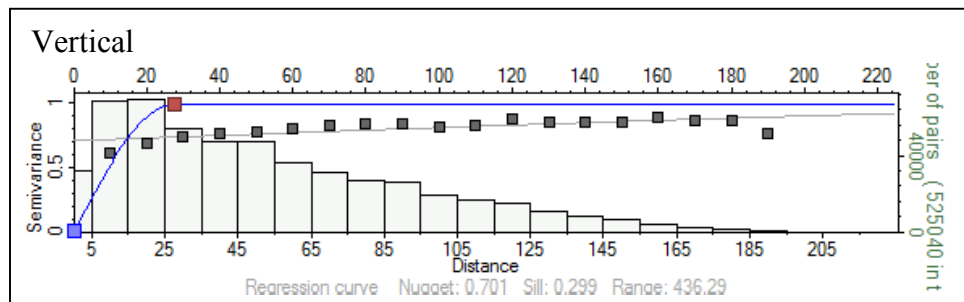
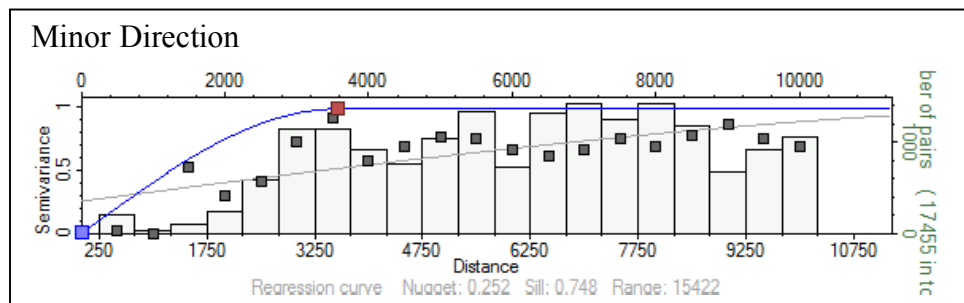
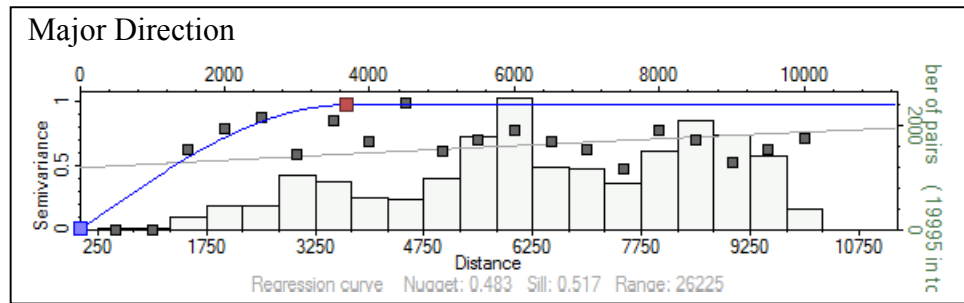
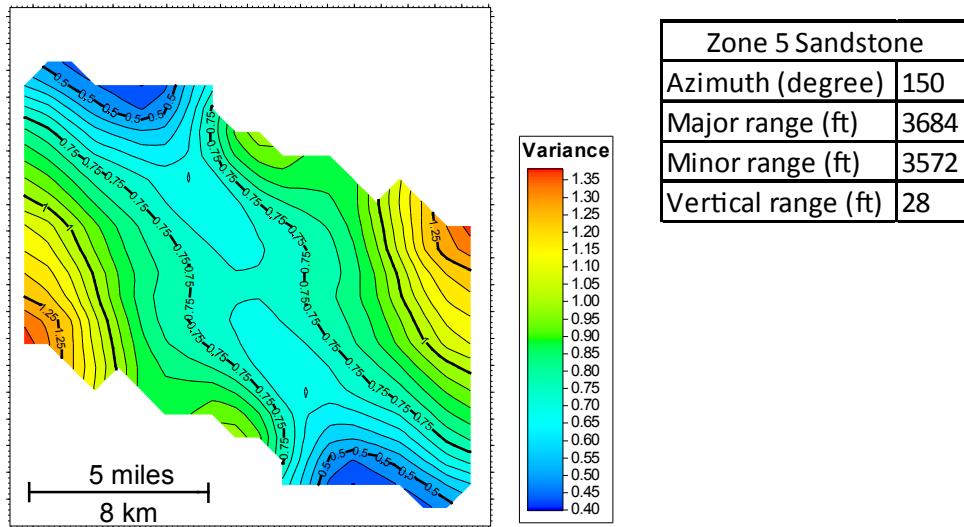


Figure K-15 Variogram models and, horizontal variogram map for conglomerate in Marmaton F Wash zone.

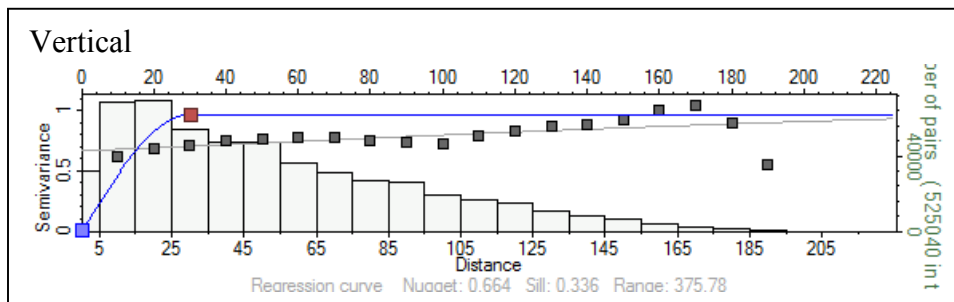
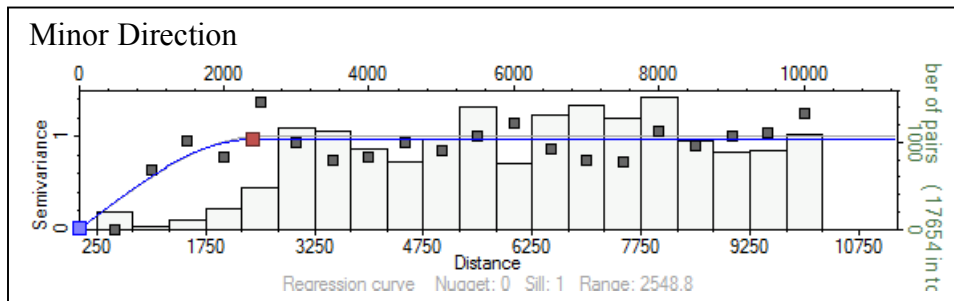
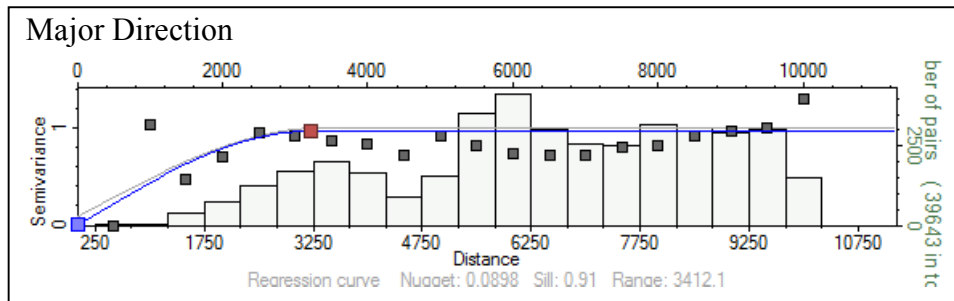
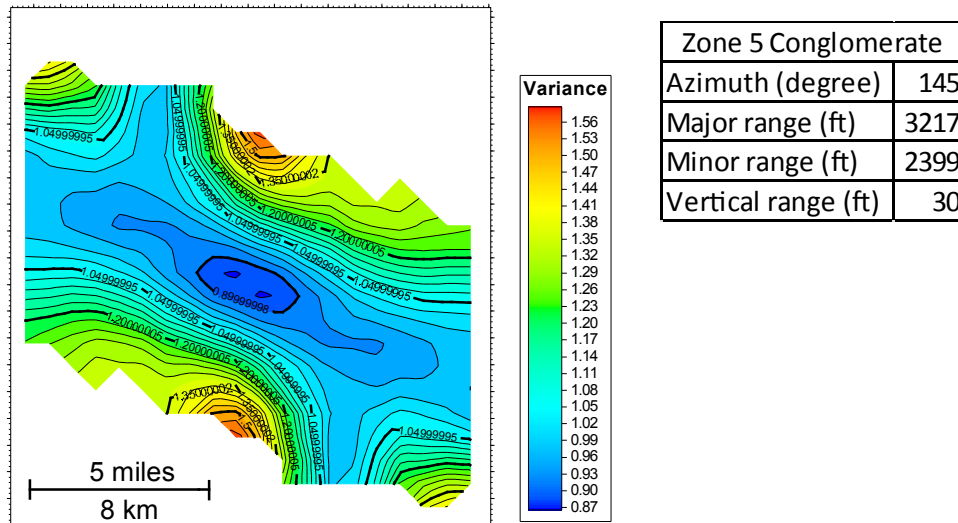
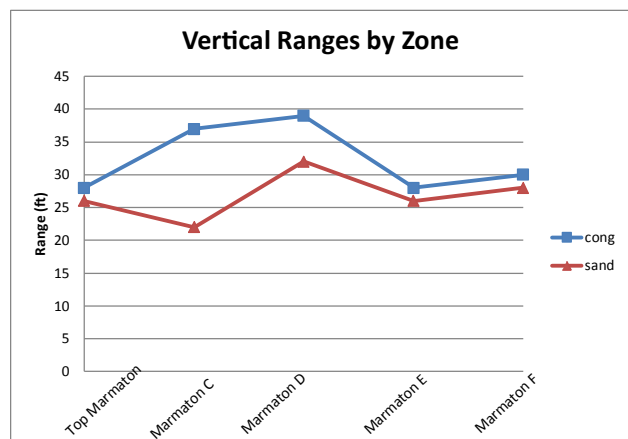
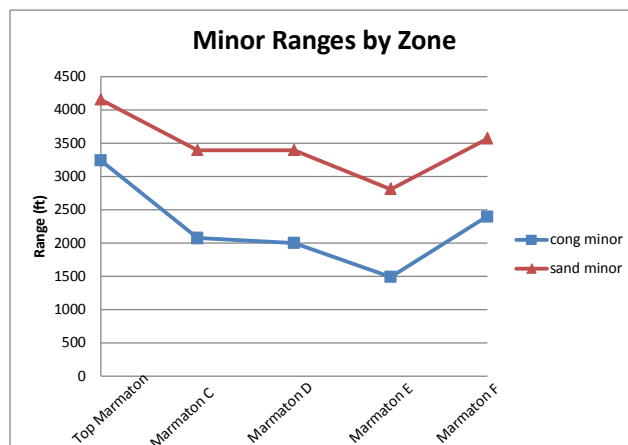
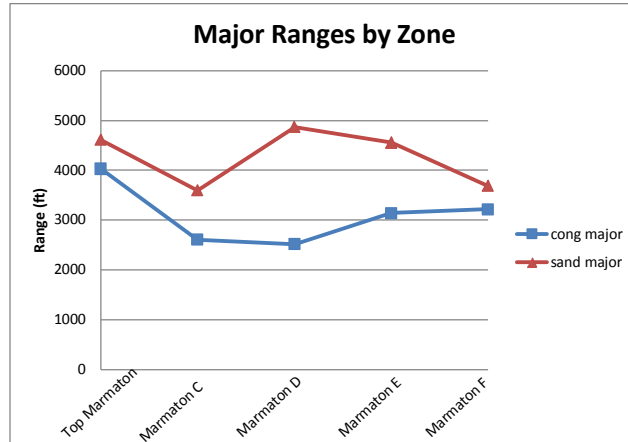


Figure K-16. Major, minor and vertical ranges of sandstone and conglomerate by zone. Sandstone has higher horizontal range while conglomerate has higher vertical range.

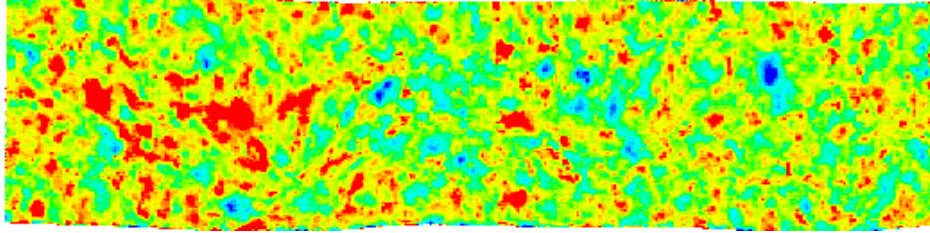


## Appendix L: Porosity Modeling

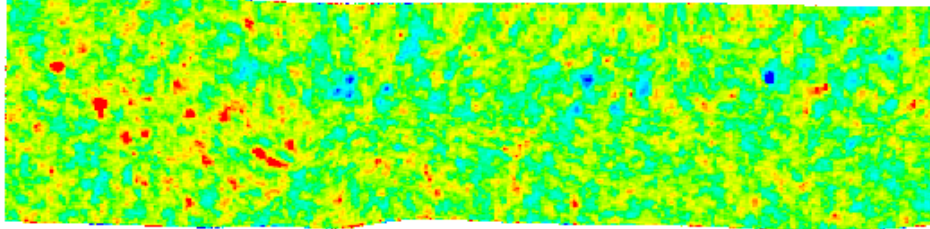
Table L-1. Variogram ranges of porosity at each lithology per zone.

Zones	Lithology	Major range (ft)	Minor range (ft)	Vertical range (ft)
<b>Top Marmaton</b>	Conglomerate	2000	2000	19
	Sandstone	2600	2600	17
	Mudstone	2500	2500	16
<b>C Wash</b>	Conglomerate	1600	1600	16
	Sandstone	2600	2600	14
	Mudstone	1500	1500	15
<b>D Wash</b>	Conglomerate	1800	1800	29
	Sandstone	2500	2500	14
	Mudstone	2000	2000	14
<b>E Wash</b>	Conglomerate	1400	1400	21
	Sandstone	2500	2500	14
	Mudstone	1400	1400	13
<b>F Wash</b>	Conglomerate	2250	2250	21
	Sandstone	3000	3000	11
	Mudstone	2500	2500	14

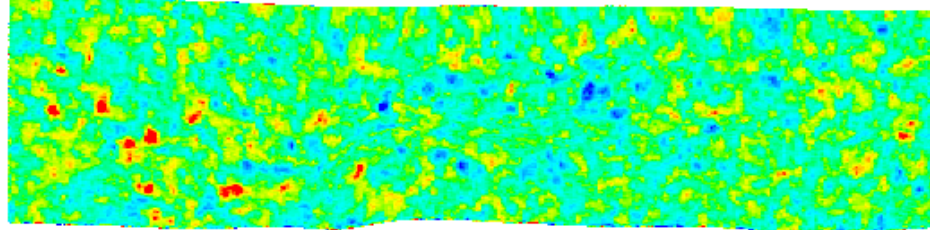
Marmaton A-B



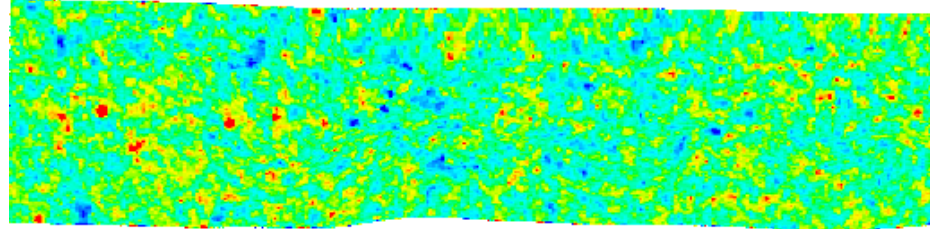
Marmaton C



Marmaton D



Marmaton E



Marmaton F

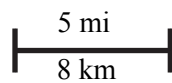
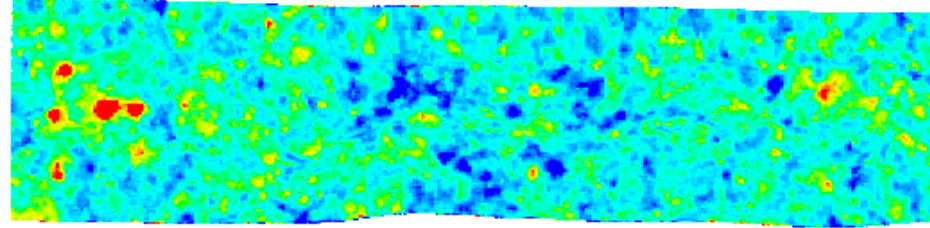


Figure L-2. Average porosity maps for each zone. Porosity increases from Marmaton F Wash through Top Marmaton Wash. This can be explained by decreasing amount of sandstone and increasing amount of conglomerate upward.

## Appendix M: Connectivity and Pore Volume

ZONES	System Tract	Total volume in BCF (x10 <sup>9</sup> ft <sup>3</sup> )	Pore volume (x10 <sup>6</sup> RB)	Connected volume in BCF	Connectivity (%)	Porosity > 5%		Porosity > 10%	
						Connected volume in BCF	Connectivity (%)	Connected volume in BCF	Connectivity (%)
<b>Marmaton A-B</b>	TST	64	1182	62	96.0	53	80.0	21	20.0
	HST	348	5156	339	97.4	287	82.5	75	21.6
	TST	32	433	25	76.6	17	53.9	6	18.3
	HST	192	2542	187	97.4	142	74.0	32	16.9
<b>Marmaton C</b>	TST	32	472	26	81.4	21	64.7	7	20.5
	HST	467	7055	456	97.6	376	80.5	121	25.9
<b>Marmaton D</b>	TST	40	590	27	67.6	22	53.6	7	17.3
	HST	479	6732	468	97.7	366	76.4	99	20.6
<b>Marmaton E</b>	TST	33	457	30	88.3	21	63.8	5	15.8
	HST	337	4913	329	97.6	264	78.3	67	19.9
<b>Marmaton F</b>	TST	44	587	39	89.1	28	63.7	7	15.4
	HST	243	2985	220	90.5	129	53.1	67	27.6
CONGLOMERATE									
ZONES	System Tract	Total volume in BCF (x10 <sup>9</sup> ft <sup>3</sup> )	Pore volume (x10 <sup>6</sup> RB)	Connected volume in BCF	Connectivity (%)	Porosity > 5%		Porosity > 10%	
						Connected volume in BCF	Connectivity (%)	Connected volume in BCF	Connectivity (%)
<b>Marmaton A-B</b>	TST	31	382	18	57.7	12	37.1	3	6.0
	HST	206	2219	186	90.3	115	55.8	13	6.3
	TST	24	257	17	69.7	10	43.3	2	7.1
	HST	117	1305	106	90.6	70	59.7	10	8.4
<b>Marmaton C</b>	TST	23	283	14	61.5	9	41.0	3	11.3
	HST	291	3303	270	92.8	173	59.5	26	8.9
<b>Marmaton D</b>	TST	35	328	25	71.3	13	37.8	1	1.6
	HST	282	2736	259	91.8	147	52.1	7	2.4
<b>Marmaton E</b>	TST	26	269	16	61.1	9	35.5	1	3.9
	HST	267	2754	256	95.9	149	55.8	14	5.1
<b>Marmaton F</b>	TST	34	324	25	73.2	12	34.2	1	3.0
	HST	359	3273	349	97.2	176	49.0	5	1.3
SANDSTONE									

Table M-1. Total volumes, connected volumes, pore volumes, and connectivities for conglomerates and sandstones at transgressive system tracts and highstand system tracts of each zone. See figure 18 for the histograms and explanation. Conglomerates and sandstones in the highstand system tracts have greater connectivities than those in transgressive system tracts. Conglomerates mostly have higher connectivities than sandstones. Highstand system tracts have greater pore volume than transgressive system tracts both for conglomerates and sandstones. Conglomerates have greater bulk volume and pore volume than sandstones except Marmaton F interval.

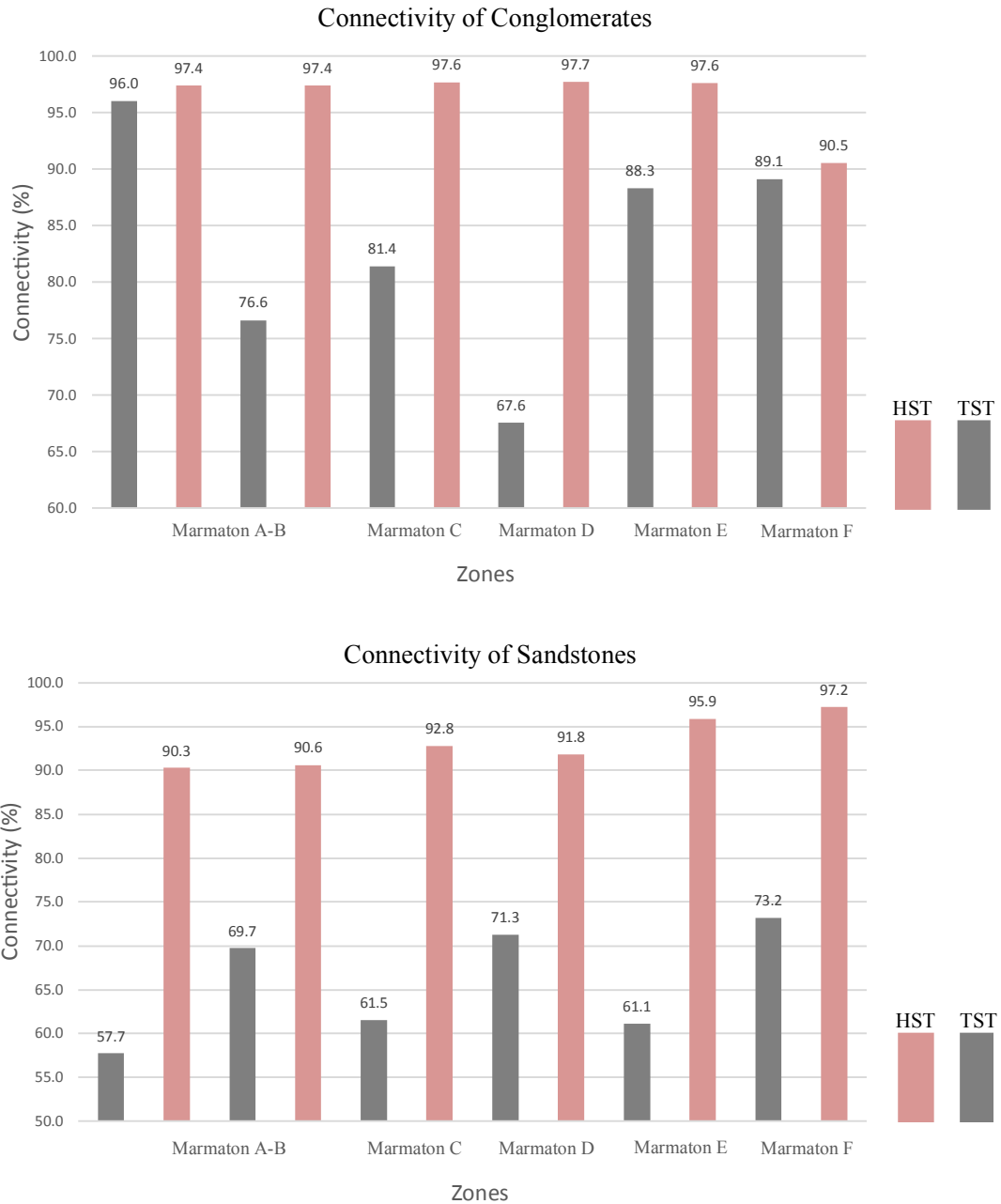


Figure M-2. Histograms showing the connectivities of conglomerates and sandstones by highstand system tracts (HST) and transgressive system tracts (TST). Conglomerates and sandstones in the highstand system tracts have greater connectivities than those in transgressive system tracts. See table M-1 for the bulk volume and connected volumes at each zone.

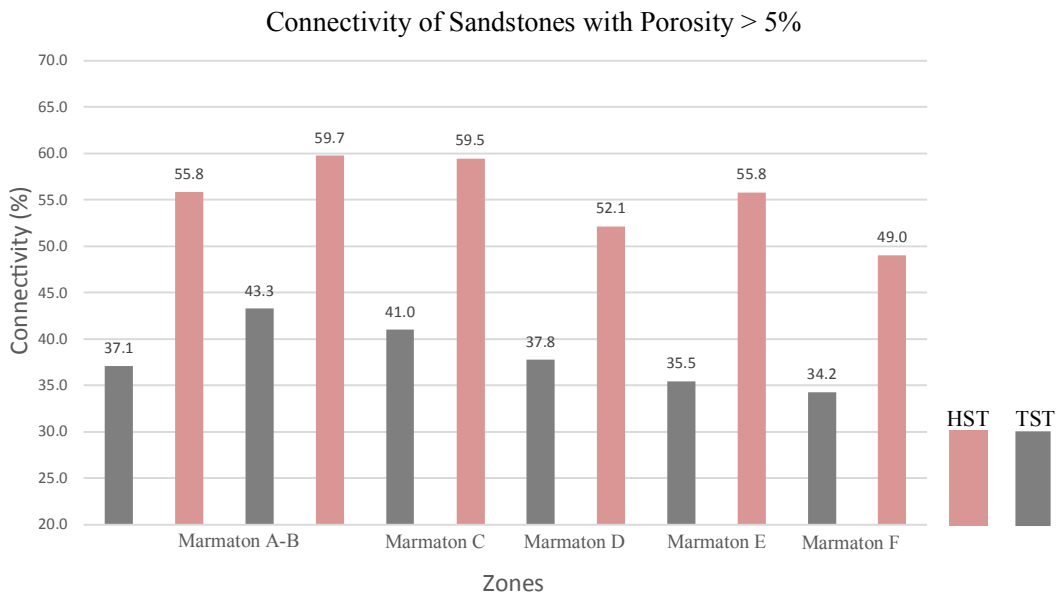
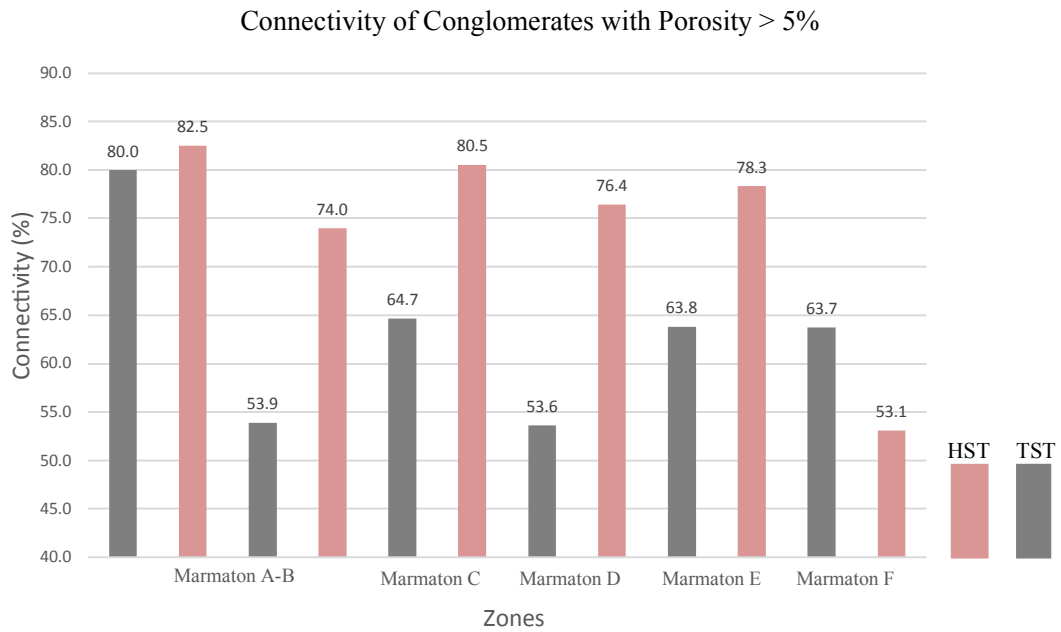
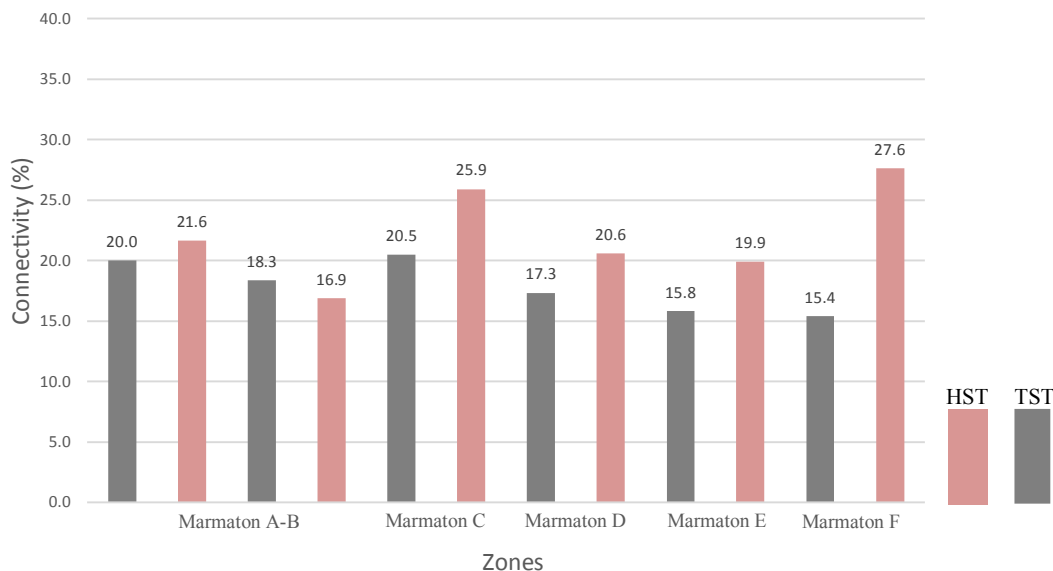


Figure M-3. Histograms showing the connectivities of conglomerates and sandstones having porosity greater than 5% by highstand system tracts (HST) and transgressive system tracts (TST). Conglomerates and sandstones in the highstand system tracts have greater connectivities than those in transgressive system tracts. See table M-1 for the bulk volume and connected volumes at each zone.



### Connectivity of Conglomerates with Porosity > 10%



### Connectivity of Sandstones with Porosity > 10%

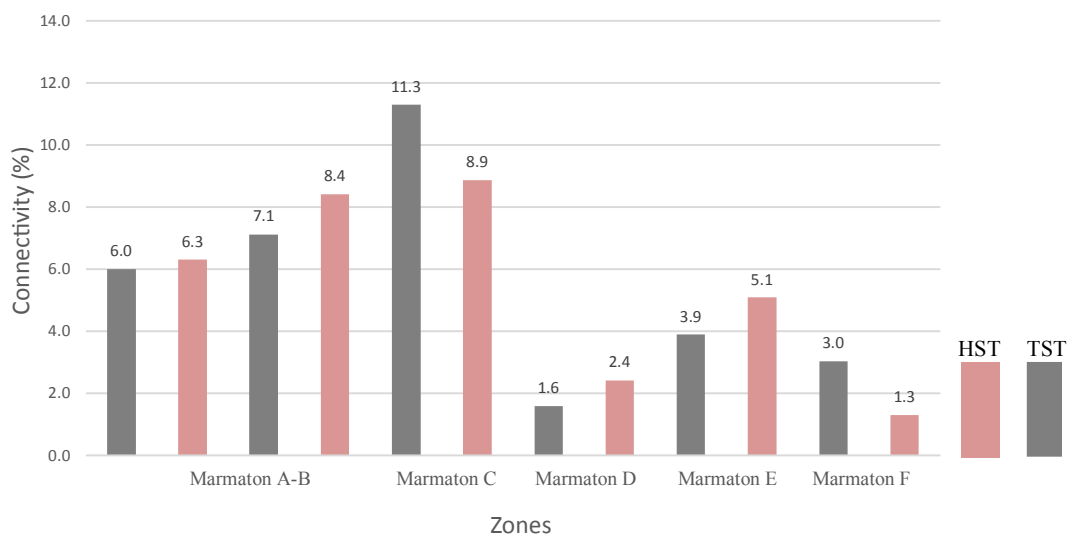


Figure M-4. Histograms showing the connectivities of conglomerates and sandstones having porosity greater than 10% by highstand system tracts (HST) and transgressive system tracts (TST). Connectivity decreases dramatically with the 10% of porosity filter. Conglomerates and sandstones in highstand and transgressive system tracts have closer connectivity. See table M-1 for the bulk volume and connected volumes at each zone.

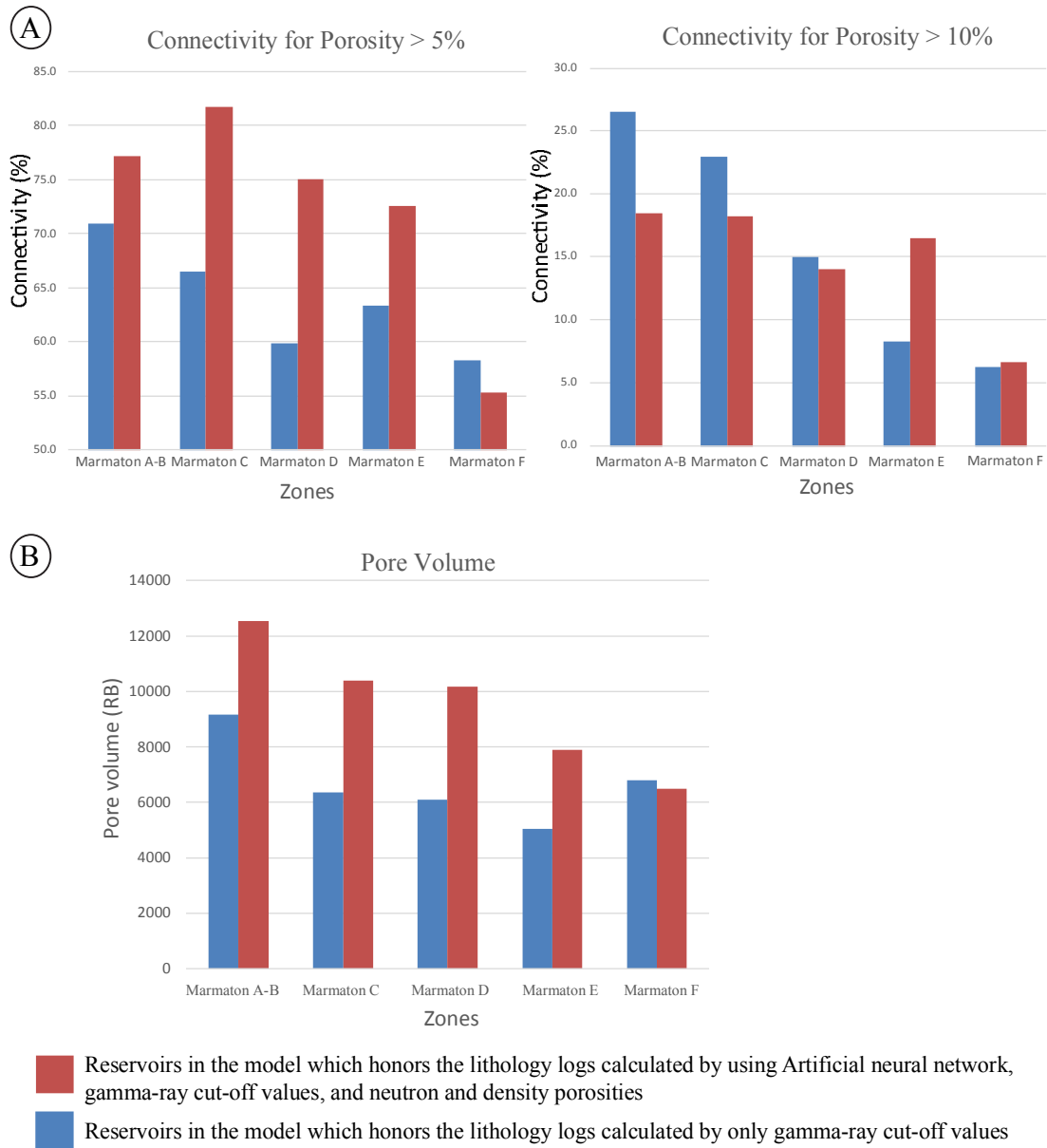


Figure M-5. Histograms showing A) the connectivity, and B) pore volume for lithology model honoring lithology logs estimated by using only gamma-ray cut-off values (blue), and lithology model honoring lithology logs created by using Artificial Neural Network, gamma-ray cut-off values, and porosity separation and cross-over (red). 5% and 10% total porosity cut-off were used as constraints to connectivity. For the reservoirs with greater than 5% porosity, and the model with the neural network estimation has greater connectivity except Marmaton F interval. Connectivity falls dramatically when the porosity filter is increased to 10%. The amount of pore volume in the model with the neural network estimation is greater than the pore volume in the model with only gamma-ray cut-off value estimation for all zones except Marmaton F interval. Closer amount of pore volume in the Marmaton F interval can be the result of closer estimation of reservoirs with two different methods.